

©2019

Praveen K. Bommareddy

ALL RIGHTS RESERVED

ONCOLYTIC HERPES SIMPLEX VIRUS - 1 FOR THE TREATMENT OF
MELANOMA

By

PRAVEEN K. BOMMAREDDY

A dissertation submitted to the

School of Graduate Studies

Rutgers, The State University of New Jersey

In partial fulfillment of the requirements

For the degree of

Doctor of Philosophy

Graduate Program in Microbiology and Molecular Genetics

Written under the direction of

Howard L. Kaufman, MD.

And approved by

New Brunswick, New Jersey

May 2019

ABSTRACT OF THE DISSERTATION
ONCOLYTIC HERPES SIMPLEX VIRUS - 1 FOR THE TREATMENT OF
MELANOMA

By
PRAVEEN K. BOMMAREDDY

Dissertation Director:
Howard L. Kaufman, MD.

Oncolytic viruses (OVs) are native or modified viruses that selectively replicate in and lyse tumor cells. The ability of OVs to selectively lyse tumor cells is attributed to disruption of both oncogenic cell signaling pathways and anti-viral machinery in cancer cells. In melanoma, rapidly dividing cells contain excessive pools of nucleotides that can also be used to enhance replication of attenuated OVs in these cells (1). In addition to the direct lytic effects, OVs are also thought to initiate innate and adaptive immune responses that contribute to both a direct and bystander effect that can promote tumor regression at injected and uninjected sites. The proof-of-concept for OVs in melanoma has recently been confirmed using Talimogene laherparepvec (Imlygic™; T-VEC), a modified form of herpes simplex virus-1 (HSV-1). T-VEC was generated from the JS1 strain of HSV-1 in which the infected cell protein (ICP) 34.5 neurovirulence genes are deleted to limit neurotoxicity and enhance cancer cell specific replication (2). T-VEC also contains a

deletion of the herpes ICP47 gene, which otherwise functions to block peptide transport through the transporter associated with antigen processing (TAP) machinery, which the virus uses to avoid immune detection. In the absence of ICP47, tumor-derived and viral peptides should be presented and result in immune recognition. To further enhance anti-tumor immunity, two copies of the human GM-CSF gene have been encoded in T-VEC to promote dendritic cell infiltration and maturation at the tumor site and enhance subsequent tumor-associated antigen presentation to T cells. Therapeutic responses to T-VEC are often limited and targeted therapies such as BRAF and MEK inhibitors often fail due to recurrence of disease in melanoma. To date, combination MAPK inhibition and oncolytic virus therapy has not been clinically tested but this may be an important regimen to consider given the potential for combining agents acting at different parts of the cancer-immunity cycle. Thus, we hypothesized that MAPK inhibition would improve oncolytic virus responses since viral infection could help activate a more robust immune response. Further, we sought to evaluate this concept in melanoma given the frequency of BRAF mutations and the availability of approved MAPK inhibitors and an oncolytic virus for clinical testing. Here, we report a synergistic *in vitro* and *in vivo* therapeutic effect for MEK inhibition administered with T-VEC in both human xenograft and immune competent melanoma models. Oncolytic activity was not dependent on BRAF mutation status but was associated with increased viral replication, and the presence of melanoma antigen specific CD8⁺ T cells and basic leucine zipper transcription factor ATF-like 3 (Batf3⁺) CD103⁺ / CD8⁺ dendritic cells. In addition, we observed that combination treatment resulted in increased PD-1 and PD-L1 expression and found that therapeutic activity could be further expanded when PD-1 blockade was added to the treatment regimen. These data support

triple combination therapy with MEK inhibition, oncolytic viruses and PD-1/PD-L1 checkpoint blockade for the treatment of melanoma. A better understanding of how T-VEC can kill melanoma tumor cells might also suggest new targets for combination therapy in melanoma and potentially other tumors permissive to oncolytic virus infection (3). Thus, next we sought to explore the molecular factors involved with T-VEC-mediated lysis melanoma cells and determine which intracellular factors are important for promoting viral replication and promoting anti-tumor immunity. We hypothesized that T-VEC would induce lysis through release of defined Damage-associated molecular patterns (DAMPs) and would promote T cell recruitment to established melanomas through type 1 interferon-related factors, as well as a pro-inflammatory gene signature profile. In addition, we found that specific components of the anti-viral machinery, such as STING, were critical for both T-VEC permissive replication and induction of host anti-tumor immunity. These data support the role of T-VEC in overcoming STING deficiency in melanoma cells and confirms how T-VEC mediates melanoma cell death and triggers innate and adaptive anti-tumor immunity. These data collectively enhance our understanding on how T-VEC can activate anti-tumor immune responses, further help to design rational clinical trials combining oncolytic Herpes simplex viruses and other approved agents in melanoma.

ACKNOWLEDGEMENT

Firstly, I would like to express my utmost gratitude to my advisor, Dr. Howard L. Kaufman, for the unwavering support, encouragement guidance throughout the graduate study, for being available at all necessary times and for his dedication and commitment towards my success not only as a graduate student but also as a scientist, his mentoring has inspired me to stay focused and enabled me to thoroughly enjoy the research experience during my graduate study

I would also like to my gratitude to Dr. Andrew Zloza for his dedication as a mentor, who is always available for feedback, motivation and constructive criticism, has enabled to make my graduate study a great experience.

I would like to sincerely thank my committee members Dr. Joseph R. Bertino, Dr. Derek Sant'Angelo, Dr. Andrew Zloza and Dr. Howard L. Kaufman for being on my committee throughout of the course of my graduate school work, I was extremely fortunate to know and receive guidance and direction from them.

I would also like to express my gratitude to Dr. Samuel D. Rabkin for giving me a chance to join brilliant and fantastic members of his lab and learn new scientific concepts, techniques and take classes at Harvard Medical School.

Additionally, I would like to thank members of Dr. Howard L. Kaufman, Dr. Andrew Zloza and Dr. Samuel D. Rabkin labs for their camaraderie and for enabling an enriching work environment. I would especially like to thank Dr. Shengguo Li, Dr. Frederick Kohlhapp and Dr. Dipongkar Saha for training and mentoring me.

I would also like to thank my amazing and brilliant friends Dr. Cole Peters and Dr. Dipongkar Saha for always being patient with my unreasonable questions and being there to celebrate my successes and conquer my failures.

My sincere thanks to core facilities at Rutgers Cancer Institute of New Jersey (CINJ), especially to Dr. Daniel Medina for always willing to discuss science and to be supportive. I also thank Wilson for providing resources and space and still ensuring smooth progress on administrative matters.

My special acknowledgment to Dr. Julia Kaltschmidt for not only training me on critical biological concepts and techniques but also training me well to be an excellent productive graduate student, her encouragement during the graduate school application process is invaluable. Many thanks to Dr. Juliet Zhang, Dr. Daniel Comer, Dr. Josephine Belluordo and Dr. Jarret Weinrich and other members of Kaltschmidt lab for always willing to teach and help me prepare for graduate school during my term at Memorial Sloan Kettering.

My special thanks to Dr. Derek Sant'Angelo and Dr. Lisa Denzin and their lab members for valuable suggestions, for providing resources and laboratory space

None of this would have been possible without financial support from funding sources.

Also, Shared Resources of the Rutgers Cancer Institute of New Jersey.

I would like to thank the graduate program, especially Dr. Janet Alder, Dr. Nancy Walworth and Dr. Rick Padgett, and for providing well-rounded support during the course of my graduate study. I also thank Diane Murano, Tina Marottoli, and Perry Dominguez for always being helpful with administrative processes.

Ultimately, I would like to thank my family, whose endless support and encouragement throughout life has made this a possibility for me, I especially thank my Parents, my wife Sireesha Alla and my daughter Mayra Bommareddy, who always missed all their vacations and stayed home as I was busy in the lab.

I acknowledge that this work includes materials, which are currently published or in the process of submission for publication. This dissertation contains and is constructed from obtaining documents directly from the following publications.

Bommareddy, P. K., Patel, A., Hossain, S. & Kaufman, H. L. Talimogene laherparepvec (T-VEC) and other oncolytic viruses for the treatment of melanoma. *Am. J. Clin. Dermatol.* 18, 1–15 (2017)

Bommareddy, P. K., Silk, A. W. & Kaufman, H. L. Intratumoral approaches for the treatment of melanoma. *Cancer J.* 23, 40–47 (2017).

Bommareddy, P. K., Peters, C., Saha, D., Rabkin, S. D. & Kaufman, H. L. Oncolytic herpes simplex viruses as a paradigm for the treatment of cancer. *Annu. Rev. Cancer Biol.* 2, 155–173 (2018).

Bommareddy, P. K., Shettigar, M. & Kaufman, H. L. Integrating oncolytic viruses in combination cancer immunotherapy. *Nat. Rev. Immunol.* 18, 498–513 (2018)

Bommareddy PK, Aspromonte S, Zloza A, Rabkin SD, Kaufman HL. 2018. MEK inhibition enhances oncolytic virus immunotherapy through increased tumor cell killing and T cell activation. *Sci Transl Med.* 10, (2018).

Bommareddy PK, Zloza A, Rabkin SD, Kaufman HL. Oncolytic virus induces immunogenic cell death and rescues STING deficiency in melanoma – *manuscript in review.*

TABLE OF CONTENTS

| | |
|---|----|
| ABSTRACT OF THE DISSERTATION | ii |
| ACKNOWLEDGEMENT | v |
| LIST OF TABLES | xi |
| LIST OF FIGURES | xi |
| CHAPTER ONE: Introduction | 1 |
| Melanoma | 1 |
| Oncolytic viruses | 3 |
| Talimogene laherparepvec | 5 |
| CHAPTER TWO: Materials and Methods | 8 |
| Cell lines | 8 |
| Viruses | 8 |
| Cytotoxicity and plaque assays | 9 |
| Drugs | 9 |
| Immunoblotting | 10 |
| Danger Associated Molecular Pattern (DAMP) Factor Analysis | 10 |
| shRNA and CRISPR Studies | 11 |
| Lumacyte Analysis | 11 |
| Murine treatment studies | 12 |
| Immune cell depletion studies | 14 |
| Immunohistochemistry | 15 |
| Flowcytometry analysis | 17 |

| | |
|--|-----------|
| Gene signature profile..... | 18 |
| CHAPTER THREE: RESULTS..... | 20 |
| SECTION:1 | |
| MEK inhibition enhances oncolytic virus immunotherapy through increased tumor cell killing and T cell activation | |
| MEK inhibition augments T-VEC-mediated cell lysis <i>in vitro</i> and increases viral replication..... | 20 |
| T-VEC and MEK Inhibition Inhibits Tumor Growth in Melanoma Xenograft Model..... | 24 |
| T-VEC and MEK Inhibition Enhances Therapeutic Effectiveness and Improves survival in the Immune-competent D4M3A Murine Melanoma model..... | 28 |
| T-VEC and MEKi Combination Therapy is CD8⁺ T cell-dependent..... | 31 |
| Combination treatment with T-VEC and MEKi augments melanoma antigen-specific T cell responses..... | 34 |
| Combination treatment with T-VEC and MEKi is Dependent on Batf3⁺ Dendritic cell..... | 38 |
| Combination T-VEC and MEK Inhibition Induces an Inflammatory Gene Signature and Increases PD-L1 Expression in the Tumor Microenvironment..... | 41 |
| Triple Treatment with T-VEC, MEK Inhibition and PD-1 Blockade Further Enhances Therapeutic Activity..... | 44 |
| Discussion..... | 49 |
| SECTION:2 | |
| Oncolytic virus immunotherapy induces immunogenic cell death and overcomes STING deficiency in melanoma..... | 56 |
| Human melanoma cell lines are permissive to T-VEC infection and oncolysis..... | 59 |

| | |
|---|-----------|
| T-VEC infection induces immunogenic cell death and DAMP release from melanoma cell line..... | 62 |
| Anti-viral machinery elements are deficient in some melanoma cell lines..... | 64 |
| STING contributes to T-VEC resistance..... | 66 |
| STING deficiency alters cytokine release induced by T-VEC infection..... | 68 |
| T-VEC treatment induces tumor regression in a STING-deficient murine Melanoma model..... | 70 |
| T-VEC induces anti-viral and systemic anti-tumor immunity in STING deficient melanoma..... | 74 |
| Discussion..... | 79 |
| CHAPTER FOUR: Conclusion..... | 84 |
| Summary and Conclusions..... | 84 |
| Future Directions..... | 86 |
| Concluding Remarks..... | 88 |
| REFERENCES..... | 90 |
| APPENDIX..... | 96 |
| APPENDIX A. ABBREVIATIONS USED..... | 96 |
| APPENDIX B. SUPPLEMENTARY TABLES..... | 96 |
| Table S1. Antibodies..... | 98 |
| Table S2. Chemicals..... | 99 |
| Table S3. Commercial Assays..... | 99 |
| Table S4. Experimental cell lines..... | 100 |
| Table S5. Experimental Models..... | 100 |

LIST OF TABLES

| | |
|--|----|
| Table S1. Antibodies..... | 93 |
| Table S2. Chemicals..... | 94 |
| Table S3. Commercial Assays..... | 94 |
| Table S4. Experimental cell lines..... | 95 |
| Table S1. Experimental Models..... | 95 |

LIST OF FIGURES

| | |
|---|----|
| Figure 1. BRAF inhibitors enhance T-VEC cell killing in BRAF mutant melanoma cell lines..... | 21 |
| Figure 2. MEK inhibition augments T-VEC mediated cell lysis <i>in vitro</i> and increases viral replication..... | 22 |
| Figure 3. Lumacyte laser flow cytology analysis..... | 24 |
| Figure 4. MEK inhibition enhances T-VEC-induced inhibition of human melanoma Xenograft growth <i>in vivo</i> and promotes tumor cell apoptosis..... | 26 |
| Figure 5. T-VEC and MEK inhibitor induced apoptosis..... | 27 |
| Figure 6. Characterization of murine D4M3A cells | 29 |
| Figure 7. MEK inhibition enhances T-VEC-induced tumor regression in an immune competent murine melanoma model..... | 30 |
| Figure 8. Validation of immune cell depletion. | 32 |

| | |
|---|----|
| Figure 9. Depletion of CD8 ⁺ T cells abrogates the effects of T-VEC and MEKi combination therapy..... | 33 |
| Figure 10. Time course analysis of tumor infiltrating CD8 ⁺ T cells during mT-VEC treatment..... | 35 |
| Figure 11. Combination T-VEC and MEK inhibition induces viral-specific CD8 ⁺ T cells and increases melanoma antigen-specific CD8 ⁺ T cell responses..... | 36 |
| Figure 12. Analysis of CD8 ⁺ T cells from spleen during mT-VEC + MEKi treatment... | 37 |
| Figure 13. Characterization of D4M3A tumor cells in Batf3 knockout mice..... | 39 |
| Figure 14. Batf3 ⁺ dendritic cells play a role in anti-tumor activity and antigen spreading associated with combination T-VEC and MEK inhibition treatment..... | 40 |
| Figure 15. T-VEC and MEK inhibition reprograms immune silent tumors in to immune inflamed tumors and induce expression of PD-1 and PD-L1..... | 42 |
| Figure 16. NanoString gene expression heat maps for all genes profiled and by gene function..... | 43 |
| Figure 17. Triple combination treatment with T-VEC, MEK inhibition and PD-1 blockade improves therapeutic treatment of melanoma and colon cancer models..... | 46 |
| Figure 18. Mean fluorescence intensity (MFI) expression of PD-1 expression and frequency of PD-1 ⁺ cells..... | 47 |
| Figure 19. Individual tumor growth curves of BALB/c mice bearing CT26 tumors..... | 48 |
| Figure 20. Human melanoma cell lines exhibit differential sensitivity to T-VEC mediated lysis <i>in vitro</i> | 60 |
| Figure 21. Human melanoma cell lines exhibit differential expression of HSV-1 cell entry receptors. | 61 |

| | |
|---|----|
| Figure 22. T-VEC induces immunogenic cell death and release DAMPs..... | 63 |
| Figure 23. Melanoma cell lines display variable levels of anti-viral machinery..... | 65 |
| Figure 24. STING contributes to resistance to T-VEC mediated lysis in melanoma cells..... | 67 |
| Figure 25. STING deficiency alters cytokine profiles following T-VEC treatment..... | 69 |
| Figure 26. D4M3A cells exhibit low levels of STING protein expression and are susceptible to T-VEC infection..... | 71 |
| Figure 27. D4M3A cells do not respond to PD-1 blockade but are sensitive to T-VEC treatment..... | 72 |
| Figure 28. T-VEC has therapeutic activity in STING deficient melanoma <i>in vivo</i> | 73 |
| Figure 29. T-VEC treatment induces host immunity in STING-deficient melanoma model..... | 75 |
| Figure 30. Global gene expression of injected and contralateral tumors during T-VEC treatment..... | 77 |
| Figure 31. T-VEC treatment induces a systemic pro-inflammatory gene signature in STING-deficient tumors <i>in vivo</i> | 78 |

CHAPTER ONE: INTRODUCTION

Melanoma

Melanoma is a metastatic tumor arising from melanocytes located in the stratum basale of the epidermis, mucosal membranes and middle layer of the uvea. Cutaneous melanoma is the most common variant and arises in skin and typically undergoes an initial radial growth phase during which complete surgical excision is often curative (4). If not treated, melanoma enters a vertical growth phase during which tumor cells may enter subdermal lymphatics and can metastasize to regional lymph nodes, and eventually to almost any visceral organ, including the central nervous system (5). Metastatic melanoma has historically been associated with dismal prognoses but systemic therapy has been transformed over the past decade, largely by advances in molecular therapy targeting the RAS-RAF-MEK-ERK mitogen activated protein kinase (MAPK) pathway in patients with tumors that harbor BRAF V600E/K mutations, and by immunotherapy, most notably with immune checkpoint blockade targeting cytotoxic T lymphocyte antigen 4 (CTLA4; via ipilimumab) and programmed cell death 1 (PD-1; via nivolumab or pembrolizumab) (6). Combination approaches within drug classes have shown improved therapeutic benefit but treatment is associated with drug resistance and increased toxicity. For example, combination immune checkpoint blockade with ipilimumab and nivolumab results in improved progression-free and overall survival compared to ipilimumab alone but was also associated with a 59% incidence of grade 3 or greater adverse events compared to 21% with nivolumab alone and 28% with ipilimumab alone (7, 8) New combination strategies with agents that enhance therapeutic responses while limiting toxicity have become a high

priority for drug development in melanoma. Approximately 40-50% of cutaneous melanomas harbor mutations in BRAF, which serve as oncogenic drivers of the MAPK pathway promoting tumor progression. Small molecule inhibitors of BRAF and MEK in treatment-naïve melanoma patients whose tumors harbor V600E or V600E BRAF mutations have shown significant improvements in relapse-free and overall survival (9). Following approval of two single-agent BRAF inhibitors, vemurafenib in 2011 and dabrafenib in 2013, further follow-up suggested that drug resistance frequently emerged with most patients relapsing within 7 months of initial treatment response (10). In some cases, resistance was associated with transcriptional alterations or secondary downstream driver mutations, such as in the mitogen/extracellular signaling regulated kinase (MEK) (11). Both of the two MEK isoforms (MEK1 and MEK2) phosphorylate ERK1 and/or ERK2 downstream of Ras and BRAF and MEK is known to be a critical mediator of constitutively active MAPK signaling in many types of cancer (12). In melanoma, inhibition of MEK has demonstrated improved clinical outcomes compared to chemotherapy in patients with BRAF-mutated melanoma and resulted in FDA approval of trametinib in 2013 (13). Subsequent studies of combined BRAF and MEK inhibitors demonstrated improved therapeutic effectiveness with acceptable toxicity profiles and several regimens (e.g. dabrafenib and trametinib, vemurafenib and cobimetinib) of combined treatment were approved for treatment-naïve, metastatic melanoma patients with BRAF-mutated melanoma (9, 14, 15). Pre-clinical studies have further suggested improved therapeutic activity of combination MAPK inhibition and immune checkpoint blockade (16). Although these findings await further clinical validation, the potential for combining MAPK inhibition with immunotherapy is particularly appealing since MAPK inhibitors act

directly on mutated tumor cells resulting in release of soluble tumor-associated antigens while immunotherapy acts on immune cells to promote innate and adaptive immune responses and/or prevent suppression of host anti-tumor immunity (17). This section is directly obtained from *Bommareddy et al Sci. Translational Medicine 2018 (3)*.

Oncolytic viruses

Oncolytic viruses (OVs) are a highly versatile platform for the treatment of cancer by mediating anti-tumor activity through multiple mechanisms of action (2, 18). Viruses have evolved sophisticated mechanism for evading and interacting with host immune systems and these features can be used to develop therapeutic agents wherein native anti-viral immunity can be usurped to induce host anti-tumor immunity. In addition, local injection of OVs into a single tumor site can induce an abscopal effect, in which distant, un-infected tumors, may also undergo immune-mediated rejection (19). This occurs through the multiple actions of therapeutic viruses that begins with direct immunogenic tumor cell killing, in which soluble tumor-associated antigens are released along with pathogen-associated molecular pattern (PAMP) factors derived from the virus and intracellular danger-associated molecular pattern (DAMP) factors derived from the tumor cells (20, 21). The local danger signals will promote rapid recruitment of innate lymphoid cells and immature dendritic cells (DCs) allowing for early transition of immune deserted or excluded microenvironments. In addition, local production of type 1 interferons and chemokines will attract additional lymphoid cells into the tumor microenvironment and help maintain effector functions of TIL. The presence of antigen-presenting cells along with soluble antigens derived from lysed tumor cells and interferon-mediated increases in

major histocompatibility complex (MHC) class I and II expression also result in improved antigen cross presentation and adaptive immunity shaped by individual tumor neoantigens (22, 23). Further, the interferon response can induce expression of immune checkpoints, such as PD-L1, CTLA-4, T-cell immunoglobulin and mucin-domain containing gene 3 (Tim-3) and lymphocyte activation gene 3 (LAG-3), promoting sensitivity to immune checkpoint blockade (24, 25). In addition, OV's are thought to regulate endothelial cell function and interaction with lymphoid cells by increasing lymphocyte adhesion molecules promoting influx of lymphoid cells and may block nutrient and oxygen delivery by tumor neovasculature (26, 27). Furthermore, OV's can be used to deliver therapeutic genes into the tumor cell or encode immune modulatory factors that can help promote and shape the local anti-viral and anti-tumor immune response (28, 29). Thus, OV's are highly flexible agents that integrate elements of virology, immunology, vascular biology and gene therapy to provide a critical "on" switch promoting lymphoid infiltration into immune deserted and excluded tumor microenvironments and can reverse immune suppression within immune-infiltrated tumor landscapes. The first therapeutic OV based on an attenuated herpes simplex virus, type 1 (HSV-1) encoding granulocyte-macrophage colony-stimulating factor (GM-CSF) demonstrated improved durable responses with a tolerable safety profile in a randomized clinical trial in patients with advanced melanoma leading to FDA approval in 2015 (30). More recently, early phase clinical trials have supported the combination of OV's with immune checkpoint inhibitors showing enhanced therapeutic activity with acceptable toxicity (31-33). This section is directly obtained from *Bommarreddy et al Nature reviews immunology 2018(1)*.

Talimogene laherparepvec

The proof-of-concept for OV_s in melanoma has recently been confirmed using Talimogene laherparepvec (ImlygicTM; T-VEC), a modified form of herpes simplex virus-1 (HSV-1). T-VEC was generated from the JS1 strain of HSV-1 in which the infected cell protein (ICP) 34.5 neurovirulence genes are deleted to limit neurotoxicity and enhance cancer cell specific replication. T-VEC also contains a deletion of the herpes ICP47 gene, which otherwise functions to block peptide transport through the transporter associated with antigen processing (TAP) machinery, which the virus uses to avoid immune detection (20). In the absence of ICP47, tumor-derived and viral peptides should be presented and result in immune recognition. To further enhance anti-tumor immunity, two copies of the human GM-CSF gene have been encoded in T-VEC to promote dendritic cell infiltration and maturation at the tumor site and enhance subsequent tumor-associated antigen presentation to T cells. T-VEC is delivered as a direct injection into melanoma lesions that can be clinically visualized or palpated, or imaged using bedside ultrasound guidance. The initial dose is 1×10^6 plaque-forming units (PFU) per milliliter (mL) up to a total of 4 mLs per visit with the actual volume to each tumor based on the largest diameter measured. This low dose administration allows all seronegative patients to convert and three weeks later patients are treated with a higher dose of 1×10^8 PFU/mL up to 4 mLs and then repeated every two weeks until maximal response, unequivocal disease progression or unacceptable toxicity. In a phase I clinical trial that included patients with a variety of accessible tumors, T-VEC was associated with an acceptable safety profile that included low grade constitutional symptoms and local injection site reactions (34). In this trial, the virus was found exclusively within tumor cells, GM-CSF expression was confirmed, and post-

treatment tumor necrosis was identified in biopsy specimens. Furthermore, all seronegative patients converted after initial exposure to T-VEC and no correlation between anti-viral titers and clinical response or toxicity profile was observed. Based on these data, a multi-institutional phase II clinical trial was developed in which an open-label design was used to test T-VEC in patients with unresectable stage IIIc-IV melanoma (35). The primary endpoint was response rate as defined by standard RECIST criteria. In the intent-to-treat population, 74% of the subjects had received prior systemic therapy. Adverse events were again limited to transient constitutional symptoms, such as fever, chills and fatigue and local injection site reactions. The objective response rate was 26%, which included 8/50 (16%) complete responses in which all injected and non-injected tumor underwent complete regression. Ten additional patients (20%) had stable disease and responses appeared to be durable with 92% of patients maintaining responses for 7-31 months after treatment. Treatment was associated with an increase in tumor-infiltrating MART-1-specific CD8+ T cells in injected lesions and a decrease in CD4+FoxP3+ regulatory T cells and myeloid-derived suppressor cells (36). These data supported a randomized phase III clinical trial of T-VEC in melanoma (termed the OPTiM [Oncovex^{GM-CSF} Pivotal Trial in Melanoma] trial), which enrolled patients from 2009-2011. In the OPTiM trial, 436 patients with stage IIIB-IV accessible melanoma metastases were treated in a 2:1 fashion with T-VEC or recombinant GM-CSF (37). The primary endpoint of this trial was durable response rate (DRR), defined as an objective response based on modified World Health Organization (WHO) criteria, beginning within one year of treatment and lasting 6 months or longer. In the trial, T-VEC met the primary study endpoint with a DRR of 16.3% compared to 2.1% ($p < 0.001$) for patients treated with GM-CSF. In addition, T-VEC was

associated with an improvement in objective response rate (26.4% vs. 5.7%; $p < 0.001$), median overall survival (23.3 vs. 18.9 months; $p = 0.051$). Subset analyses supported a particular strong effect for patients with stage IIIB/C disease (response rates 33% vs. 0 for GM-CSF-treated subjects) and stage IV M1a (16% vs. 2%). A similar trend favoring T-VEC in the treatment naïve setting (24% vs. 0%) was also seen when compared to patients who received T-VEC after first-line therapy (10% vs. 4%). Treatment was associated with low-grade constitutional symptoms and injection site reactions with the only grade 3 or greater event occurring in more than 2% of subjects being a self-limited cellulitis. In a careful assessment of individual lesion responses, T-VEC administration was associated with $\geq 50\%$ regression in 64% of injected lesions, 34% of un-injected non-visceral lesions and 15% of un-injected visceral lesions (37). These data resulted in approval of T-VEC for the treatment of advanced melanoma in the United States and Australia and the treatment of stage IIIB/C and IV M1a melanoma in Europe. This section is directly obtained from *Bommareddy et al Cancer J. 2017 (38)*.

CHAPTER TWO: Materials and Methods

Cell Lines

Human melanoma cells SK-MEL-28, SK-MEL-2, and SK-MEL-5 (ATCC) and mouse cell line CT26 (ATCC) were cultured in monolayers using RPMI supplemented with 10% heat inactivated bovine serum (Thermo Fisher Scientific), 10mM L-glutamine (Corning), and 0.5% penicillin G-streptomycin sulfate (Corning). Cells were detached using 0.25% trypsin EDTA (Corning) for passaging. The murine melanoma cell line D4M3A was generated from *Tyr::CreER;Braf^{CA};Pten^{lox/lox}* mice (39) and kindly provided by Dr. David Mullins (Dartmouth University, Hanover, NH). D4M3A cells were cultured as previously described (39). All cells were low-passage and confirmed to be mycoplasma-free (LookOut mycoplasma kit; Sigma).

Viruses

T-VEC is a modified JS1 strain of HSV-1 encoding human GM-CSF and has been previously reported (18). T-VEC is commercially available and was purchased from the Rutgers Cancer Institute Pharmacy. For immune competent murine studies, a modified virus (mT-VEC) in which the human GM-CSF gene was replaced by murine GM-CSF, was used and generously provided by Dr. Pedro Beltran (Amgen Inc). All human cell lines and xenograft experiments were performed using T-VEC and all murine cell line and syngeneic experiments were performed using mT-VEC.

Cytotoxicity and Viral Plaque Assays

Human and murine melanoma cells (7.5×10^3) were seeded on 96-well plates, treated with vehicle or MEKi (trametinib) (10 nM for SK-MEL-28, 5 nM for SK-MEL:5, 1.25 nM for SK-MEL-2, and 5 nM for D4M3A). Six to eight hours later, cells were treated with T-VEC at the indicated MOI. After 5 days (SK-MEL-28, SKMEL:5, SK-MEL-2) or 3 days (D4M3A) of incubation, MTS assay was performed following manufacturer's instruction (Promega). For plaque assays, cells were plated and treated with T-VEC alone or T-VEC and trametinib as above. Cells were treated with trametinib 6-8 h before T-VEC infection. For T-VEC infection, the virus was diluted using RPMI and seeded over a cell monolayer at the indicated MOI for 2 hours (plates were gently rocked every 15 min to ensure even spread of virus). Whole cell lysates were collected at indicated times and viral titers obtained by plaque assay on a monolayer of Vero cells. Each experimental condition was performed in triplicate and all experiments were conducted three times.

Drugs

The MEK inhibitor trametinib (GSK1120212) and BRAF inhibitor vemurafenib were purchased from MedChem Express (Monmouth Junction, NJ). Both drugs were dissolved in DMSO to make a 10 mM stock solution for *in vitro* studies. The highest DMSO concentration (0.001% DMSO) used for *in vitro* studies was non-toxic to the cells. For *in vivo* studies, trametinib powder (0.5 mg/kg) was dissolved in 0.5% hydroxypropyl methylcellulose and 0.2% Tween-80 (Sigma Aldrich) to make a homogenous suspension and was administered by oral gavage.

Immunoblotting

Total cell lysates were obtained from human and murine melanoma cells and 40 µg of lysate was loaded onto an SDS-PAGE gel, electrophoresed, and transferred to a PVDF membrane. Antibodies against HSV-1 glycoprotein D (gD) (1:50) (Genetex), cleaved PARP (1:50), total ERK1/2 (1:100), phospho ERK1/2 (1:100), Protein Kinase R (PKR) (1:500), Stimulator of Interferon genes (STING) (1:1000), Cyclic GMP-AMP synthase cGAS (1: 500), Vinculin (1:1000) and GAPDH (1:1000) (Cell Signaling Technologies) were used.

Danger Associated Molecular Pattern (DAMP) Factor Analysis

SK-MEL-28 cells (5×10^5) were mock infected or treated with 1 MOI T-VEC and cell supernatants collected at 24 and 48 hrs. Cell culture supernatants were collected and passed through 40 µm filters, further centrifuged at 5000 rpm for 10 min at 4°C. High mobility group box 1 (HMGB1) in cell supernatants were detected using an Enzyme linked immunosorbent assay (ELISA) kit according to the manufacturers (Chondrex) instructions. Adenosine triphosphate (ATP) levels in cell supernatants at indicated times were detected using a standard ATP determination kit according to the manufacturers (ThermoFisher) instructions. For surface calreticulin expression SK-MEL-28 cells (1×10^5) were plated in a 6 well chamber slide and treated the next day with phosphate buffer saline (mock) or 1 MOI of T-VEC and stained with anti-calreticulin (CALR) antibody (1:100) and incubated at 4°C overnight, then washed twice with PBS. FITC-anti-Rb antibody was used as a secondary antibody (1:200), incubated for 2 hours at room temperature. Finally, cells are

cover slipped using nuclear reactive dye and images were taken using Olympus fluorescent microscope.

shRNA and CRISPR Studies

For shRNA studies, LOX-IMVI cells (3×10^5) were plated in a 6 well plate and 12 – 16 hrs. later cells were infected with 10 MOI of either PKR or STING shRNA from Santa Cruz biotechnology. After 36 – 48 hrs., cells were washed with PBS and replaced with normal media containing 0.5 $\mu\text{g/ml}$ of puromycin and selected for 5 days. Western blot analysis was performed on cells that passed puromycin selection to confirm the knock down of targeted gene(s). CRISPR studies were performed using Santa Cruz CRISPR-HDR system according to the manufacturers guidelines. In short, LOX-IMVI cells (3×10^5) were plated in a 6 well plate and 12 – 16 hr. later cells are transfected with the CRISPR plasmid and HDR plasmid using Lipofectamine 300. After 8-12 hrs., cells were replaced with normal media and grown to 50 - 60% confluence. Cell selection was performed in 0.5 $\mu\text{g/ml}$ of puromycin for 5 days and single cell clones were isolated using fluorescence-activated cell sorting (FACS).

Lumacyte Analysis

SK-MEL-28 cells were seeded into 24-well plates at a density of 500,000 cells/mL and infected with T-VEC or treated with trametinib or both as described above. At the specified time points, cells were detached from the wells using TrypLE (Thermo Fisher Scientific), resuspended in culture medium and then analyzed using a Radiance instrument (LumaCyte). The threshold velocity (which in this case defines the infection metric), was

calculated based on the velocity at which approximately 5% of the control cells have a velocity above the infection metric. This is similar to gating for fluorescence in flow cytometry. A principal component analysis (PCA) was performed using XLStat. Input data included the infection metric, average velocity, and average size of each sample. This combination resulted in components (F1 and F2) that represented the largest possible variance in the data.

Murine treatment studies

All animal experiments were approved by Rutgers Institutional Animal Care and Usage Committee. For survival experiments mice were monitored for tumor-growth and euthanized before tumors reached 400 mm². Kaplan-Meier curves were used to calculate survival. Mice were weighed twice a week and no weight loss was observed during the treatment. For xenograft melanoma models, SK-MEL-28 cells (8×10^6) were injected into the right flank of NSG mice in 100 μ l PBS. Mice were treated with either mT-VEC (1×10^5 pfu) or sterile water via intratumoral injection on days 35, 40, and 45. Trametinib (MEKi; 0.5 mg/kg) or vehicle control was given on days 35-43 via oral gavage. Mice in the combination treatment group received both mT-VEC and MEKi at the above doses and schedule. The vehicle control consisted of a mixture of 0.2% Tween 80 and 0.5% hydroxypropyl methylcellulose (HPMC). For syngeneic melanoma tumor studies, C57BL/6J mice (n = 9/group) were implanted s.c. with 3×10^5 D4M3A murine melanoma cells in the right flank on day 0 and treated with mT-VEC (1×10^6 pfu) or sterile water via i.t. injection on days 15, 19, 22, 26, 29 and 33, and MEKi (0.5 mg/kg) or vehicle (0.2% Tween 80 and 0.5% HPMC) was gavaged from days 15-27. For tumor re-challenge studies

in mT-VEC and MEKi studies, cured mice (n = 7 from 2 independent experiments) from the combination (mT-VEC + MEKi) group were re-challenged on day 96 with a two-fold increased number of D4M3A cells (6×10^5) in the contralateral (left) flank. Age matched (21 to 22-week-old) naïve mice were implanted as controls (n = 7). For flow cytometry analysis of tumors from T-VEC and MEKi combination therapy, C57BL/6J mice implanted s.c. with 3×10^5 D4M3A cells on day 0, treated with T-VEC (1×10^6 pfu) or sterile water on days 15, 19 and 22 and MEKi (trametinib; 0.5 mg/kg) or vehicle gavaged orally once daily from days 15-19 (n = 5/group), and euthanized on day 24. Tumors were harvested and FACS was performed as described in the flow cytometry analysis section of methods. Mice that had completely regressed primary tumors and survived long-term were re-challenged with an increased number of D4M3A cells (6×10^5) in the contralateral flank (left) at day 96. For Batf3^{-/-} mouse studies Batf3^{-/-} or C57BL/6J mice were implanted with (3×10^5) D4M3A cells on day 0 and treated with mT-VEC or sterile water via i.t. injection and/or trametinib or vehicle control via oral gavage. For triple combination studies using mT-VEC + MEKi + α PD-1 antibody, C57BL/6J mice (n = 7/group) were implanted subcutaneously in the right flank with 3×10^5 D4M3A murine melanoma cells on day 0 and treated with mT-VEC (1×10^6 pfu) or sterile water via intratumoral injection on days 15, 19, 22, 26, 29 and 33, MEKi (0.5 mg/kg) or vehicle control on days 15-27 via oral gavage and α PD-1 antibody (clone: RMP1-14, 10 mg/kg) via intra-peritoneal (i.p.) injection on days 15, 19, 22, and 26. In addition, groups received doublet combination treatment with mT-VEC and MEKi (and rat IgG isotype control) or triplet therapy with mT-VEC, MEKi and α PD-1 antibody. For re-challenge experiments during triple combination, cured mice (n = 10 from 2 independent experiments) from mT-VEC + MEKi

+ α PD-1 therapy was re-challenged on day 130 with a two-fold increased number of D4M3A cells (6×10^5) in the contralateral (left) flank. Age matched (26 to 28-week-old) naïve mice were implanted as controls ($n = 5$). For flow cytometry studies during triple combination, B6 mice ($n=6$ per group) were implanted subcutaneously in the right flank with D4M3A cells (3×10^5) on day 0 and treated with mT-VEC (1×10^6 pfu) or sterile water via intratumoral injection on days 15, 19 and 22, MEKi (0.5 mg/kg) or vehicle control on days 15-19 via oral gavage and α PD-1 antibody (clone: RMP1-14, 10 mg/kg) via i.p. injection on days 15, 19 and 22. In addition, groups received double combination treatment with mT-VEC and MEKi (and rat IgG isotype control) or triple. Tumors were collected on day 24 and flow cytometry analysis of tumor infiltrating lymphocytes was performed as described in supplemental methods. For triple combination studies in CT26 tumor model, BALB/c mice ($n=10$ per group) were implanted s.c. in the right flank with CT-26 cells (2×10^5) on day 0 and treated with mT-VEC (5×10^5 pfu) or sterile water via i.t. injection on days 8, 12, 15, 19 and 22, MEKi (0.5 mg/kg) or vehicle control on days 8-20 via oral gavage and α PD-1 antibody (clone: RMP1-14, 7.5 mg/kg) via i.p. injection on days 8, 12, 15 and 19. In addition, groups received double treatment with mT-VEC + α PD-1, MEKi + α PD-1, mT-VEC + MEKi and rat IgG isotype control or triple therapy with m-TVEC, MEKi and α PD-1 antibody.

Immune Cell Depletion Studies

For depletion studies, C57BL/6J mice ($n = 5$ /group) were implanted s.c. with 3×10^5 D4M3A murine melanoma cells in the right flank on day 0 and treated with T-VEC (1×10^6 pfu) or sterile water via i.t. injection on days 15, 19, 22, 26, 29 and 33 and MEKi

(trametinib; 0.5 mg/kg) or vehicle (0.2% Tween 80 and 0.5% HPMC) gavaged from days 15-27. For depletion of immune cell populations, mice administered via intraperitoneal (i.p.) injection anti-mouse CD8 α (clone 2.43; 10 mg/kg), anti-mouse CD4 (clone GK1.5; 10 mg/kg), or clodronate liposomes (first injection 50 mg/kg, followed by 25 mg/kg) on days 12, 15, 18, 21, 25, 28, and 32. Mock group received sterile water (i.t.) + vehicle (0.2% Tween 80 and 0.5% HPMC) + control rat IgG (i.p.) + empty liposomes (i.p.). Isotype group received T-VEC (i.t.) + MEKi (i.p.) + control rat IgG (i.p.) + empty liposomes (i.p.) as above. Anti-CD4 or anti-CD8 group received T-VEC + MEKi + anti-CD4 or anti-CD8 + empty liposomes, whereas Clodronate group received T-VEC + MEKi + control rat IgG + clodronate liposomes. For flow cytometry analysis in depletion studies C57BL/6J mice implanted s.c. with 3×10^3 D4M3A murine melanoma cells in the right flank on day 0, treated with mT-VEC (1×10^6 pfu) or sterile water administered via i.t. injection on days 15, 19, and 22 and MEKi (trametinib; 0.5 mg/kg) or vehicle was gavaged from days 15-19. For depletion of immune cell populations, mice were injected i.p. with anti-mouse CD8 α (clone 2.43; 10 mg/kg), anti-mouse CD4 (clone GK1.5; 10 mg/kg), or clodronate liposomes (first injection 50 mg/kg, followed by 25 mg/kg) on days 12, 15, 18, and 21. Tumors were harvested on day 24 and flow cytometry was performed as described in flow cytometry section of methods.

Immunohistochemistry

Tumors were harvested at indicated time points and sections were deparaffinized using Xylene twice for 10 min each, followed by gradual rehydration using 100%, 90% and 70%

ethanol treatment (5 min each). Sections were left in distilled water for 10 min, followed by dipping sections in a hematoxylin container for 1 min, washing in tap water for 5 min, dipping in Eosin Y (1% alcoholic) for 30 s. This was followed by gradual dehydration using 95% ethanol (twice 5 min each) and 100% ethanol (twice 5 min each), treating with Xylene twice for 10 min each, and mounting in Xylene-based media (Cytoseal XYL; Thermo Scientific). To examine proliferation (Ki67 and pERK1/2), apoptosis (cleaved caspase 3), and T-VEC prevalence (HSV-1 gB) in the SK-MEL-28 xenograft model, NSG mice (n=5) were implanted with human melanoma SK-MEL-28 cells (8×10^6) on day 0 and treated with either T-VEC (5×10^5 pfu) or sterile water via i.t. injection on days 30 and 34 or trametinib (0.5 mg/kg) or vehicle control on days 30-34 via oral gavage. Mice in the combination group received both T-VEC and trametinib. Animals were euthanized on day 36 and tumors were removed and fixed in 10% formalin for 24-36 h, embedded in paraffin, and 5 μ m-sections subjected to immunohistochemistry with indicated antibodies (Key Resources Table, IHC), followed by incubation with appropriate secondary antibodies (Vector Laboratories). To examine the presence of CD8⁺ T cells in syngeneic C57BL/6J mice treated with combination (mT-VEC + trametinib) therapy, C57BL/6J mice were implanted with 3×10^5 D4M3A cells and treated with mT-VEC (10^6 pfu i.t.) for 3 doses on days 15, 19 and 22 and/or trametinib (0.5 mg/kg) orally once daily on days 15-19. Mice were euthanized on day 24 and tumors were removed and fixed in 10% formalin for 24-36 h, embedded in paraffin, and 5 μ m-sections subjected to immunohistochemistry with indicated antibodies (Key Resources Table, IHC), followed by incubation with appropriate secondary antibodies (Vector Laboratories) as described above. For positive cell counting, annotated whole tumor regions were subjected to unsupervised quantification using Visio

Pharm quantitative digital pathology software. Positive cell density was computed as positive cell count / mm² tissue area for cleaved caspase 3, Ki67, pERK1/2 and CD8. HSV-1 staining was quantified as an average brown staining intensity of HSV-1 glycoprotein (gB) over the tumor area.

Flow Cytometry Analysis

Annexin-V expression was detected on SK-MEL-28 cells after culture for 24 h with or without T-VEC at the indicated MOI and/or trametinib at 5 nM. Cells were centrifuged, counted, re-suspended in FACS buffer (2% inactivated fetal calf serum in PBS), incubated with 7-AAD (BD Biosciences) and FITC-conjugated antibody for 30 min, washed, fixed in 4% paraformaldehyde, washed, re-suspended in FACS buffer, and analyzed using an LSRII flow cytometer (BD Biosciences) and FlowJo software (v.10.4; Tree Star).

For multi-color flow cytometry analyses, flank tumors from treated groups were harvested, mechanically dissociated using a gentleMacs Octo Dissociator (Miltenyi), incubated with collagenase (1 mg/ml, Sigma Aldrich) and DNase I (10 U/ml; Promega) for 30 minutes with rocking at 37°C, mechanically dissociated again, passed through a 40 µm screen, re-suspended in FACS buffer, and stained with fluorochrome-conjugated anti-mouse antibodies, as well as appropriate isotype control antibodies. Fixable live/dead viability Kit (Invitrogen) was used to stain dead cells. We followed a 'no-wash' sequential staining protocol (BioLegend) to stain dead cells and for surface staining. Intracellular FoxP3 staining was performed following the FoxP3 intracellular staining protocol (BioLegend). For antigen-specific CD8⁺ T cell determination, tumor samples were stained for 45 min at

4°C with fluorochrome-conjugated MHC-I dextramers (Immudex) for HSV-1 gB, murine gp100 or murine TRP2 prior to extra-cellular staining and all other steps were followed according to manufacturer's guidelines. For single-color compensation controls, spleens from naïve C57BL/6J mice were treated with ACK Lysis Buffer (Sigma Aldrich) to lyse red blood cells, and single cells were stained with each of ten fluorescent-conjugated antibodies according to manufacturer's instructions. All samples were analyzed using a BD LSRII flow cytometer. Data were analyzed with FlowJo software (v.10.4; Tree Star). Technicians acquiring and analyzing the data were blinded to the treatments.

Gene Signature Profiles

C57BL/6J mice implanted with D4M3A cells (3×10^5) were treated with mT-VEC (10^6 pfu) via i.t. injection for 3 doses on days 15, 19 and 22 and/or trametinib (0.5 mg/kg) orally once daily on days 15-19. Tumors were harvested on day 24 and total RNA was isolated using a Qiagen RNeasy kit. Gene expression analysis was performed using the NanoString PanCancer Immune panel. Per sample, 50 ng of total RNA in a final volume of 5 μ l was mixed with a 3' biotinylated capture probe and a 5' reporter probe tagged with a fluorescent barcode from the custom gene expression code set. Probes and target transcripts were hybridized at 65°C for 12-16 h. Hybridized samples were run on the NanoString nCounter preparation station using the recommended manufacturer protocol, in which excess capture and reporter probes were removed and transcript-specific ternary complexes were immobilized on a streptavidin-coated cartridge. The samples were scanned at maximum scan resolution on the nCounter Digital Analyzer. Data were processed using

nSolver Analysis Software and the nCounter Advanced Analysis module. For gene expression analysis data were normalized using the geometric mean of housekeeping genes selected by the GeNorm algorithm.

CHAPTER THREE: RESULTS Section:1

MEK inhibition enhances oncolytic virus immunotherapy through increased tumor cell killing and T cell activation

MEK inhibition augments T-VEC-mediated cell lysis *in vitro* and increases viral replication

We sought to investigate whether combining T-VEC and MAPK inhibition can augment tumor cell killing in melanoma. T-VEC was able to replicate in and kill melanoma cell lines harboring BRAF V600E mutations and wild-type N-Ras (SK-MEL-28 and SK-MEL-5; Fig. 1A-B) and those cells with wild-type BRAF, but an NRAS Q61R mutation (SK-MEL-2; Fig. 1C). Infected cells exhibited dose-dependent cytotoxicity following viral infection at doses starting at 0.003 multiplicity of infection (MOI) (Fig. 1A-C). In addition, the BRAF-mutated murine D4M3A cell line (39) was susceptible to T-VEC at high doses (MOI ≥ 1 ; Fig. 1D). Cytotoxicity was increased in all cell lines when they were pre-treated with trametinib, a selective MEK inhibitor (MEKi; Fig. 2A-D, left panel). Independent assays with vemurafenib, a selective BRAF inhibitor, enhanced T-VEC-mediated cytotoxicity in BRAF V600E mutated SK-MEL-28 and SK-MEL 5 cell lines, but not in BRAF wild-type SK-MEL-2 line (Fig. 1E-G). Increased viral replication was confirmed by plaque assay (Fig. 2A-D right panels) and Western blot showing increased amounts of HSV-1 glycoprotein D during combination treatment in the SKMEL-28 cell line (Fig. 2E). In order to confirm viral replication within infected cells we utilized single-cell laser radiance-based quantitative technology (40) that allows detection of viral infection at a single cell level (Fig. 3A).

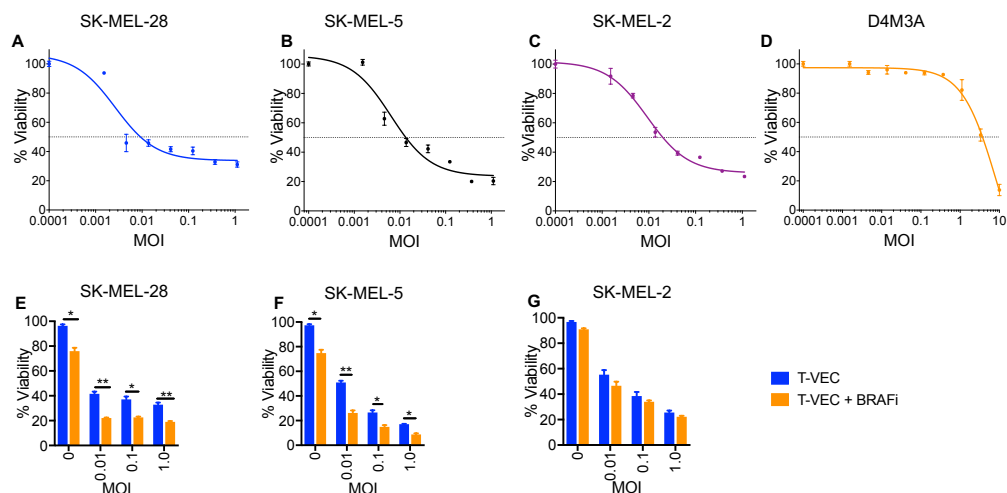


Figure 1. BRAF inhibitors enhance T-VEC cell killing in BRAF mutant melanoma cell lines

Cytotoxic effects of T-VEC in human (A) SK-MEL-28, (B) SK-MEL-5, (C) SK-MEL-2 and mouse (D) D4M3A melanoma cell lines. Cells (7.5×10^3) were seeded on 96-well plates and treated with T-VEC at the indicated MOI or control (sterile water). After 5 days (SK-MEL-28, SK-MEL-5, SK-MEL-2) or 3 days (D4M3A) of incubation, an MTS (3-(4,5-dimethylthiazol-2-yl)-5-(3-carboxymethoxyphenyl)-2-(4-sulfophenyl)-2H-tetrazolium) assay was performed to measure cell viability. (E-G) Cytotoxic effects of T-VEC and vemurafenib (BRAF inhibitor, BRAFi) in human (E) SK-MEL-28, (F) SK-MEL-5 and (G) SK-MEL-2. Cells (7.5×10^3) were seeded on 96-well plates and treated with vehicle or BRAFi (0.5 μ M) six to eight hours later, cells were treated with T-VEC at the indicated MOI. After 5 days of incubation, an MTS assay was performed to measure cell viability. This experiment was conducted at least twice with similar results. Data are presented as mean \pm SEM and statistical differences between groups were measured by two-tailed student *t* test. * $p < 0.05$, ** $p < 0.01$, *** $p < 0.001$, **** $p < 0.0001$. Only significant values are indicated.

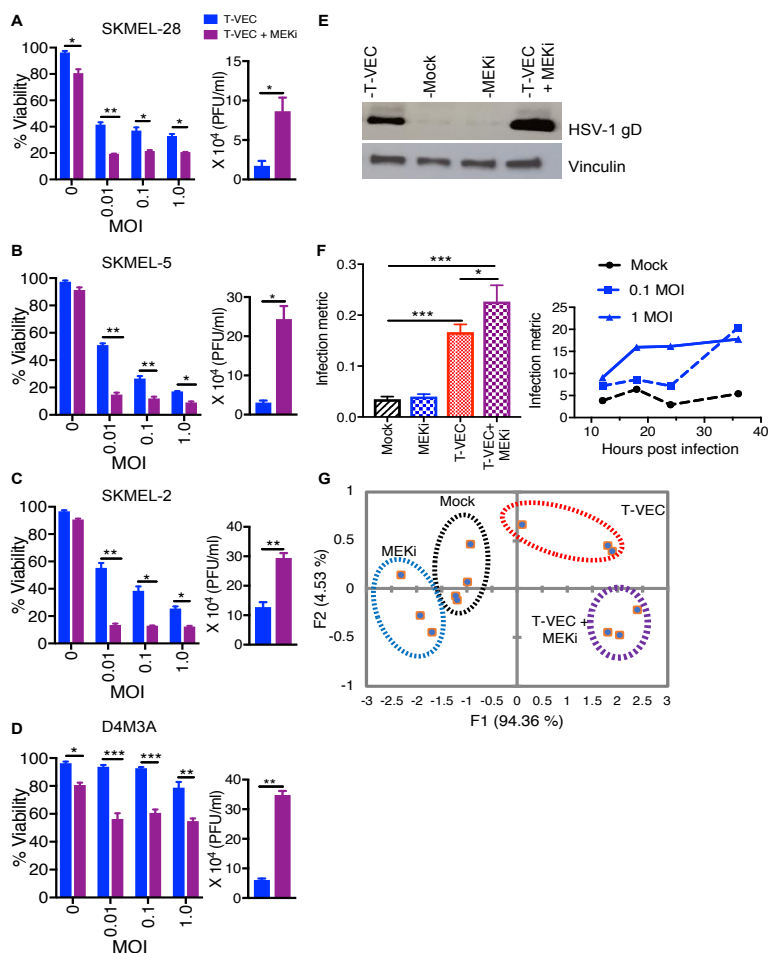


Figure 2. MEK inhibition augments T-VEC-mediated cell lysis *in vitro* and increases viral replication.

Cell viability determined by MTS assay. Cells were treated with either T-VEC alone or trametinib or combination T-VEC and trametinib (**A-D**, left panels). The right panels (**A-D**) show HSV-1 titers as measured by plaque assay from cells treated with either T-VEC alone (blue bar) or T-VEC and trametinib (purple bar). (**E**) Western blot of cell lysate collected at 24 hours after mT-VEC (0.1 MOI) infection of SK-MEL-28, mock infected, MEKi (10 nM) or combination treatment. (**F**) Infection metric analysis by Lumacyte (left panel) of SK-MEL-28 cells (mock), treated with 10 nM trametinib (MEKi), 1 MOI T-VEC or trametinib and T-VEC. The right panel shows a time course for untreated cells (black line), or those treated with 0.1 MOI of T-VEC (dotted blue line) or 1 MOI of T-VEC (solid blue line). (**G**) Principle component analysis (PCA) of the infection metric. Each experiment was conducted at least twice with similar results. Data are presented as mean \pm SEM and statistical differences between groups was measured by using two-tailed student *t* test. **p* < 0.05, ***p* < 0.01, ****p* < 0.001, *****p* < 0.0001.

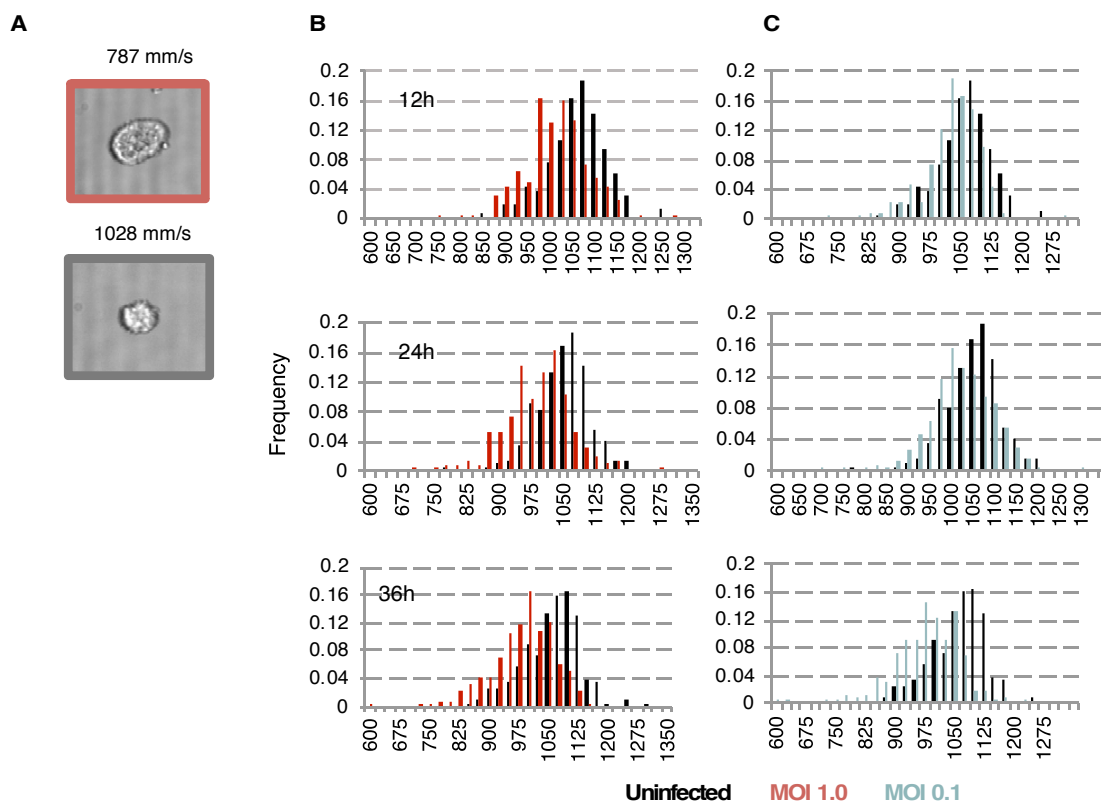


Figure 3. Lumacyte laser flow cytometry analysis

SK-MEL-28 cells were infected with T-VEC at 0.1 MOI and subjected to single cell laser flow cytometry. **(A)** Photomicrograph showing that a virus-infected cell is larger and has a corresponding lower velocity through single cell capillary chamber (787 mm/s; upper panel) compared to uninfected cells that are smaller and have higher velocity (1028 mm/s; lower panel). SK-MEL-28 cells were infected with 1 MOI T-VEC, 0.1 MOI T-VEC or uninfected, and subjected to velocity measurement in single cell capillary chamber. **(B)** Standard velocity histograms generated at 12 h. (top), 24 h. (middle) and 36 hrs. (bottom) for uninfected cells (black bars) or 1 MOI T-VEC (red bars). **(C)** Standard velocity histograms show indicated time points same as **(B)** for uninfected cells (black bars) and 0.1 MOI T-VEC-infected cells (grey bars). These data are calculated using an infection metric as described in the Materials and Methods. This experiment was conducted twice, similar results were obtained.

As shown in Figure 2F, the infection metric was increased at 18 hours for virally infected cells with the highest value seen in cells treated with T-VEC and MEKi (Fig. 2F, left). A time-course analysis on cells infected with T-VEC at low (0.01) or high (1.0) MOI or uninfected control cells showed the expected rapid increase in infection metric for cells infected with 1 MOI, while cells infected with 0.01 MOI demonstrated a delayed increase in infection metric at 36 hours when more virus had replicated (Fig. 2F, right). Principal component analysis (PCA) based on cell size (F1) and radiance (F2) was able to differentiate each of the treated cell populations (Fig. 2G).

T-VEC and MEK Inhibition Inhibits Tumor Growth in Melanoma Xenograft Model.

Next, we sought to determine if T-VEC and MEK inhibition had therapeutic activity *in vivo*. We utilized a murine xenograft model using the human SK-MEL-28 cell line (Fig. 4A). Delayed tumor growth was observed with MEK inhibition alone and T-VEC alone, but combination treatment was associated with a significant decrease in tumor growth and tumor regression compared to mock or monotherapy treatments ($p < 0.001$; Fig. 4B). Previously, MEK inhibition was shown to induce tumor cell apoptosis (41), therefore, we sought to determine how cells were killed in this model. We found combination of T-VEC and MEKi is associated fewer proliferating cells, based on Ki-67 immunostaining, compared to either treatment alone (Fig. 4C). HSV-1 in tumors was detected by immunostaining for the HSV-1 glycoprotein D, which was seen in the T-VEC alone-treated tumors and significantly increased in tumors of mice treated with T-VEC and MEKi (Fig. 4D). We also observed decreased levels of phosphorylated (p)ERK in tumor cells treated

with MEKi, as well as tumors treated with T-VEC alone, which was further decreased in tumors treated with the combination (Fig. 4E). Finally, while T-VEC treatment alone resulted in significant increase in caspase 3 cleavage compared to mock treatment, combination therapy resulted in higher tumor cell apoptosis *in vivo* (Fig. 4F). To confirm melanoma cell apoptosis, we treated SK-MEL-28 cells *in vitro* and found an increase in Annexin-V staining in cells treated with the combination compared to monotherapy or mock treatment (Fig. 5A-B), and this effect was partially blocked by a pan-caspase inhibitor (Z-VAD), (Fig. 5C). Further, there was increased cleaved PARP in tumor cells treated with both T-VEC and trametinib (Fig 5D). Collectively, these data demonstrate that combination T-VEC and MEK inhibition can delay melanoma xenograft growth *in vivo*

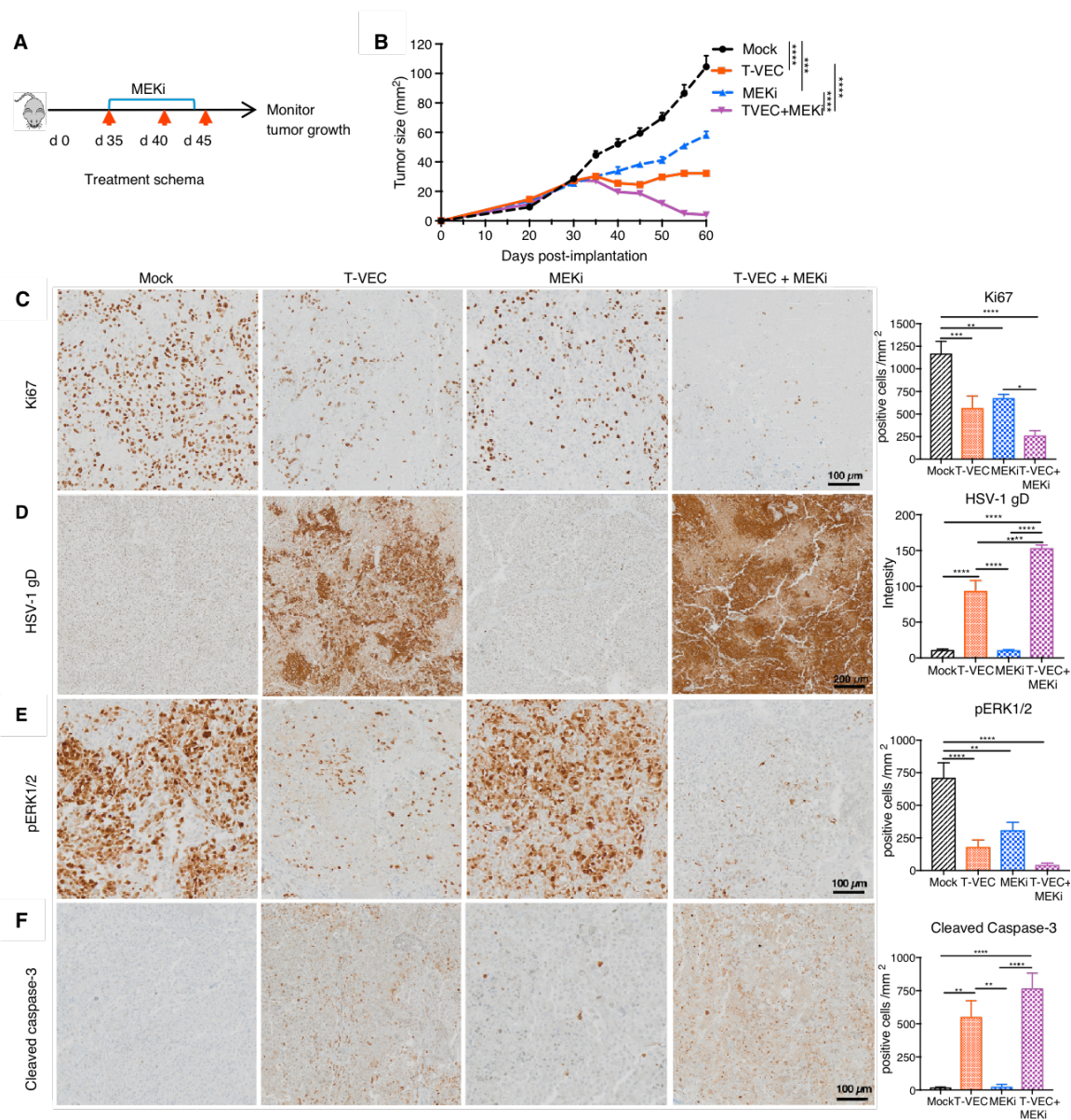


Figure 4. MEK inhibition enhances T-VEC-induced inhibition of human melanoma xenograft growth *in vivo* and promotes tumor cell apoptosis.

(A) NSG mice (n = 5/group) were implanted subcutaneously (s.c.) with human melanoma SK-MEL-28 cells (8×10^6) on day 0, treated via intratumoral (i.t.) injection with sterile water or T-VEC (1×10^5 pfu) on days 35, 40 and 45, and MEKi (trametinib; 0.5 mg/kg) or vehicle (0.2% Tween 80 and 0.5% hydroxypropyl methyl cellulose (HPMC) was given from days 35-43 via oral gavage. Red arrows indicate days when T-VEC was injected and top blue bar indicates days of trametinib (MEKi) treatment. (B) Mean tumor area. (C)

Representative images obtained from immunohistochemical staining of tumors for Ki67 at day 36; **(D)** HSV-1 gD; **(E)** pERK1/2; and **(F)** cleaved caspase 3. Right panels indicate quantification of positive cells. Scale bars are as indicated. Each experiment was repeated at least twice with similar results. Data are presented as mean \pm SEM and statistical differences between groups was measured by using one-way ANOVA. * $p < 0.05$, ** $p < 0.01$, *** $p < 0.001$, **** $p < 0.0001$. Only significant differences are indicated.

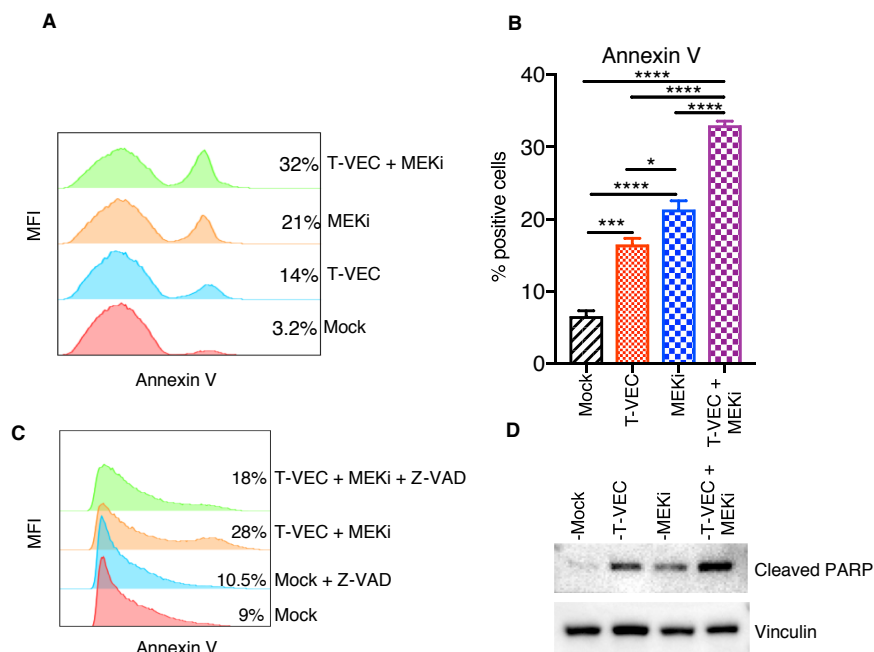


Figure 5. T-VEC and MEK inhibitor induced apoptosis

(A) Flow cytometry analysis of Annexin V staining in SK-MEL-28 cells treated with either T-VEC or MEKi or both. SK-MEL-28 cells were treated with vehicle or MEKi (trametinib; 10 nM) for 6-8 hours. Afterwards, PBS or T-VEC (MOI 1) was added to cells and cells were cultured for 24 h, stained for Annexin V (apoptosis), and analyzed by flow cytometry. **(B)** Quantitative analysis of A. **(C)** Annexin-V staining of cells SKMEL-28 cells treated with T-VEC and MEKi or T-VEC, MEKi and Z-VAD (pan caspase inhibitor). Annexin-V staining could be blocked by treatment with Z-VAD FMK (20 μ M). **(D)** Western blot analysis of cleaved PARP. SK-MEL-28 Cells (3.5×10^5) were seeded in 6-well plate, treated with vehicle or MEKi (trametinib; 10 nM) as in A. six to eight hours later cells were inoculated with T-VEC (MOI 1). 24 h post-viral infection, total cell lysates were harvested and cleaved PARP level is detected by immunoblotting. This experiment was conducted twice, similar results were obtained. Data are presented as mean \pm SEM and statistical differences between groups were measured by one-way ANOVA. * $p < 0.05$, ** $p < 0.01$, *** $p < 0.001$, **** $p < 0.0001$. Only significant differences are shown.

T-VEC and MEK Inhibition Enhances Therapeutic Effectiveness and Improves Survival in the Immune-competent D4M3A Murine Melanoma model

To determine the effects of combination T-VEC and trametinib (MEKi) in an immune-competent D4M3A BRAFV600E melanoma model, we used a modified T-VEC encoding murine GM-CSF (mT-VEC), as described in the Materials and Methods. D4M3A cells are susceptible to T-VEC infection and killing (Fig. 6A) and exhibit upregulation of pERK, characteristic of BRAFV600E mutated cells (Fig. 6B). In D4M3A tumor-bearing mice, mT-VEC alone exhibited no significant delays in tumor growth (Fig 7B-C) while MEKi alone showed significant delays in tumor growth (Fig. 7B-C). Combination treatment, however, was associated with significant tumor growth inhibition and improved survival with complete tumor eradication in 4 of 9 (44%) mice (Fig. 7C). Mice with complete tumor regression remained tumor free (Fig. 7C) and were re-challenged with twice the number of D4M3A cells implanted in the opposite flank (left). In this experiment, 70% (5/7) of mice completely rejected re-challenged tumor (Fig. 7D). We further observed a significant increase in tumor infiltrating CD8⁺ T cells in mice treated with combination therapy (Fig. 7E). CD8⁺ T cells exhibited increased levels of interferon- γ , Granzyme B and Ki-67 (Fig. 7E), indicative of an activated cytotoxic phenotype (Fig. 7E). The increased number of CD8⁺ T cells was further confirmed by immunohistochemistry (Fig. 7F-G). Both mT-VEC and MEKi demonstrated an increase in CD8⁺ T cells following treatment, which were further increased by combination therapy (Fig. 7F-G). There was no significant change in the total number of CD3⁺CD4⁺ T cells (Fig. 7H), but there was a decrease in CD4⁺FoxP3⁺ regulatory T cells (Tregs) in mice treated with mT-VEC alone or in

combination with MEKi (Fig. 7H). This resulted in a significant increase in the CD8⁺/Treg ratio in mice treated with mT-VEC alone and in combination with MEKi (Fig. 7H).

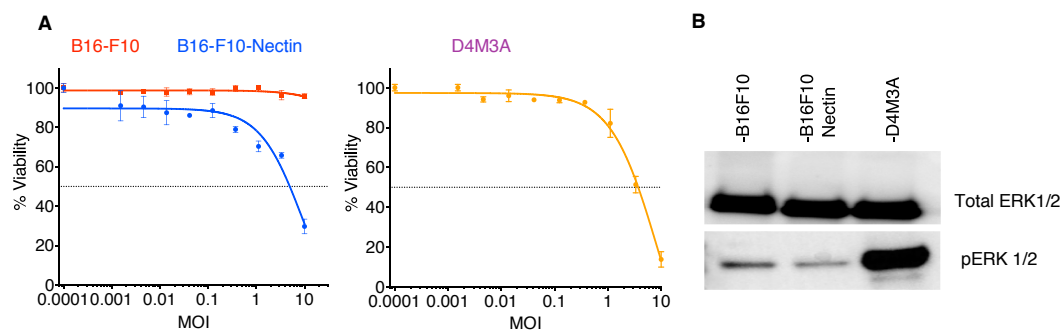


Figure 6. Characterization of murine D4M3A cells

(A) MTS assay measuring cell viability of B16-F10 (red) B16-F10-Nectin-1 (blue) and D4M3A (yellow) at 3 days post T-VEC treatment. (B) Immunoblot measuring the levels of phosphorylated ERK1/2.

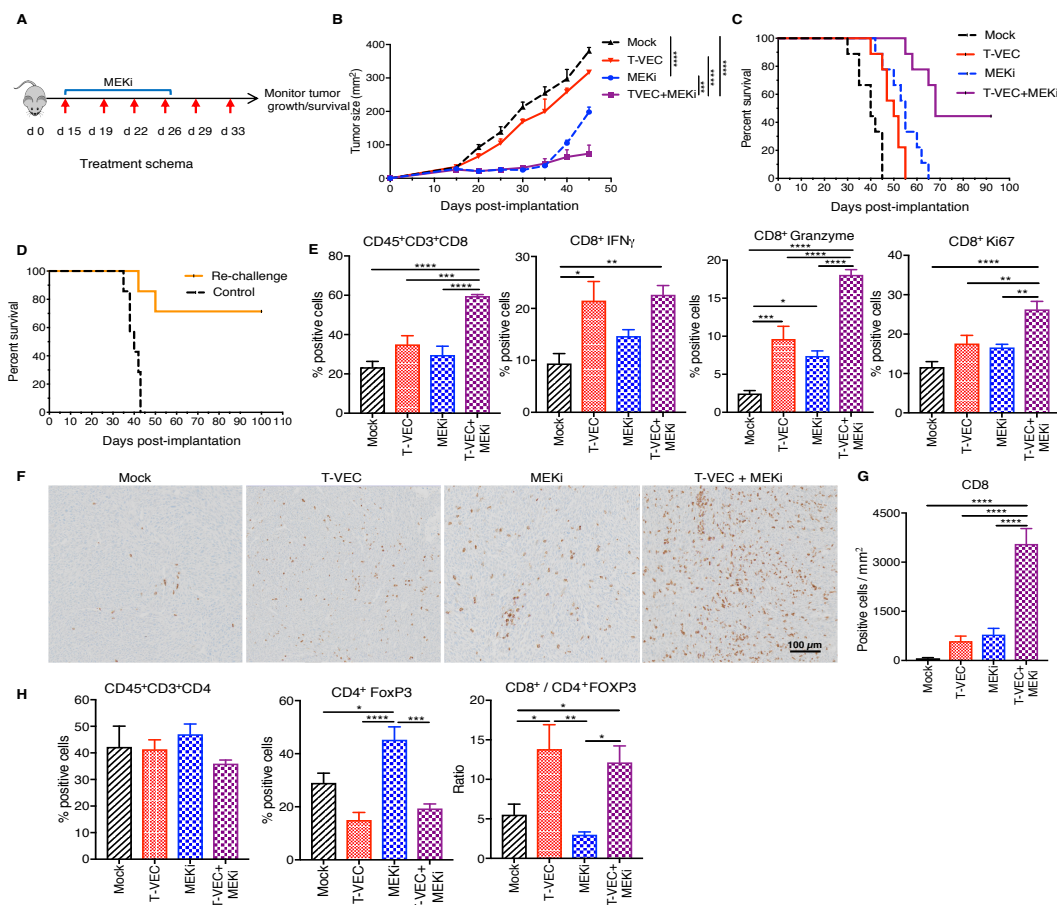


Figure 7. MEK inhibition enhances T-VEC-induced tumor regression in an immune competent murine melanoma model, promotes recruitment of CD8⁺ T cells and establishes long-term memory

(A) Treatment schema: red arrows indicate days of mT-VEC treatment and top blue bar indicates trametinib (MEKi) treatment. (B) Mean tumor area of mice from treated groups at day 45. (C) Survival of mice. (D) Re-challenge of mice cured in 3C. (E-F) Flow cytometry analysis of tumors at day 24. (E) Bar graphs (n=6) indicating the percent positive CD8 T cells, CD8+IFN- γ , CD8+GranzymeB, and CD8+Ki67 T cells respectively. (F) Immunohistochemical staining of CD8⁺ T cells in the tumor. Scale bar as indicated. (G) Quantification of CD8 positive cells. (H) Bar graph indicating CD4⁺ and CD4⁺FoxP3 (Tregs) and ratio of CD8⁺ T cells to Tregs. Each experiment was conducted at least twice with similar results. Data are presented as mean \pm SEM and statistical differences between groups was measured by using one-way ANOVA. *p < 0.05, **p < 0.01, ***p < 0.001, ****p < 0.0001. Only significant differences are indicated.

T-VEC and MEKi Combination Therapy is CD8⁺ T cell-dependent

To determine which immune cells are involved in the anti-tumor activity, we repeated the *in vivo* tumor experiments using depletion antibodies against CD4⁺ and CD8⁺ T cells, and liposomal clodronate to deplete macrophages. All cell depletions were confirmed by FACS analysis of splenocytes (Fig. 8A-B). Mice bearing D4M3A tumors were treated as described in the survival experiments in Fig. 7 and depletion antibodies were injected as shown in (Fig. 9A) and described in Materials and Methods. Neither macrophage depletion nor CD4⁺ T cell depletion significantly impacted anti-tumor activity, but CD8⁺ cell depletion completely abrogated the anti-tumor activity and survival benefit (Fig. 9B-C). FACS analysis confirmed the loss of CD4⁺ and CD8⁺ T cells in tumors collected from mice treated with immune cell depleting antibodies (Fig 9D, E). A compensatory increase in CD4⁺ T cells in the tumor microenvironment of mice depleted of CD8⁺ cells (Fig. 9D) and increased CD8⁺ T cells in tumors of mice depleted of CD4⁺ cells (Fig 9E) was seen.

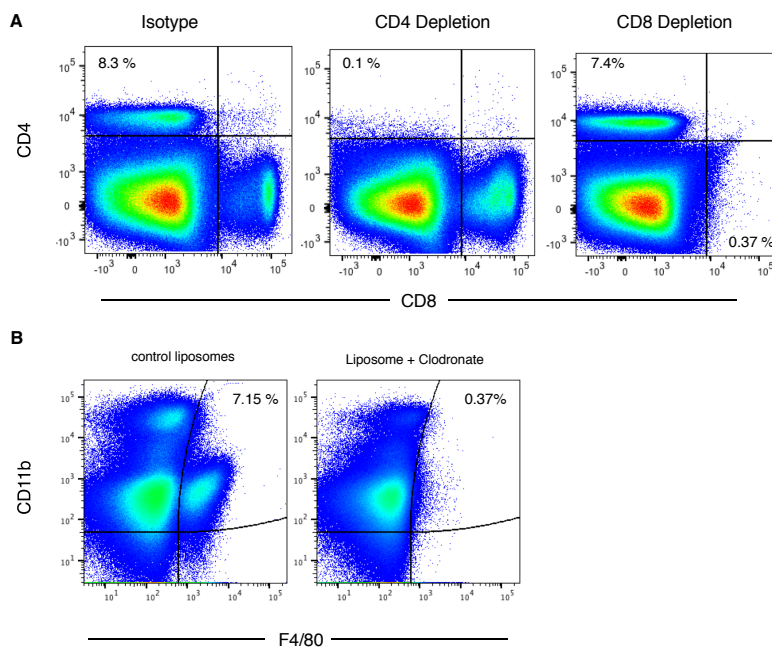


Figure 8. Validation of immune cell depletion

In vivo effects of depletion antibodies (α CD4 and α CD8) on CD4⁺ and CD8⁺ cell populations (**A**), and clodronate liposomes on macrophage (CD11b+F4/80+) populations (**B**) in splenocytes from treated mice. B6 mice were injected with either anti-mouse CD8 α (clone 2.43; 10 mg/kg), or anti-mouse CD4 (clone GK1.5; 10 mg/kg), control liposomes or clodronate liposomes (first dose 50 mg/kg followed by 25 mg/kg) were given by intraperitoneal (i.p.) injection every 72 hours for 3 doses. Mice were sacrificed 24 h. after the last dose, splenocytes isolated, and stained with or without anti-mouse CD4 (clone 129.19) and CD8a (clone 53-6.7) antibodies, or anti-mouse CD11b and F4/80 antibodies, and analyzed by flow cytometry.

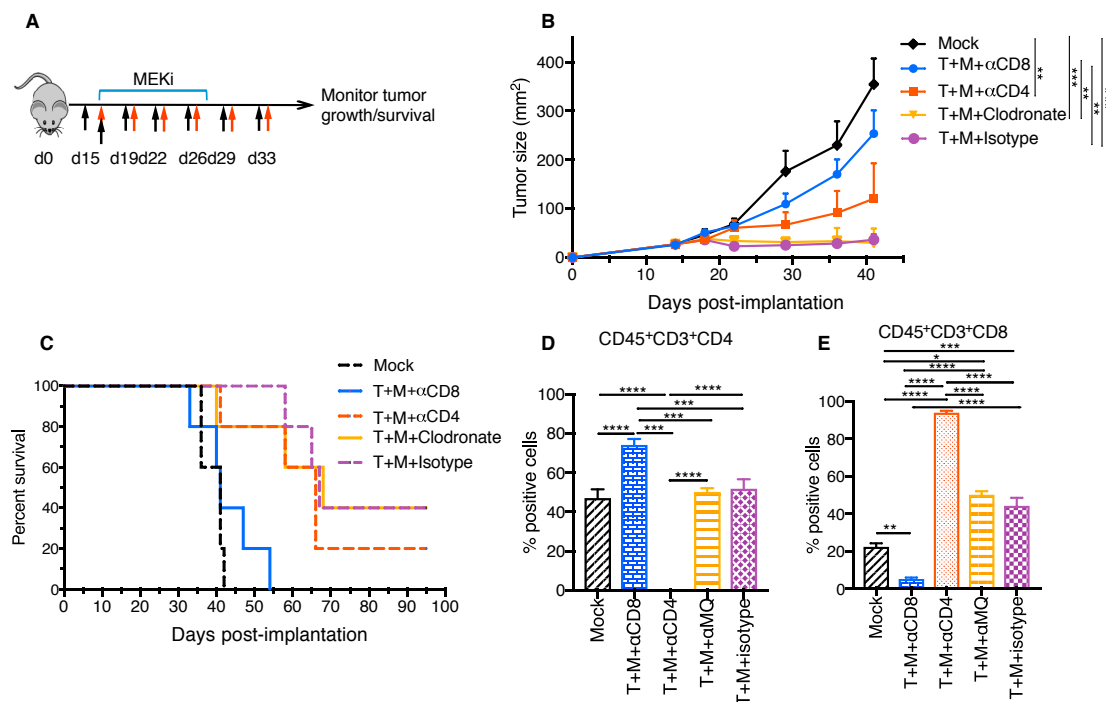


Figure 9. Depletion of CD8⁺ T cells abrogates the effects of T-VEC and MEKi combination therapy.

(A) C57BL/6J mice ($n = 5/\text{group}$) were implanted with D4M3A murine melanoma cells and mice were treated as indicated, described in methods. Red arrows indicate days of mT-VEC treatment, top blue bar indicated days of trametinib (MEKi) treatment, and black arrows indicating days where depletion antibodies against CD4, CD8 and clodronate were injected. (B) Mean tumor area of mice treated from different groups as indicated at day 40. (C) Survival of mice. (D-E) Flow cytometric analysis of tumor infiltrating T cells on day 24. (D) Bar graphs show the percentage CD45⁺CD3⁺CD4⁺ and (E) CD45⁺CD3⁺CD8⁺ cells. Each experiment was repeated at least twice with similar results. Data are presented as mean \pm SEM and statistical differences between groups was measured by using one-way ANOVA. * $p < 0.05$, ** $p < 0.01$, *** $p < 0.001$, **** $p < 0.0001$. Only significant differences are indicated.

Combination treatment with T-VEC and MEKi augments melanoma antigen-specific T cell responses

We sought to further characterize the antigen specificity of the CD8⁺ T cell responses in mice treated with mT-VEC/MEKi combination therapy. Initially, flow cytometry using MHC-I dextramers for two defined melanoma antigens, gp100 and TRP2 and one viral antigen, HSV-1 gB, was used to determine antigen specificity of tumor infiltrating CD8⁺ T cells during T-VEC treatment alone in a time course study (Fig. 10). We saw an initial increase of HSV-1 gB-specific CD8⁺ T cells at day 19 which plateaued by day 24 (Fig. 10). Gp100- and TRP2-specific CD8⁺ T cells emerged between days 19-24 (Fig. 10). mT-VEC treatment induced HSV-1 gB-specific CD8⁺ T cells (Fig. 11A) and combination mT-VEC and MEKi resulted in a significant increase in the relative frequency of tumor-infiltrating HSV-1 gB-specific CD8⁺ T cells (Fig. 11A). We also observed an increase in gp100- and TRP2-specific CD8⁺ T cells during combination treatment (Fig. 11B-C). Although the increase in melanoma-specific CD8⁺ T cells was especially high within the tumor-infiltrating lymphocyte population, we did not detect HSV-1-specific CD8⁺ T cells in the spleen of treated animals but did observe a minimal, but significant, increase in both gp100- and TRP2-specific CD8⁺ T cells in the spleen (Fig. 12). These data suggest that T-VEC and MEKi can induce antigen spreading.

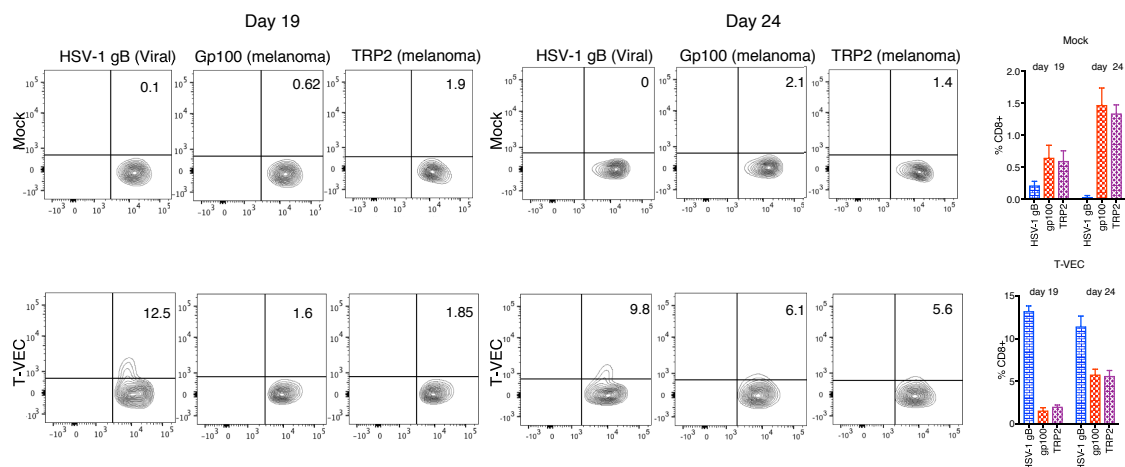


Figure 10. Time course analysis of tumor infiltrating CD8⁺ T cells during mT-VEC treatment

Day 19: Mice bearing D4M3A tumors were treated with 1×10^6 pfu of mT-VEC on days 15 and 18 and tumors collected on day 19. Bar graph indicating the % CD8⁺ antigen specific T cells as indicated.

Day 24: Mice bearing D4M3A tumors were treated with 1×10^6 pfu of mT-VEC on days 15, 18, 21 and 23 and tumors harvested on day 24. Bar graph indicating the % CD8⁺ antigen specific T cells as indicated.

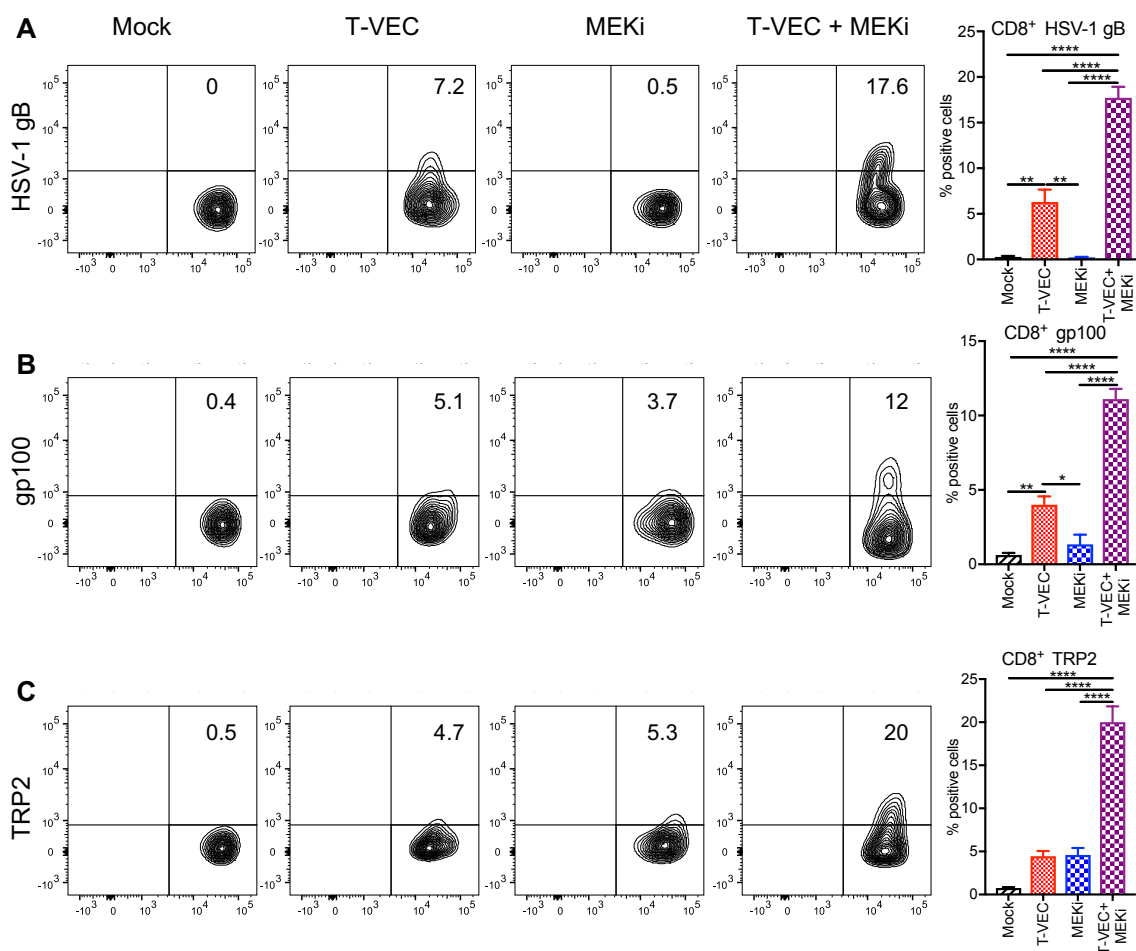


Figure 11. Combination T-VEC and MEK inhibition induces viral-specific CD8+ T cells and increases melanoma antigen-specific CD8+ T cell responses.

C57BL/6J mice implanted s.c. in the right flank with 3×10^5 D4M3A cells and treated with mT-VEC (1×10^6 pfu) or sterile water i.t. for 3 doses on days 15, 19 and 22 and or trametinib (0.5 mg/kg) or vehicle (0.2% Tween 80 and 0.5% Hydroxypropyl methyl cellulose) orally once daily on days 15-19. Tumors were harvested on day 24, cells dissociated and analyzed by flow cytometry. Percentages of live CD45+ cells, CD3+ cells, and CD3+ sorted CD4+ and CD8+ subsets from the Mock, T-VEC monotherapy, MEKi monotherapy, and T-VEC + MEKi combination groups were analyzed and compared. Tumor-infiltrating CD8+ T cells were analyzed with (A) HSV-1-specific H-2K^b-HSV-1gB dextramer, (B) melanoma antigen specific H-2D^b-gp100 dextramer, (C) H-2K^b-TRP2 dexamers. Quantitative analysis is shown in the bar graphs on the right. These experiments were conducted at least twice with similar results. Data are presented as mean \pm SEM and statistical differences between groups was measured by using one-way ANOVA. * $p < 0.05$, ** $p < 0.01$, *** $p < 0.001$, **** $p < 0.0001$. Only significant differences are indicated.

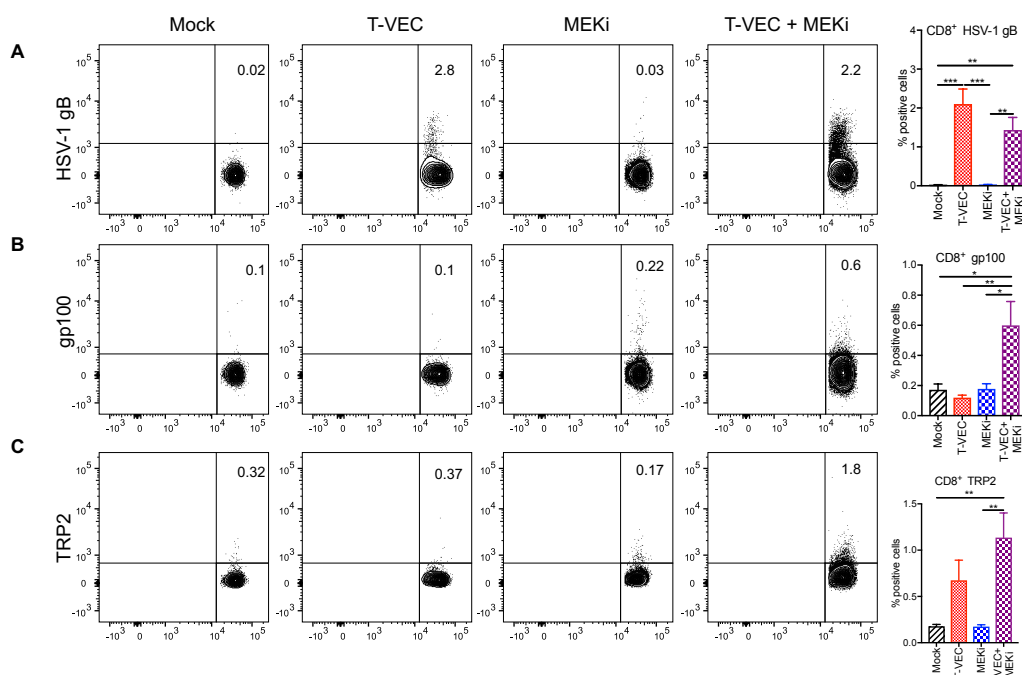


Figure 12. Analysis of CD8⁺ T cells from spleen during mT-VEC + MEKi treatment

C57BL/6J mice implanted s.c. in the right flank with 3×10^5 D4M3A cells and treated with mT-VEC (1×10^6 pfu) or sterile water i.t. for 3 doses on days 15, 19 and 22 and or trametinib (0.5 mg/kg) or vehicle (0.2% Tween 80 and 0.5% Hydroxypropyl methyl cellulose) orally once daily on days 15-19. Spleens were harvested on day 24 and flow cytometry was performed. Cells were gates on live, CD45⁺, CD3⁺, CD8⁺ and further analyzed for antigen specificity.

(A) Representative plots and bar graph showing quantification of HSV-1-specific H-2Kb-HSV-1gB dextramer positive CD8 T cells from spleen. (B) Representative plots and bar graph showing quantification of melanoma antigen specific H-2Db-gp100 dextramer positive CD8 T cells from spleen. (C) Representative plots and bar graph showing quantification of melanoma antigen specific H-2Kb-TRP2 dextramer positive CD8 T cells from spleen. Data presented as mean \pm SEM and the statistical differences between groups was measured by one-way ANOVA. * $p < 0.05$, ** $p < 0.01$, *** $p < 0.001$, **** $p < 0.0001$. Only significant values are indicated.

Combination treatment with T-VEC and MEKi is Dependent on Batf3⁺ Dendritic Cells.

To determine the role of CD8⁺CD103⁺ DCs in mediating anti-tumor immunity (42, 43), we implanted D4M3A tumors into *Batf3*^{-/-} mice. The lack of CD8⁺CD103⁺ DCs in *Batf3*^{-/-} mice did not alter the ability to establish D4M3A tumors (Fig. 13A-B). Tumors from *Batf3*^{-/-} mice had significantly reduced frequency of CD45⁺MHCII⁺CD11c⁺CD103⁺ cells, as well as CD45⁺MHCII⁺CD11c⁺CD8⁺ cells after combination therapy (Fig. 13C). To determine the effects of Batf3⁺ DCs on combination therapy, D4M3A tumors were implanted in C57BL/6J and *Batf3*^{-/-} mice and treated as described in Fig. 7. Although combination treatment resulted in delayed tumor growth in C57BL/6J mice, as previously seen (Fig. 7C), this effect was significantly diminished in *Batf3*^{-/-} mice (Fig. 14A-B). Treated *Batf3*^{-/-} mice demonstrated a significant decrease in the percent and number of CD8⁺ T cells compared to C57BL/6J (B6) (Fig. 14C). There was also a significant decrease in the percent of CD8⁺ T cells expressing IFN- γ and Granzyme B (Fig. 14D) and proliferating (Ki67⁺) CD8⁺ T cells (Fig. 14D) and increased Tregs, (Fig. 14E) seen after combination treatment. We also observed a significant decrease in gB-specific CD8⁺ T cells and gp100- and TRP2-specific CD8⁺ T cells in *Batf3*^{-/-} mice compared to wild-type mice treated with combination therapy (Fig. 14F).

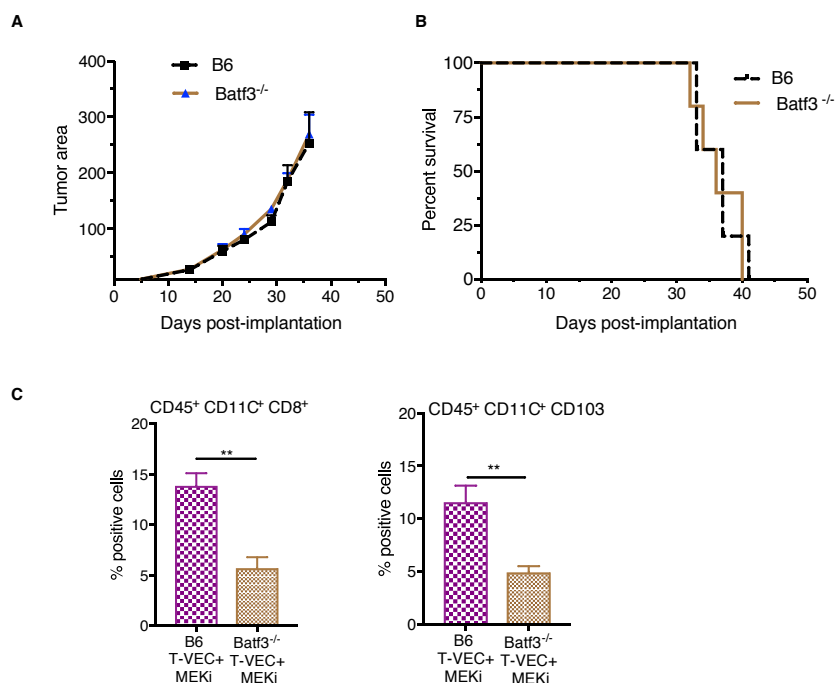


Figure 13. Characterization of D4M3A tumor cells in Batf3 knockout mice

In order to test growth kinetics of D4M3A cells in Batf3^{-/-} mouse model compared to C57BL/6J mice, age-matched C57BL/6J and Batf3^{-/-} mice were implanted subcutaneously in the right flank with 3×10^5 D4M3A murine melanoma cells on day 0. (A) Tumor growth and (B) Survival were monitored (C) C57BL/6J (n = 5) mice and Batf3^{-/-} mice (n = 5) were treated as in Fig. 6C and mice were euthanized on day 24. Tumors were harvested, dissociated cells stained with fluorochrome-conjugated anti-mouse antibodies, and multicolor flow cytometry performed. (C) Bar graph indicating frequency of live CD45⁺ MHC II⁺ CD11b⁻ CD11c⁺ CD8⁺ cells (left panel) and CD45⁺ MHC II⁺ CD11b⁻ CD11c⁺ CD103 (right panel) cell subsets from B6 and Batf3^{-/-} mice. Data are presented as mean \pm SEM and the statistical differences between groups was measured by two-tailed student *t* test. **p* < 0.05, ***p* < 0.01, ****p* < 0.001, *****p* < 0.0001. Only significant differences are indicated

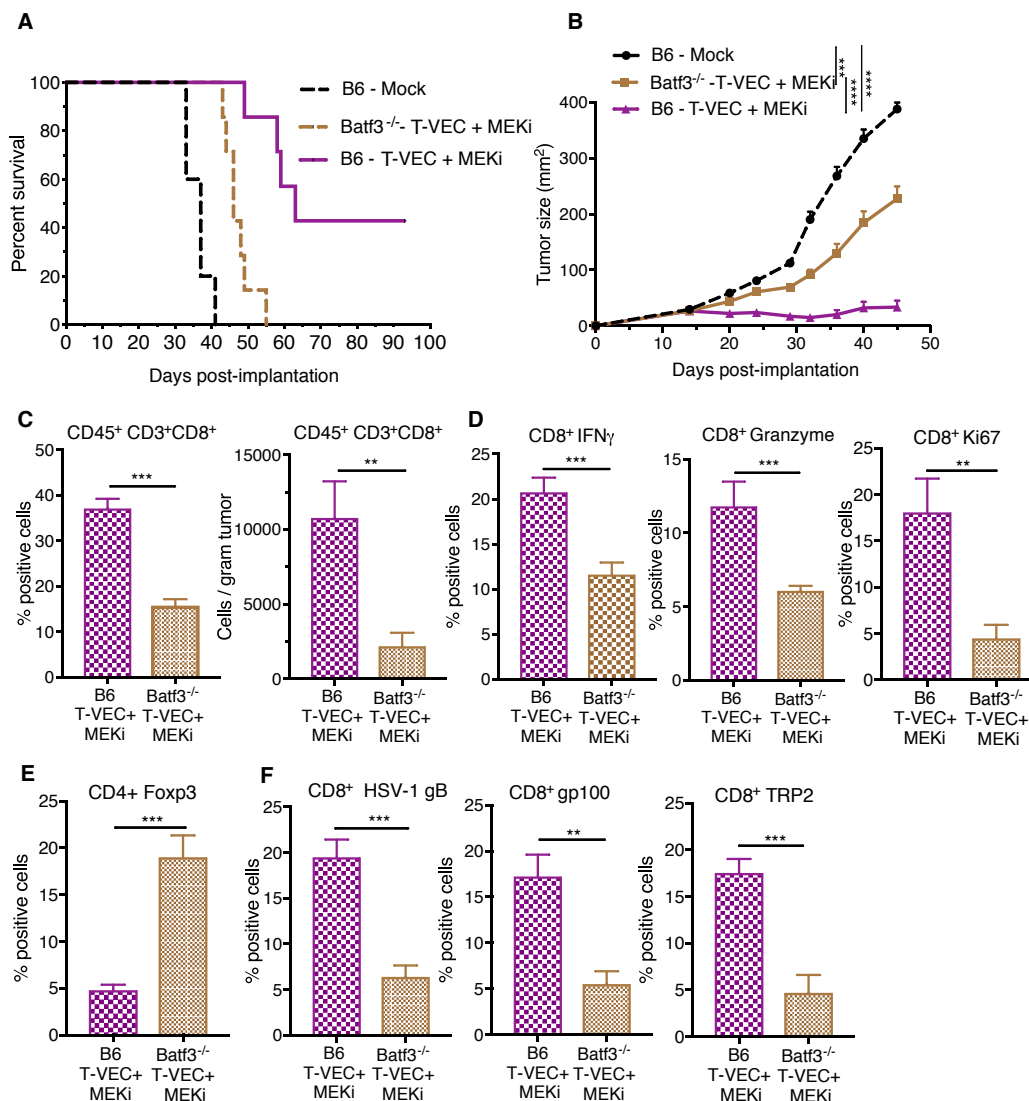


Figure 14. Batf3⁺ dendritic cells play a role in the anti-tumor activity and antigen spreading associated with combination T-VEC and MEK inhibition treatment.

C57BL/6J mice (B6, n = 7) and Batf3^{-/-} mice (n = 7) were implanted with D4M3A murine melanoma cells and either mock treated or treated with T-VEC and trametinib as described in Materials and Methods. **(A)** Mean tumor area at day 45. **(B)** Survival of mice. **(C-F)** Flow cytometry analysis of tumors obtained from B6 and Batf3^{-/-} mice on day 24. **(C)** Bar graph indicating the percentage, number, of tumor-infiltrating total CD8⁺ T cells and the frequency of CD8⁺IFN- γ ⁺ and CD8⁺GranzymeB⁺ T cells respectively. **(D)** CD8⁺Ki67⁺ T cells. **(E)** CD4⁺FoxP3⁺ Tregs. **(F)** Percentage of HSV1-gB⁺, murine gp100⁺ and TRP2⁺ CD8⁺ T cells respectively. These experiments were repeated at least twice with similar results. Data presented as mean \pm SEM and the statistical differences between groups was measured by two-tailed student *t* test. **p* < 0.05, ***p* < 0.01, ****p* < 0.001, *****p* < 0.0001.

Combination T-VEC and MEK Inhibition Induces an Inflammatory Gene Signature and Increases PD-L1 Expression in the Tumor Microenvironment

Previous studies have identified an inflammatory gene signature in patients responding to PD-1 checkpoint blockade (44). Since T-VEC is associated with type 1 interferon release and CD8⁺ T cell recruitment to the tumor microenvironment, we evaluated the established D4M3A tumors on day 24 from mice treated with mT-VEC, MEKi or both for inflammatory gene expression profile. Treatment with mT-VEC was associated with an increased inflammatory signature compared to both mock- and MEKi-treated tumors, and that this profile was highest in tumors treated with combination mT-VEC and MEKi (Fig. 15A). We also restricted the gene expression profile to 5 genes related to T cell activation (*interferon- γ* , *CD8 α* , *tumor necrosis factor- α* , *granzyme B* and *perforin 1*) and found a correlation between T cell activation gene expression and therapeutic effects (Fig. 15B; Fig. 16A), as well as categories of genes related to immune cells and anti-viral immunity (Fig 16B-C). While MEKi inhibited expression of most anti-viral genes, the combination of mT-VEC and MEKi resulted in increased gene expression compared to mT-VEC alone, except for *interleukin-34* (IL34) and *NKG2D ligand* (UL16 binding protein 1; Ulbp1). While PD-1 and PD-L1 expression was significantly increased in the inflammatory gene panel in T-VEC and MEK inhibitor-treated animals (Fig. 15C), this was confirmed by flow cytometry analysis of CD45⁺ cells harvested from the tumor microenvironment at day 24 as described in Fig. 7D. An increase in both PD-1 and PD-L1 was observed in tumors treated with mT-VEC alone, but they were highest in tumors treated with the combination (Fig. 15D).

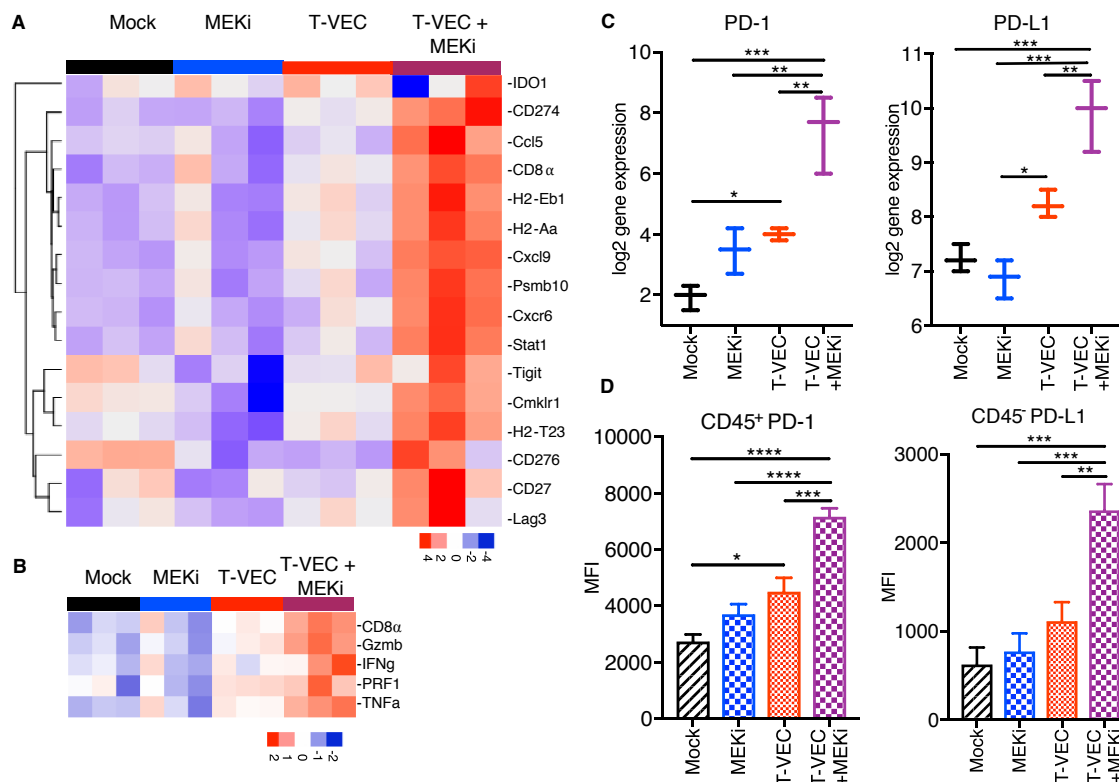


Figure 15. T-VEC and MEK inhibition reprograms immune silent tumors into immune inflamed tumors and induces expression of PD-1 and PD-L1.

C57BL/6J mice were implanted s.c. in the right flank with 3×10^5 D4M3A cells and treated with mT-VEC (1×10^6 pfu) i.t. for 3 doses on days 15, 19 and 22 and or trametinib (0.5 mg/kg) orally once daily on days 15-19. Tumors were harvested on day 24, total RNA was isolated and gene expression analysis performed using the NanoString PanCancer Immune panel as described in the Materials and Methods. **(A)** An inflammatory 16-gene expression profile was generated from mice ($n=3$) treated (as described in Fig 3D) with mock control (black), trametinib alone (MEKi; blue), mT-VEC alone (red), or combination mT-VEC and MEKi (purple). **(B)** A selected 5-gene expression signature represented by genes highly associated with CD8⁺ T cell activation. **(C)** Gene expression of PD-1 (right panel) and PD-L1 (left panel). **(D)** Bar graphs show the mean fluorescence intensity (MFI) of CD45⁺PD-1⁺ (left panel) and CD45⁻PD-L1⁺ (right panel). Each experiment was performed at least twice with similar results. Data are presented as mean \pm SEM and the statistical differences between groups were measured by two-tailed student *t* test. **p* < 0.05, ***p* < 0.01, ****p* < 0.001, *****p* < 0.0001.

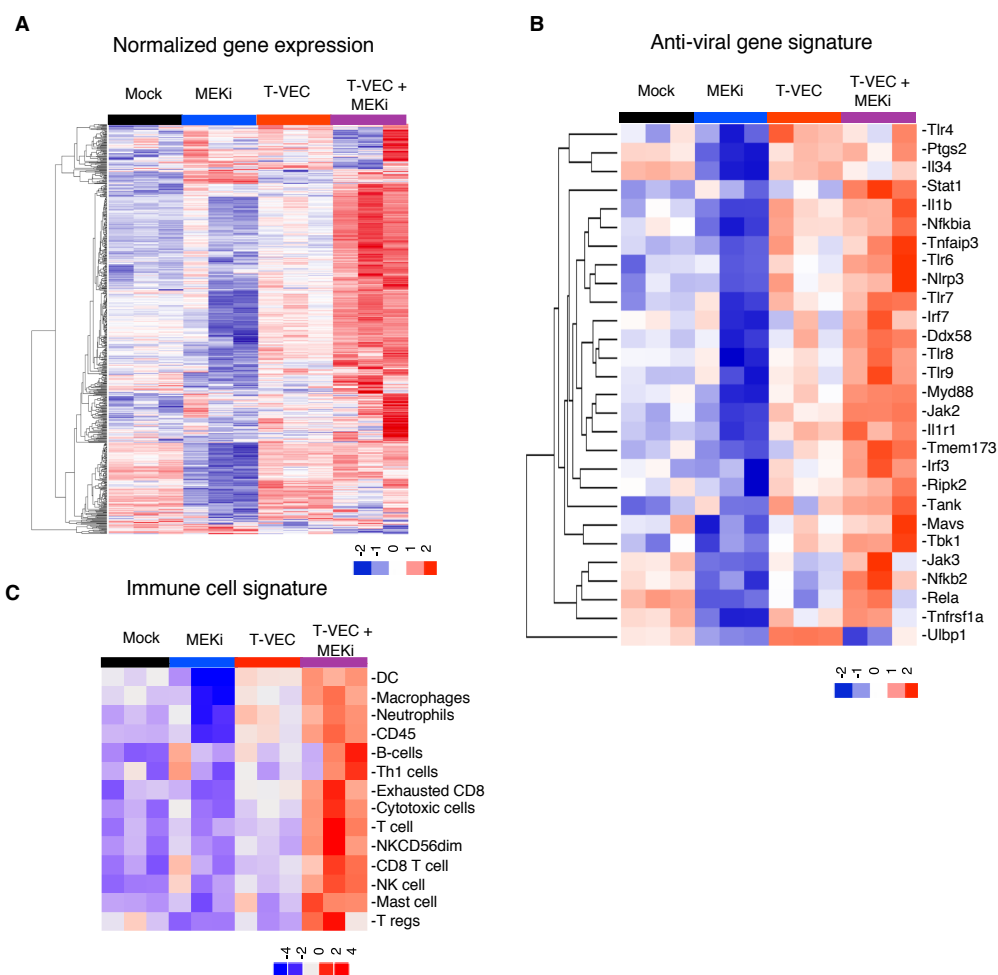


Figure 16. NanoString gene expression heat maps for all genes profiled and by gene function.

C57BL/6J (n=3) mice implanted with 3×10^3 D4M3A cells on day 0, treated with sterile water or mT-VEC (10^6 pfu) on days 15, 19 and 22 and vehicle or MEKi (trametinib; 0.5 mg/kg) gavage orally once daily from days 15-19 (n = 5/group), and euthanized on day 24. Tumors were harvested, total RNA was isolated using Qiagen RNAeasy kit and gene expression analysis was done using the PanCancer Immune panel as described in the Materials and Methods. N= (3). This experiment was conducted twice with similar results. **(A)** Heat map representing normalized gene expression of all genes included in the NanoString PanCancer Immune panel. **(B)** Heat map representing the normalized gene expression signature of genes associated with innate anti-viral immune responses. **(C)** Heat map representing the normalized gene expression signature of genes associated with specific immune cell function.

Triple Treatment with T-VEC, MEK Inhibition and PD-1 Blockade Further Enhances Therapeutic Activity.

Although combination therapy using mT-VEC and MEK inhibition reduced tumor burden and enhanced survival of treated mice (Fig. 7B, C), tumors were completely eradicated in only 30-40% of mice. Based on the flow cytometry analysis and gene expression profiling showing an increase in PD-1 and PD-L1 expression in the tumor microenvironment (Fig. 15D), we reasoned that therapeutic activity might be further expanded by addition of PD-1 blockade to the combination regimen. To test this, we treated D4M3A tumor-bearing mice with mT-VEC, MEKi, or both as previously described in Fig. 7C, and with or without α PD-1 antibody. There was limited impact of α PD-1 when given with mT-VEC alone or MEK inhibition alone (Fig. 17B, C), as compared to monotherapy (Fig. 7B, C). However, the combination of α PD-1 with both mT-VEC and MEKi resulted in complete durable responses in almost all mice (6/7), compared to 2/7 mice with mT-VEC and MEKi (Fig. 17C). All mice who cleared primary tumors with mT-VEC/MEKi/ α PD-1 therapy rejected subsequent tumor re-challenge (Fig. 17D). Flow cytometry analysis performed on tumors showed a significant decrease in CD45⁺PD-1⁺ and CD8⁺PD-1⁺ cells in mice treated with triple therapy compared to mT-VEC and MEKi (Fig. 17E, Fig. 18). No significant changes were observed in Tregs or the CD8⁺/Treg ratio (Fig. 17F). Triple combination elicited an increase in the percentage of total CD8⁺ T cells (Fig. 17G, left panel), as well as granzyme B and Ki67 expression (Fig. 17G). There was no overt toxicity observed in the mice as evidenced by changes in body weight, feeding habits, stool frequency or coat appearance, including the absence of vitiligo.

Finally, to test the efficacy of triple combination in a different model we tested the triple combination in BALB/c mice bearing established CT26 murine colon cancer tumors. In the CT26 model, both mT-VEC/MEKi and mT-VEC/ α PD-1 antibody dual combinations elicited significant anti-tumor activity, with regression observed in 5/10 mice (Fig 17H, Fig. 19). In addition, the triple combination, using mT-VEC/MEKi/ α PD-1, caused regression of all tumors, producing complete responses not observed with double therapy treatment (Fig 17H, Fig. 19). There were no signs of toxicity or weight loss in any of these animals.

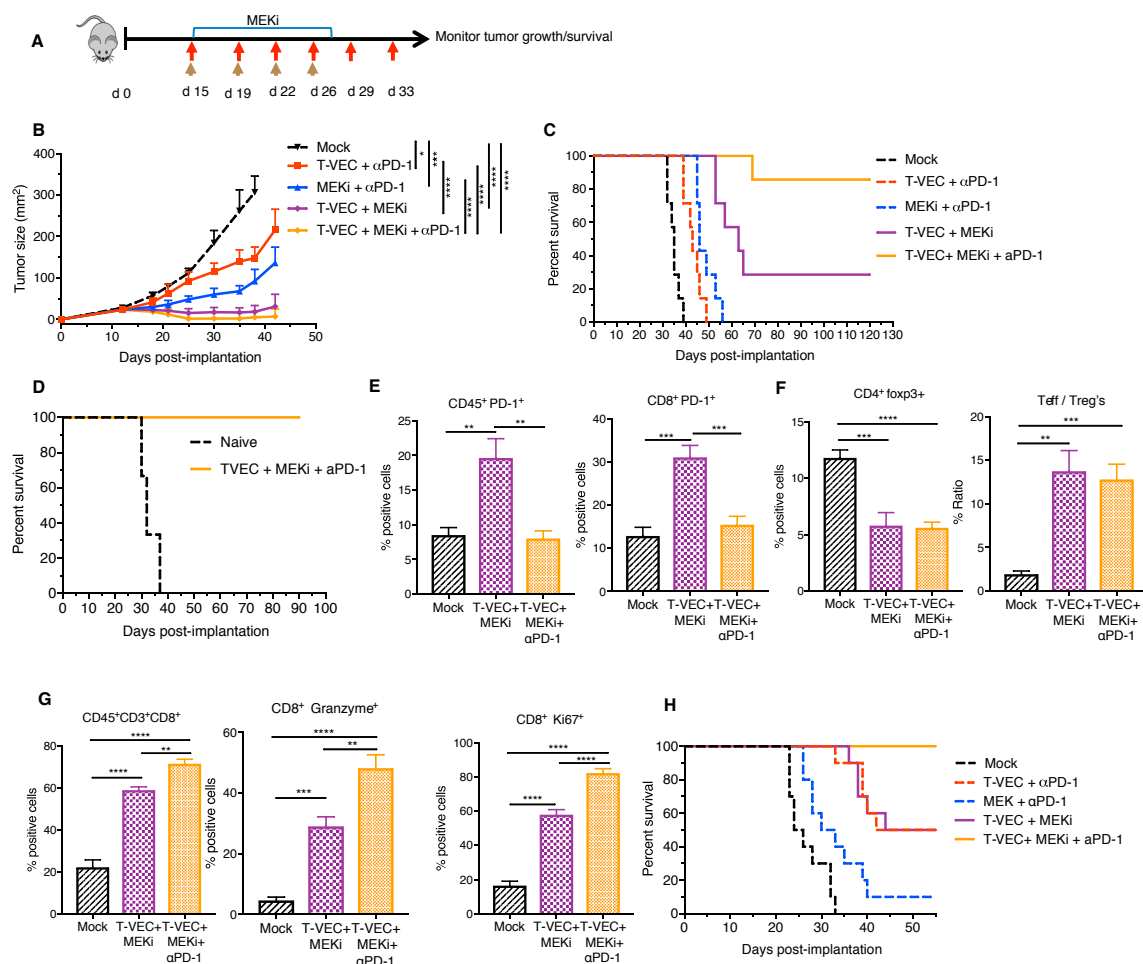


Figure 17. Triple combination treatment with T-VEC, MEK inhibition and PD-1 blockade improves therapeutic treatment of melanoma and colon cancer models.

(A) Treatment schema: red arrows indicate T-VEC, top blue bar indicates trametinib and brown arrows indicate α PD-1. (B) Mean tumor area. (C) Survival of mice. (D) Re-challenge of mice cured from B. (E-F) Flow cytometry of tumors at day 24. Bar graph indicating percent positive (E) CD45⁺PD-1⁺ cells (right panel) and CD45⁺CD8⁺PD-1⁺ cells (left panel), (F) CD4⁺FoxP3⁺ (right panel) and ratio of effector T cells to Tregs (left panel) (G) CD8⁺ T cells, granzyme B⁺ CD8 T cells, and Ki67⁺ CD8 T cells respectively. (H) Evaluation of triple combination in CT26 murine colon carcinoma model. Mice were treated as described in Materials and Methods. Each experiment was conducted at least twice with similar results. Data are presented as mean \pm SEM and statistical differences between groups were measured by two-tailed student *t* test. **p* < 0.05, ***p* < 0.01, ****p* < 0.001, *****p* < 0.0001.

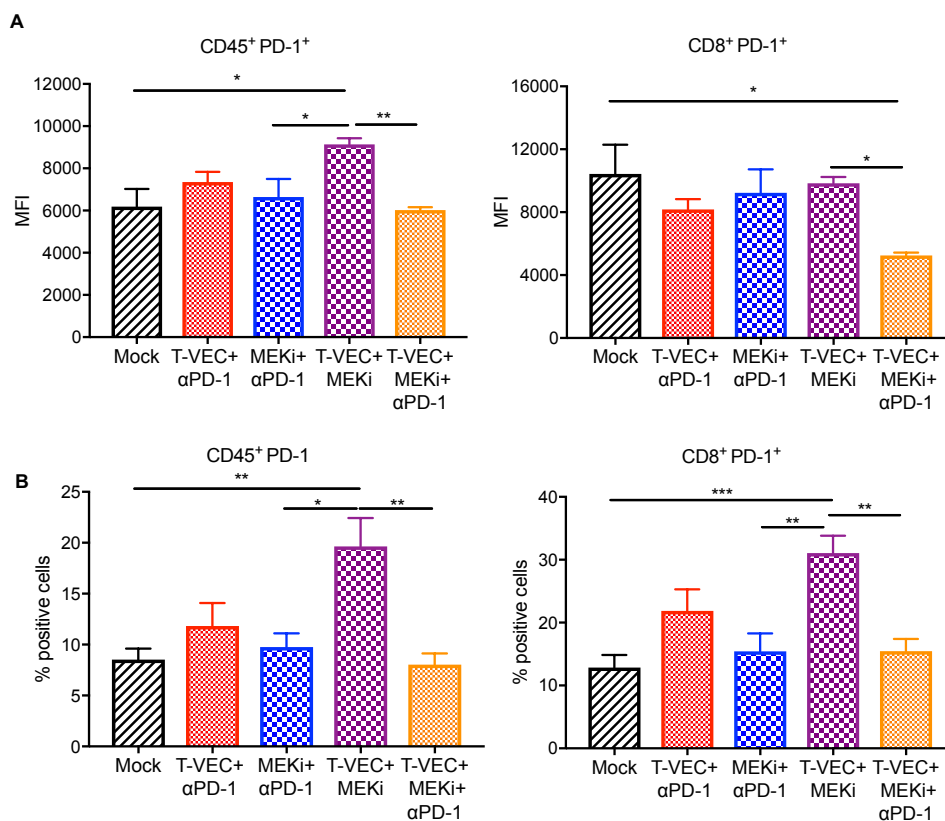


Figure 18. Mean fluorescence intensity (MFI) expression of PD-1 expression and frequency of PD-1⁺ cells

C57BL/6J mice (n=5 per group) were implanted subcutaneously in the right flank with D4M3A cells (3×10^5) on day 0 and treated with T-VEC (1×10^6 pfu) or sterile water via intra-tumoral injection on days 15, 19 and 22, trametinib (0.5 mg/kg) or vehicle control on days 15-19 via oral gavage and αPD-1 antibody (clone: RMP1-14, 10 mg/kg) via i.p. injection on days 15, 19 and 22. In addition, groups received double combination treatment with T-VEC and trametinib (and rat IgG isotype control) or triple therapy with m-TVEC, trametinib, and αPD-1 antibody. **(A)** Bar graph indicating the mean fluorescence intensity (MFI) of CD45⁺PD-1⁺ (right panel) and CD45⁺CD8⁺PD-1⁺ (left panel). **(B)** Bar graph indicating the percent positive CD45⁺PD-1⁺ (right panel) and percent positive CD45⁺CD8⁺PD-1⁺ (left panel). Each experiment was repeated at least two times with similar results. Data are presented as mean ± SEM and statistical differences between groups were measured by using one-way ANOVA *p < 0.05, **p < 0.01, ***p < 0.001, ****p < 0.0001. Only significant differences are indicated.

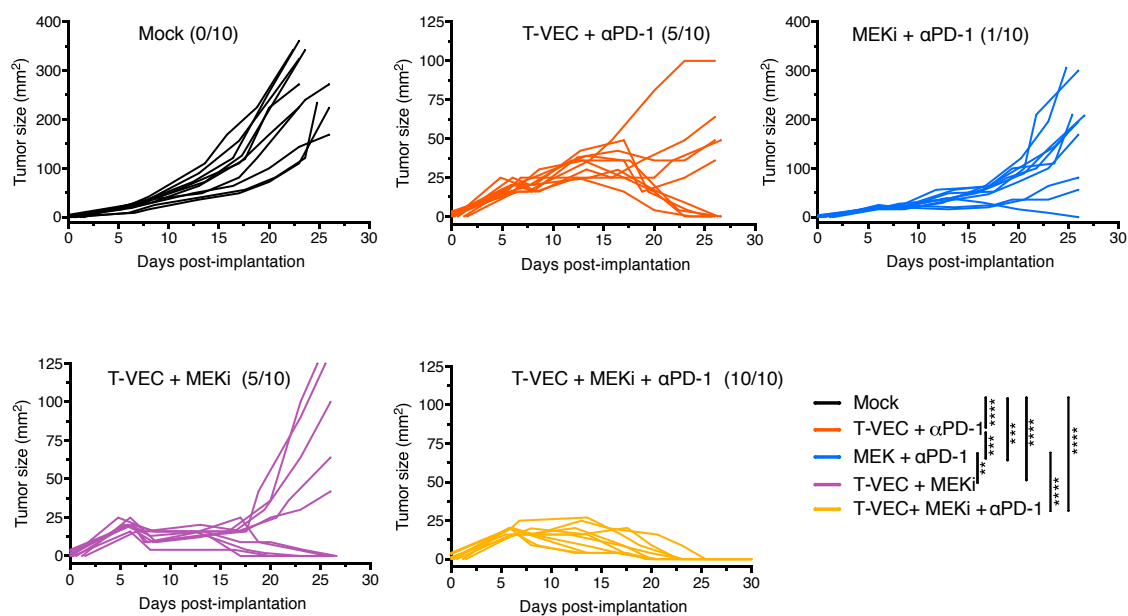


Figure 19. Individual tumor growth curves of BALB/c mice bearing CT26 tumors.

Growth curves from two individual experiments. BALB/c mice (n=10 per group) were implanted subcutaneously in the right flank with CT26 cells (2×10^5) on day 0 and treated with T-VEC (5×10^5 pfu) or sterile water via intratumoral injection on days 8, 12, 15, 19 and 22, MEKi (0.5 mg/kg) or vehicle control on days 8-20 via oral gavage and αPD-1 antibody (clone: RMP1-14, 7.5 mg/kg) via i.p. injection on days 8, 12, 15 and 19. In addition, groups received equivalent doses of double combination treatment with mT-VEC and MEKi (and rat IgG isotype control) or triple therapy with TVEC, MEKi and αPD-1 antibody. Mean tumor area across groups was calculated on day 26 and statistical differences between groups were measured by one-way ANOVA, *p < 0.05, **p < 0.01, ***p < 0.001, ****p < 0.0001. Only significant differences are shown.

DISCUSSION

In this study, we demonstrate that the combination of T-VEC and MEK inhibition increases melanoma tumor cell killing through increased viral replication and apoptosis *in-vitro* and enhances melanoma specific adaptive immune responses *in-vivo*. Previous reports have described interactions between MAPK pathway inhibition and different OV's (45, 46). MEK inhibition was found to increase oncolytic adenovirus replication and tumor cell killing, possibly through upregulation of coxsackievirus and adenovirus receptor (CAR) (47). In glioma cells, MEK inhibitor PD98059 inhibited autophagy and increased cell killing without increasing oncolytic adenovirus replication (48). Oncolytic reovirus increased tumor cell killing due to increased endoplasmic reticulum (ER) stress-induced apoptosis and not increased virus replication (45). The effects of MEK inhibition is more complex with oncolytic HSV and depend on the particular virus mutation. An internal repeat-deleted oncolytic HSV-1 inhibited p-MAPK activation *in vitro* and synergized with PD98059 in killing triple negative breast cancer (TNBC) cells lines (46). In contrast, the tumor cell cytotoxicity of ICP34.5-deleted oncolytic HSV-1 (R3616) *in vitro* correlated with constitutive MEK activation, due to suppression of PKR, so that MEK inhibition reduced virus replication by about 15-fold (49). The R3616 virus was also found to be more effective *in vivo* against tumors with high MEK activity (50). Compared to R3616, T-VEC has an additional ICP47 deletion, resulting in early Us11 expression and PKR suppression, which likely explains the favorable interaction of T-VEC with trametinib. Thus, different OV's interact with MEK inhibition in different ways that may depend on cancer cell type.

These data suggest that different OV's may enhance therapeutic responses through a variety of mechanisms.

Furthermore, it is important to point out that in our model we utilized trametinib which is a more selective MEK 1/2 inhibitor and has been previously shown to have less side effects compared to other MEK inhibitors (51). Thus, in the context of combination therapy, trametinib might provide a paradoxical improvement in therapeutic activity while limiting toxicity and, hence, promoting a more favorable therapeutic window. Another factor known to influence the replicative ability of viruses is the status of the anti-viral machinery. These include intra-cellular factors that detect viral nucleic acids and molecular elements that promote viral clearance, such as type 1 interferon, and initiate innate immune responses, such as cGAS-STING. The expression of the anti-viral machinery is typically defective in tumor cells, which adds to the ability of OV's to preferentially replicate in tumor cells (52). In our model with trametinib and T-VEC, further interrogation of the Nanostring data confirmed that MEK inhibition was associated with a decrease in anti-viral response factors *in vivo*, including STING (Tmem173) and interferon response factors (IRFs) 3 and 7. While MEK inhibition alone inhibits expression of these factors it establishes favorable intra-cellular conditions for increased viral replication. When T-VEC is added to the treatment regimen, increased viral replication drives interferon production and ultimately increases innate immune gene expression.

While MEK inhibition in tumor cells may promote apoptosis and drive immunogenic cell death, MEK inhibition may also block T cell activation (53). Thus, it may be surprising

that we demonstrated strong anti-viral and anti-tumor CD8⁺ T cell responses in our model (Figs 7 and 11). One explanation may have related to a recent finding that MEK inhibition selectively blocks activation of naïve T cells but not antigen-experienced effector T cells (16). Others have shown that MEK inhibition selectively suppresses alloreactive T cells in a model of graft-versus-host disease (GVHD), demonstrating that trametinib blocks GVHD-inducing CD8⁺ T cells but spares graft-versus-tumor (GVT)-specific CD8⁺ T cells *in vivo* (54). Thus, established tumors may contain antigen experienced T cells and, in this setting, MEK inhibition would be expected to promote T cell activation, consistent with the Nanostring data from tumor bearing mice treated with trametinib and mT-VEC. The increased expression of anti-viral machinery genes, including STING and TLRs, may also promote recruitment of anti-tumor CD8⁺ T cells as induction of these innate immune sensors has been associated with restoration of effective anti-tumor immunity (55).

Another important observation in our study was that BRAF inhibition only enhanced T-VEC oncolysis in BRAF-mutant tumor cells (Fig. 1G). In contrast, MEK inhibition improved T-VEC replication and oncolytic activity in both BRAF-mutant and BRAF wild-type cell lines (Fig. 2C, E). This suggests that MEK inhibition may be better than BRAF inhibitors in combination with HSV-based OV therapy and might be active regardless of BRAF mutation status. This will, however, require further clinical validation.

In our studies, therapeutic effectiveness was seen in both human xenograft and immune-competent melanoma models. While human melanoma cells are highly sensitive to HSV-1 infection, murine melanoma cells have been generally resistant. To our knowledge, this

is the first report demonstrating that spontaneous murine D4M3A cells are sensitive to HSV-1 infection and exhibit high levels of phosphorylated ERK. This also provides a physiologically relevant model to assess host anti-tumor immunity. We found that combination T-VEC and MEK inhibition is associated with an increased accumulation of activated CD8⁺ T cells, characterized by production of IFN- γ and Granzyme B (Fig. 7E), within the tumor microenvironment as well as a decrease in CD4⁺FoxP3⁺ regulatory T cells. We also confirmed the importance of CD8⁺ T cells through selective immune cell depletion studies. This is consistent with prior reports in melanoma patients treated with single-agent T-VEC in which injected tumors have been found to have higher numbers of MART-1-specific effector CD8⁺ T cells and decreased numbers of CD4⁺ Foxp3⁺ Tregs (36). Since HSV-1 can promote IFN production, we also found an increase in PD-1 and PD-L1 expression within the tumor microenvironment and this is likely related to the counter-regulatory induction of immune checkpoints in the setting of excessive IFN- γ (56). This comports with recent clinical data showing increased PD-L1 expression in tumors from melanoma patients treated with T-VEC and pembrolizumab (32) and provides a biologic rationale for the addition of PD-1 blockade to T-VEC and MEKi treatment, where we showed over 80% complete tumor eradication and increased survival without overt signs of toxicity. This triple drug regimen is particularly appealing since all three agents are currently FDA-approved for the treatment of melanoma, and it is consistent with recent reports suggesting MAPK pathway inhibition and PD-1/PD-L1 blockade are associated with improved therapeutic responses in pre-clinical models (16, 57).

The Batf3⁺ (CD8⁺CD103⁺) DC population was initially identified as critical for priming anti-viral CD8⁺ T cells responses (42, 58). These DCs have also recently been identified as critical for anti-tumor immunity and recruitment of lymphocytes through chemokines, such as CXCL9 (59). We demonstrated that Batf3⁺ DCs are also critical for the recruitment of CD8⁺ T cells in our melanoma model following treatment with T-VEC and trametinib. We further observed an increase in CXCL9 as evidenced by NanoString gene expression profiling. These data support a role for Batf3⁺ DCs, which likely prime both anti-herpes and anti-tumor CD8⁺ T cells. Enhanced CXCL9 expression also helps recruit effector CD8⁺ T cells into the tumor microenvironment. The antigen specificity of the CD8⁺ T cells has not been previously evaluated, but we found evidence for both viral (HSV gB-specific) and melanoma (gp100- and TRP2-specific) CD8⁺ T cell responses. This is consistent with initial viral responses and cross presentation of tumor-associated antigens (60). Antigen spreading has previously been reported as a predictive biomarker of therapeutic responses for other forms of immunotherapy, including tumor vaccines and immune checkpoint inhibitors (61, 62).

We applied an IFN- γ -regulated gene signature profile that has been associated with therapeutic responses to PD-1 blockade in patients with melanoma (44) and found a strong correlation between this gene signature and responses in mice treated with T-VEC and MEK inhibition, supporting this as a more universal profile for immunotherapy. These findings also support the ability of T-VEC and MEK inhibition to transform the tumor microenvironment into a more lymphocyte-predominant state that likely favors immune-mediated regression with immunotherapy. We were also able to identify a strong

correlation with a 5-gene T cell activation signature supporting the importance of effector CD8⁺ T cell function in the anti-tumor activity of the combination treatment and highlighting a potential predictive biomarker for further clinical validation in oncolytic virus trials. The NanoString analysis was also interesting in that minor variations were observed in selected genes and gene families suggesting potential pathways of drug resistance, which remain largely undefined for OV treatment. Finally, we added anti-PD-1 therapy to the T-VEC + MEKi combination based on gene expression data and FACS analysis showing upregulation of PD-1 and PD-L1 during therapy (Fig. 15D), which produced a superior survival benefit (Fig. 17C). This was associated with increased granzyme B-positive cytolytic CD8⁺ T cells and proliferating CD8⁺ T cells (Fig. 17F) in the tumors. Our observations support a mechanism where combination of T-VEC + MEKi can enhance immune cell infiltration and augment antitumor responses but eventually leads to upregulation of PD-1 and PD-L1, which can suppress anti-tumor immunity. Addition of PD-1 blockade to T-VEC + MEKi further augments anti-cancer immunity. We also observed a similar therapeutic effect for triple combination in the genetically distinct BALB/c murine CT26 model suggesting that this approach may be broadly applicable for solid tumors beyond melanoma.

Finally, our data may also have implications for other microbial pathogens being evaluated as cancer therapeutics. In a patient-derived orthotopic xenograft model, treatment with *Salmonella typhimurium* combined with vemurafenib or trametinib resulted in improved therapeutic responses in a BRAF V600E mutated melanoma (63). In a syngeneic pancreatic cancer orthotopic murine model, *S. typhimurium* was also associated with recruitment of

CD8⁺ T cells into the tumor microenvironment. In addition, *S. typhimurium* has shown enhanced therapeutic benefit when combined with cytotoxic chemotherapy (64, 65). Recent studies using non-oncogenic viruses such as influenza have shown to influence anti-tumor immune responses (66). Thus, it may be intriguing to test oncolytic viruses, such as T-VEC with other targeted therapies and cytotoxic chemotherapy to further optimize therapeutic potential.

In summary, we evaluated the combination of MAPK inhibition and T-VEC in murine and human melanoma cell lines and found an unexpected synergistic effect between T-VEC and MEK inhibition regardless of BRAF mutation status. The combination was associated with therapeutic activity in human xenograft and immune competent murine melanoma models, as well as in the CT26 colon carcinoma model. Therapeutic responses are associated with induction of viral- and tumor-specific CD8⁺ T cells and immunologic memory. Combination treatment also induced an interferon- γ -related inflammatory gene signature, which resulted in increased expression of PD-L1 so that therapeutic responses could be further improved by addition of anti-PD-1 therapy. In our studies, we did not observe overt signs of toxicity in mice supporting a more favorable therapeutic window even with triple combination therapy, although clinical confirmation is needed. Collectively, these data provide pre-clinical rationale for triple combination treatment of T-VEC, MEK inhibition and PD-1 blockade in patients with melanoma.

CHAPTER THREE: RESULTS Section:2

Oncolytic virus immunotherapy induces immunogenic cell death and overcomes STING deficiency in melanoma

RATIONALE:

Tumor immunotherapy has changed the therapeutic landscape for an increasing number of patients with cancer (1). Yet, many patients do not respond to treatment and the mechanisms of innate and acquired drug resistance are incompletely understood (2). Solid tumors are generally characterized by the presence or absence of tumor-infiltrating lymphocytes (3). Indeed, studies in metastatic melanoma patients treated with programmed cell death 1 (PD-1) inhibitors revealed an association between T-cell infiltration and clinical response to immune checkpoint blockade (4). The homeostatic mechanisms regulating the development of this so-called T cell-inflamed tumor microenvironment are being elucidated and appear to depend on patterns of intracellular signaling within tumor cells as well as innate features of the host immune system. The presence of high tumor cell mutation burden, enriched neoantigen T cell repertoire, availability of tissue resident basic leucine zipper ATF-like transcription factor 3 (Batf3)⁺ dendritic cells (DCs) and expression of an interferon-related pro-inflammatory gene expression profile have correlated with improved therapeutic responses to immunotherapy (5-9).

Recently, the cyclic guanosine monophosphate (GMP)–adenosine monophosphate (AMP) synthase (cGAS) and stimulatory of interferon genes (STING) complex has been implicated as a key intracellular regulator of host T cell recruitment to the tumor

microenvironment in melanoma (10). cGAS is a DNA sensor that responds to genotoxic cell stress by binding to abnormal DNA in neoplastic cells and activating STING, which serves as an adaptor protein that triggers innate immunity through type I interferon gene expression, release of chemokines CXCL9 and CXCL10, and ultimately recruitment of T cells (10, 11). While cGAS-STING signaling explains the presence of tumor-infiltrating T cells, this pathway also enhances expression of several counter-regulatory immune parameters, including expression of PD-1 ligand 1 (PD-L1), accumulation of CD4⁺FoxP3⁺ regulatory T cells and production of indoleamine 2,3-dioxygenase (IDO), all factors that inhibit host anti-tumor immunity (6, 12). Thus, effective immunotherapy requires both T cell recruitment to the tumor microenvironment and suppression of the homeostatic counter-regulatory pathways. This explains why the presence of T cells, *per se*, is insufficient to mediate tumor regression in the absence of immune checkpoint inhibition. In addition, re-establishing cGAS-STING activation in tumors with deficient type 1 interferon responses has been suggested as an important strategy for converting lymphoid-deficient tumors (i.e., “cold” tumors) into T cell-inflamed tumors (i.e., “hot” tumors)(13, 14).

Oncolytic viruses are viral vectors that preferentially replicate in tumor cells, inducing immunogenic cell death (ICD) and promoting host anti-tumor immune responses (13). The preferential replication in tumor cells is based on several features, including deficiencies in tumor cell anti-viral machinery elements and defective type 1 interferon signaling as compared to normal, non-neoplastic cells (15). Additionally, oncolytic viruses are thought to enhance ICD through release of danger-associated molecular pattern (DAMP) factors

and soluble tumor-associated antigens that cooperate to induce innate and adaptive immune responses, although this has not been confirmed for most oncolytic viruses (13). The ability of oncolytic viruses to recruit T cells to the tumor microenvironment and promote ICD with release of tumor-associated antigens suggests that oncolytic immunotherapy is especially well suited for converting lymphoid-deficient tumors into T cell-inflamed tumor microenvironments, which should further enhance systemic immunotherapy (16).

Thus, in this set of experiments we sought to explore the molecular factors involved with T-VEC-mediated ICD in melanoma cells and determine which intracellular factors are important for promoting viral replication and promoting anti-tumor immunity. We hypothesized that T-VEC would induce ICD through release of defined DAMPs and would promote T cell recruitment to established melanomas through type 1 interferon-related factors, including CXCL9 and CXCL10, as well as a pro-inflammatory gene signature profile. In addition, we found that specific components of the anti-viral machinery, such as STING, were critical for both T-VEC permissive replication and induction of host anti-tumor immunity. Tumors which have low levels of STING show minimal response to anti-PD-1 therapy but respond to T-VEC treatment. Further, T-VEC treatment induced a systemic anti-tumor specific CD8⁺ T cell response and increased immune inflammatory gene signature both in injected and contralateral tumors, leading to regression of un-injected tumors. These data support the role of T-VEC in overcoming STING deficiency in melanoma cells and confirms how T-VEC mediates melanoma ICD and triggers innate and adaptive anti-tumor immunity.

Human melanoma cell lines are permissive to T-VEC infection and oncolysis

We first sought to investigate the ability of T-VEC to kill a panel of melanoma cell lines included in the NCI60 cell line list. Melanoma cell lines were seeded in 96-well plates and treated with T-VEC at the indicated multiplicity of infection (MOI) and an MTS assay was performed on infected SK-MEL-2, SK-MEL-5, SK-MEL-28, M14 and LOX-IMVI cells 5 days after T-VEC infection to measure cell viability (Fig. 20A-E). The SK-MEL-5 cell line (Fig. 20B) exhibited the highest sensitivity to T-VEC induced death, while LOX-IMVI cells (Fig. 20E) were the least sensitive. The sensitivity of LOX-IMVI, M14, and SK-MEL cell lines to T-VEC infection was significantly different at low doses (0.03 MOI) (Fig. 20F). Thus, we confirmed that melanoma cells exhibited differential sensitivity to T-VEC killing, the LOX-IMVI cell line was relatively resistant to T-VEC-mediated killing. We next investigated the expression levels of several distinct entry receptors, including gD-binding herpes virus entry mediator (HVEM) and nectin-1, and low affinity nectin-2. While most cell lines seem to express one or more of the entry receptors (Fig. 21). However, the level of expression of individual receptors was variable in different cell line, with highly sensitive SK-MEL-5 cells (Fig. 21) expressing the highest levels of HVEM and nectin-1 and LOX-IMVI cell expressing relatively lower levels of major entry receptors. These data show that there is variable expression of HSV-1 cell surface receptor expression across several melanoma cell lines.

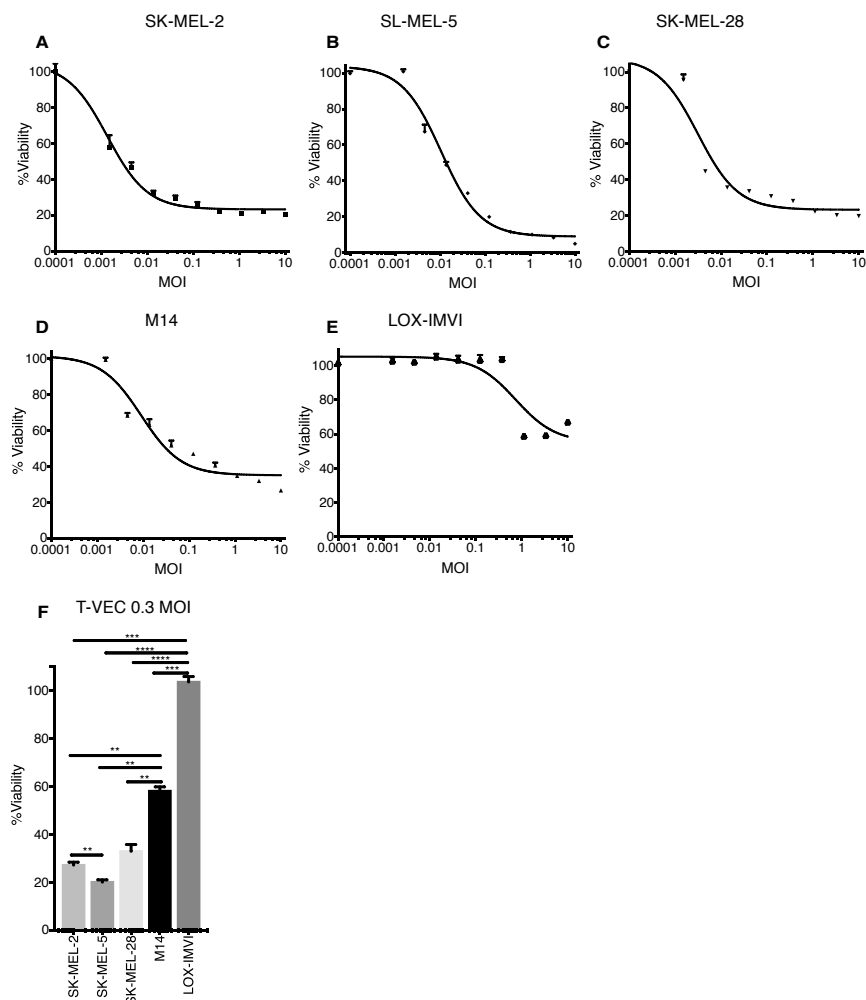


Figure 20. Human melanoma cell lines exhibit differential sensitivity to T-VEC-mediated lysis *in vitro*.

Cells (5×10^3) were seeded on 96-well plates and treated with T-VEC at the indicated multiplicity of infection (MOI) and MTS assay performed on day 5 post T-VEC infection to measure cell viability of (A) SK-MEL-2 (B) SK-MEL-5 (C) SK-MEL-28 (D) M14 and (E) LOX-IMVI at 5 days post T-VEC treatment. (F) Cell viability at 5 days post 0.3 MOI T-VEC treatment for selected cell lines. Each experiment was performed two or more times and similar results were obtained. * denotes statistical significance as per Methods

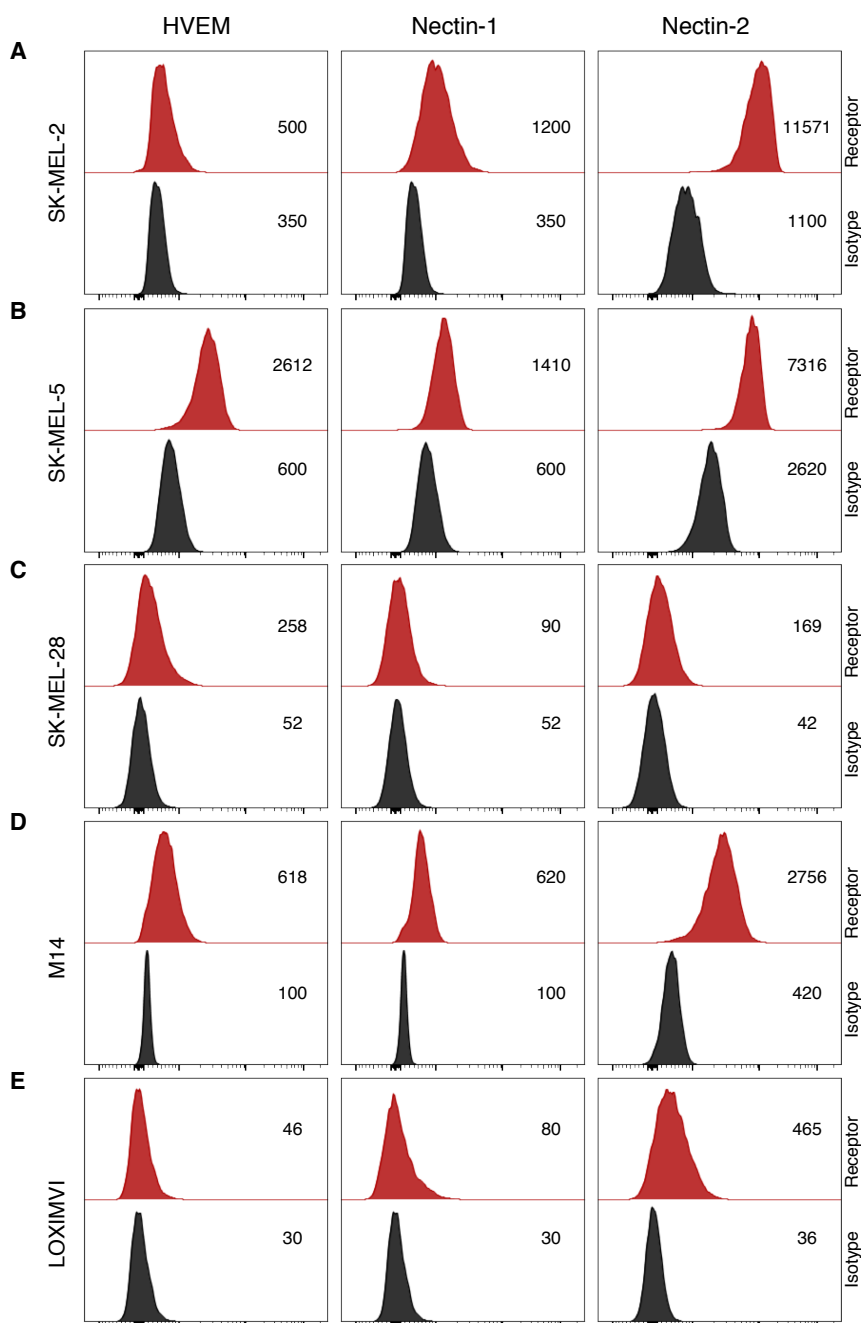


Figure 21. Human melanoma cell lines exhibit differential expression of HSV-1 cell entry receptors.

Cells (1×10^6) were collected from cultures and stained using antibodies against Herpes Virus Entry Mediator (HVEM), Nectin-1 and Nectin-2. Histograms show mean fluorescence intensity (MFI) levels of receptor expression on (A) SK-MEL-2 (B) SK-MEL-5 (C) SK-MEL-28 (D) M14 and (E) LOXIMVI. This experiment was performed two or more times and similar results were obtained.

T-VEC infection induces immunogenic cell death and DAMP release from melanoma cell lines

The induction of immunogenic cell death is associated with release of damage-associated molecular patterns (DAMPs). Although generally accepted that oncolytic viruses induce DAMP release, we sought to test whether T-VEC promoted DAMP release following infection. To test this, we selected the moderately sensitive SK-MEL-28 cell line for analysis, and infected cell monolayers with T-VEC at MOI of 1 (or mock infected) and collected cell supernatants at 24 and 48 hours after infection. First, the levels of the high mobility group box 1 (HMGB1) was assessed by ELISA and was significantly increased at 24 hours compared to mock infected cells and increased even further at 48 hours (Fig. 22A). Next, the levels of adenosine triphosphate (ATP) were assessed in cell supernatants and found to be significantly elevated at 24 hours compared to mock infected cells and levels increased further at 48 hours (Fig. 22B). Finally, the presence of ecto-calreticulin was evaluated at 24 hours and presence of ecto-calreticulin was noted by immunostaining with an antibody against calreticulin (CALR; green) and a nuclear stain (DAPI; blue) as shown in Fig. 22C. These data confirm that T-VEC induces immunogenic cell death and release of DAMPs during lysis of melanoma tumor cells.

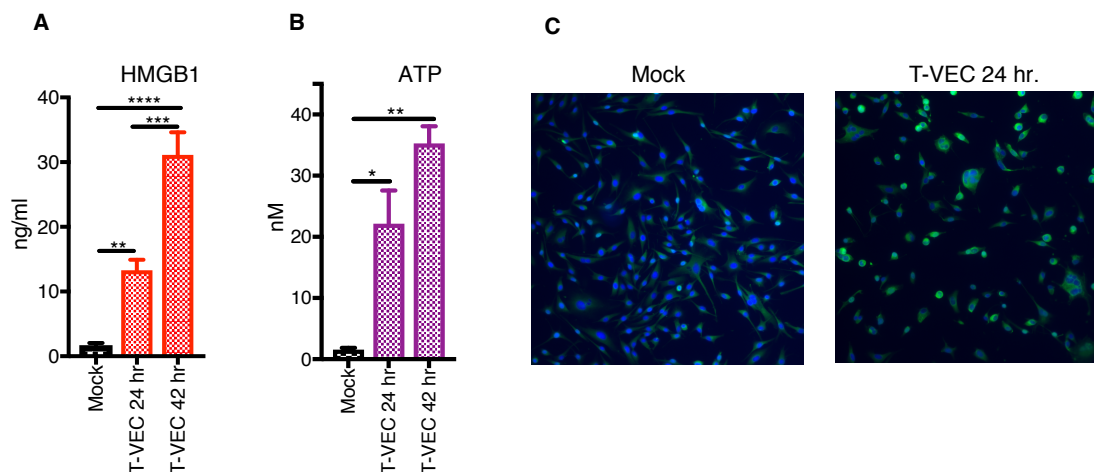


Figure 22. T-VEC induces immunogenic cell death and release of DAMPs.

(A-B) SK-MEL-28 cells (5×10^5) were mock infected or treated with 1 MOI T-VEC and cell supernatants collected at 24 and 48 hrs. post infection. (A) Bar graph indicating levels of high mobility group box 1 (HMGB1) in cell supernatants at indicated times. (B) Bar graph indicating the level of adenosine triphosphate (ATP) in cell supernatants at indicated times. (C) SK-MEL-28 cells (1×10^5) were plated in a 6 well chamber slide and treated the next day with phosphate buffer saline (mock; left panel) or 1 MOI of T-VEC (right panel) and stained with anti-calreticulin (CALR) antibody (green) and nuclear stain (DAPI; blue) 24 hrs. post T-VEC treatment. Each experiment was performed two or more times with similar results. Data are presented as mean \pm SEM and statistical differences between groups was measured by student's t test. * $p < 0.05$, ** $p < 0.01$, *** $p < 0.001$, **** $p < 0.0001$.

Anti-viral machinery elements are deficient in some melanoma cell lines

The preferential replication of oncolytic viruses in tumor cells occurs, in part, because of deficiencies in anti-viral machinery in tumor cells. The characterization of the anti-viral machinery in melanoma cells, however, has not been extensively evaluated. We hypothesized that alterations in anti-viral machinery proteins were necessary for T-VEC replication in melanoma cell lines. HSV-1 is detected in host cells by two major anti-viral pathways, the Protein Kinase R (PKR) and cGAS / STING pathways (24). The levels of PKR and cGAS/STING expression in the various melanoma cell lines was determined and compared to T-VEC cytolytic activity. Using Western blot analysis, we observed that the SK-MEL-5 cell line exhibited undetectable expression of PKR, STING and cGAS proteins (Fig 23A-B), whereas the LOX-IMVI cells exhibited the highest protein levels of PKR and STING. The undetectable PKR and cGAS/STING in the SK-MEL-5 cell line and low levels of STING in SK-MEL-2 was associated with increased sensitivity to T-VEC-mediated lysis (Fig 20). In contrast, the PKR and cGAS/STING high LOX-IMVI cells were relatively resistant to T-VEC-mediated lysis and required MOI of 1 or greater for activity (Fig 20E).

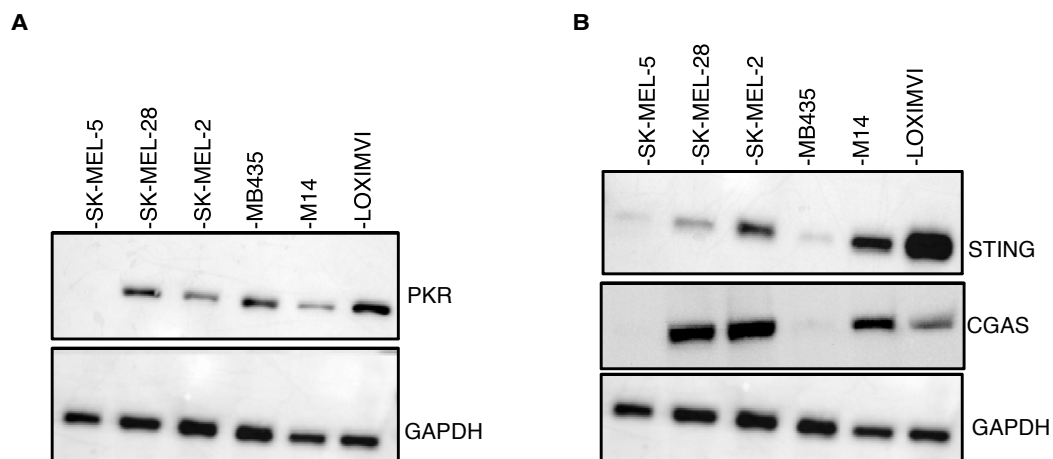


Figure 23. Melanoma cell lines display variable levels of anti-viral machinery elements.

(A-B) Total cell lysates were collected from the indicated cell lines (2×10^6) and 40 μg of lysate was loaded onto an SDS-PAGE gel and transferred to a PVDF membrane. Antibodies against protein kinase R (PKR), cyclic-GMP-AMP synthase (cGAS) and stimulator of interferon genes (STING) were used in immunoblotting assay as described in Methods. Immunoblots of PKR **(A)**, cGAS and STING **(B)**. GAPDH is loading control.

STING contributes to T-VEC resistance

In order to confirm which anti-viral machinery factor elements was responsible for resistance to T-VEC-mediated lysis, the LOX-IMVI cell line was used to generate a series of gene knockout clones. First, a LOX-IMVI-shPKR cell line was generated and clones exhibited low levels of PKR expression compared to LOX-IMVI-shScr (Fig 24A-left panel). However, no significant differences in T-VEC sensitivity were observed between LOX-IMVI shScr and LOX-IMVI-shPKR cells (Fig 24A-right panel). To test the role of STING in mediating resistance to T-VEC sensitivity, we generated LOXIMVI-shSTING and CRISPR knock-out cell lines. ShSTING reduced STING protein levels by over 50% (Fig 24B-left panel) and had only a modest effect on T-VEC cytotoxicity compared to the scrambled control (Fig 24B-right panel). Using CRISPR-Cas9 technology we generated 3 clones of LOX-IMVI cells, with clone1 and clone3 exhibiting a complete knock out of STING protein (Fig 24C). Both these clones, but not clone2 or scrambled control, were now sensitive to T-VEC at higher MOIs (Fig 24D). Cytosolic and viral DNA is detected by cGAS and other synthases which eventually leads to STING activation (25). Thus, to determine if cGAS is involved in T-VEC resistance in the LOX-IMVI cell line, we generated 3 clones of LOX-IMVI cells with cGAS knockout using CRISPR-Cas9, with complete knockout in all the three clones (Fig 24E). However, all 3 clones retained resistance to T-VEC (Fig 24F). These data collectively suggest that STING, and not cGAS or PKR, contributes to resistance to T-VEC-mediated killing in LOX-IMVI melanoma cells.

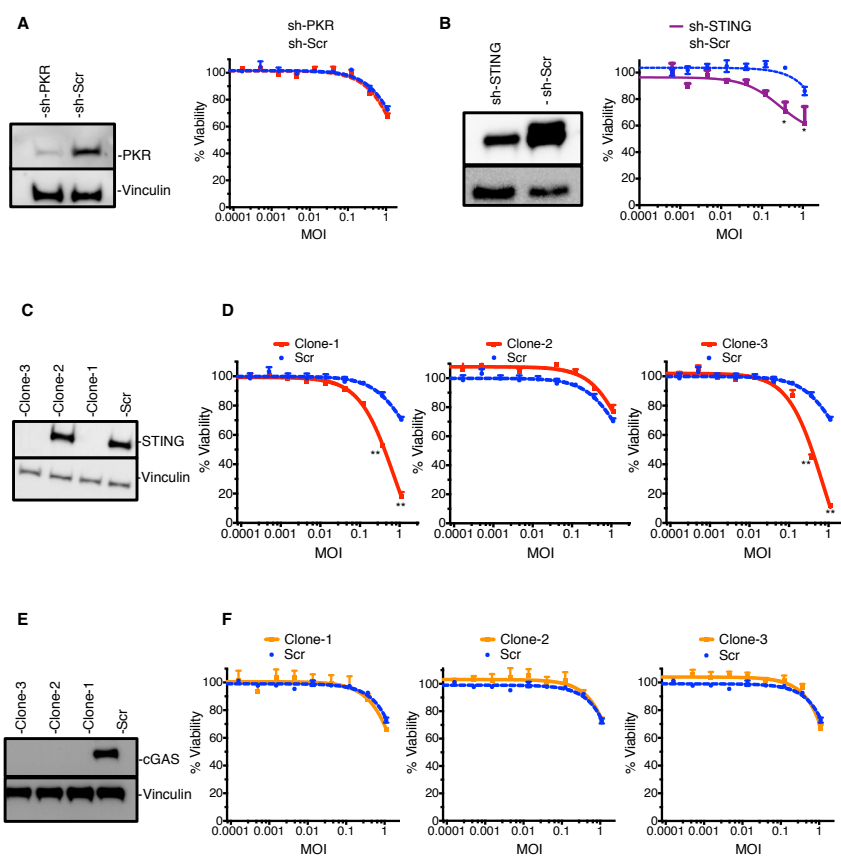


Figure 24. STING contributes to resistance to T-VEC-mediated lysis in melanoma cells.

(A) Immunoblot showing PKR protein levels from LOXIMVI-scr and LOXIMVI-shPKR cell lysates (left panel) and cell viability 5 days post T-VEC treatment (right panel). (B) Immunoblot showing STING protein levels from LOXIMVI-scr and LOXIMVI-shSTING cell lysates (left panel) and cell viability 5 days post T-VEC treatment (right panel). (C) Immunoblot showing STING protein levels from LOXIMVI-CRISPR-scr and LOXIMVI-CRISPR-STING clones 1, 2 and 3 cell lysates. (D) MTS assay measuring cell viability of LOXIMVI-CRISPR-scr and LOXIMVI-CRISPR-STING clones 1, 2 and 3 cell lines at 5 days post T-VEC treatment. (E) Immunoblot showing cGAS protein levels from LOXIMVI-CRISPR-scr and LOXIMVI-CRISPR-cGAS clones 1, 2 and 3 cell lysates. Vinculin is loading control. (F) MTS assay measuring cell viability of LOXIMVI-CRISPR-scr and LOXIMVI-CRISPR-cGAS clones 1, 2 and 3 cell lines at 5 days post T-VEC treatment. Each experiment was performed two or more times with similar results. Data are presented as mean \pm SEM and statistical differences between groups was measured by student's t test. ** $p < 0.01$, *** $p < 0.001$, **** $p < 0.0001$.

STING deficiency alters cytokine release induced by T-VEC infection

We demonstrated that loss of STING can increase sensitivity to T-VEC in LOX-IMVI cells. Since activation of STING leads to the release of several cytokines, including type 1 interferons and tumor necrosis factor alpha (TNF α) secretion that mediate anti-viral responses (26), we tested the hypothesis that STING expression was required for cytokine release in the LOX-IMVI cell line following T-VEC infection. To observe the changes in cytokine profile, we treated LOX-IMVI CRISPR-scr and LOXIMVI-CRISPR-STING-clone1 cells with T-VEC (MOI 1) and collected supernatants 24 hours later. We utilized a multiplex human anti-viral immune response array to determine the cytokine profile. There was a significant increase in levels of GM-CSF during T-VEC treatment in LOXIMVI-CRISPR-STING-clone 1 (Fig 25A), due to expression of GM-CSF by the virus and indicative of better viral replication. T-VEC also induced TNF α , which was reduced to mock-infection levels in STING knockout cells (Fig 25B). Finally, we saw a significant increase in levels of interleukin 1 beta (IL-1 β) after T-VEC, which was further increased in the knockout cells (Fig 25C). STING expression appears to be required for production of cytokines associated with inflammation and induction of innate immunity following T-VEC infection of melanoma cell lines.

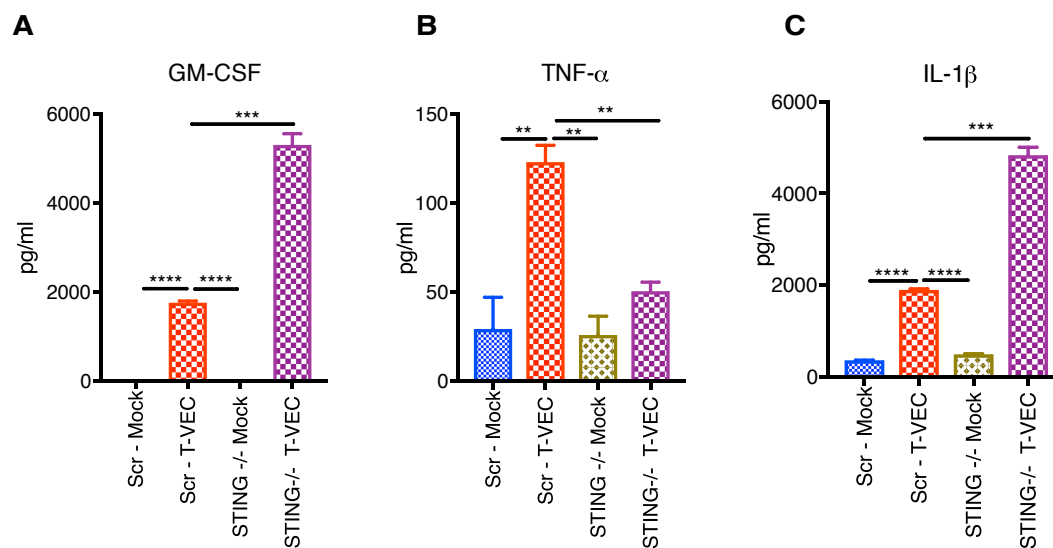


Figure 25. STING deficiency alters cytokine profiles following T-VEC treatment.

LOXIMVI-CRISPR-scr and LOXIMVI-CRISPR-cGAS clone 1 cells (5×10^5) were plated in a six well plates and infected with 1 MOI of T-VEC or mock. After 24 hrs., cell supernatants were collected and measured for cytokine release as described in Methods. Bar graphs show the levels of GM-CSF (**A**), TNF α (**B**) and IL-1 β (**C**). Each experiment was performed two or more times with similar results. Data are presented as mean \pm SEM and statistical differences between groups was measured by student's t test. ** $p < 0.01$, *** $p < 0.001$, **** $p < 0.0001$.

T-VEC treatment induces tumor regression in a STING-deficient murine melanoma model

STING has been previously implicated as a critical mediator of anti-tumor immunity in melanoma by recruiting T cells to the tumor microenvironment (10). Since T-VEC was shown to replicate more efficiently in STING-deficient cells, we sought to determine if T-VEC could overcome STING deficiency and enhance anti-tumor immunity *in vivo* compared to checkpoint blockade. To test this, we implanted STING^{lo} expressing BRAF V600E mutant D4M3A melanoma tumors in C57/BL6J mice (Fig. 26). Once tumors were palpable, mice were mock-treated, treated with T-VEC or treated with murine α PD-1 antibody as described in Methods. STING^{lo} D4M3A melanoma tumors did not respond to PD-1 blockade as no significant differences were observed between mock treated mice (Fig. 27A) and mice treated with PD-1 blockade (Fig. 27B). This was consistent with previous reports showing D4M3A cell line does not respond to PD-1 blockade (27). We did, however, observe significant tumor growth reduction in T-VEC treated mice (Fig. 27C). T-VEC treatment completely eliminated tumors in 1/5 treated mice, while treatment with α PD-1 antibody had no effect. To determine if T-VEC treatment was associated with systemic anti-tumor activity, we implanted D4M3A tumors in both the right and left flanks of C57/BL6J mice. T-VEC was injected in the right flank palpable tumors according to the study schema shown in Fig. 28A. T-VEC treatment significantly reduced tumor volume in both injected and un-injected contralateral tumors compared to mock treated mice (Fig 28B-C). T-VEC was associated with complete regression in 3/9 injected tumors and 1/9 un-injected tumors. T-VEC treatment also significantly enhanced survival of mice

compared to mock treatment (Fig 28C). These data indicate that T-VEC induced anti-tumor activity *in vivo* in STING^{lo} melanoma tumors that are resistant to PD-1 blockade.

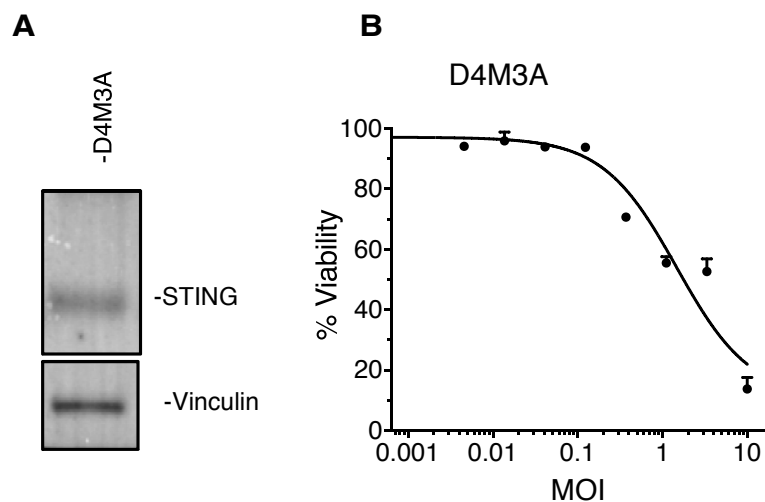


Figure 26. D4M3A cells exhibit low levels of STING protein expression and are susceptible to T-VEC infection.

(A) Immunoblot showing the levels of STING expression in D4M3A cell line. (B) MTS assay measuring cell viability of D4M3A cells at 74 hrs. post T-VEC treatment. Each experiment was performed at least twice.

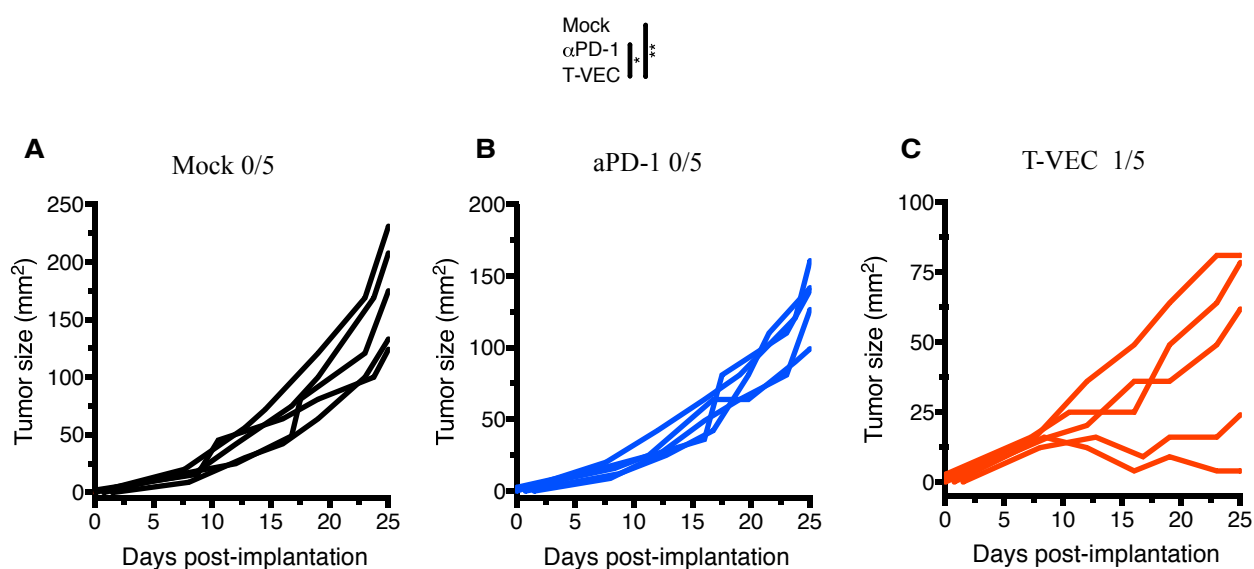


Figure 27. D4M3A cells do not respond to PD-1 blockade but are sensitive to T-VEC treatment.

(A-C) B6 mice ($n = 5/\text{group}$) were implanted subcutaneously in the right flank with 3×10^5 D4M3A murine melanoma cells on day 0 and treated either with 6×10^6 plaque forming units of T-VEC or mock at days 8, 10, 12, and 14. $\alpha\text{PD-1}$ group received 15 mg/kg of $\alpha\text{PD-1}$ antibody (clone: RMP1-14, 7.5 mg/kg) or Mock group received rat IgG2a isotype control via subcutaneous (s.c.) injection at days 8, 10, 12, and 14. (A) Individual tumor growth curves of mock treated mice. (B) Individual tumor growth curves of $\alpha\text{PD-1}$ antibody treated mice. (C) Individual tumor growth curves of T-VEC treated mice. Each experiment is performed two or more times with similar results. statistical differences between groups was measured at day 23 by one-way ANOVA. * $p < 0.05$, ** $p < 0.01$. Only significant differences are indicated.

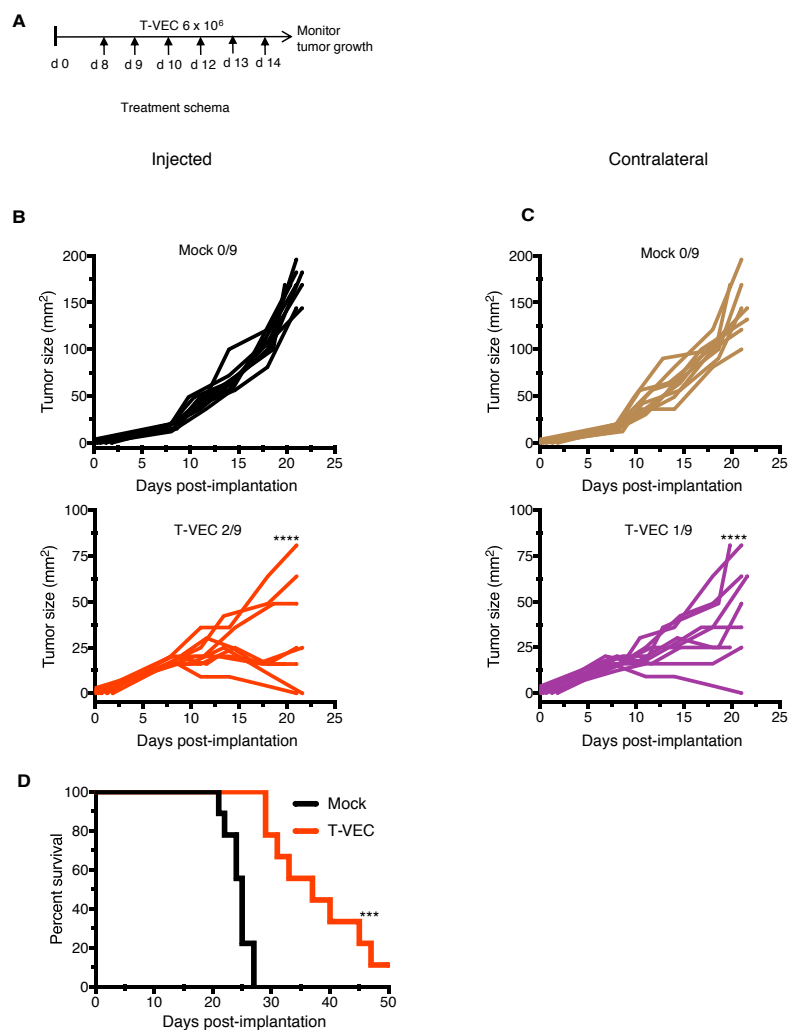


Figure 28. T-VEC has therapeutic activity in STING deficient melanoma *in vivo*.

(A) Schema of treatment studies *in vivo*. **(B)** Individual tumor growth curves of injected tumors of mice treated with mock (top panel; black curves) or T-VEC (bottom panel; red curves). **(C)** Individual tumor growth curves of contralateral tumors of mock-treated (top panel; brown curves) or T-VEC treated mice (bottom panel; purple curves). Mean tumor area of Mock injected (169.4 mm^2) was compared to mean tumor area of Mock un-injected (144 mm^2), mean tumor area of T-VEC-injected (15.33 mm^2) and mean tumor area of T-VEC-un-injected (47 mm^2) at day 21 **(D)** Kaplan-Meier survival curves from animals. Each experiment was performed twice with similar results.

T-VEC induces anti-viral and systemic anti-tumor immunity in STING deficient melanoma

We investigated whether T-VEC treatment of STING^{lo} melanoma cells induced viral or tumor-associated antigen-specific CD8⁺ T cell responses. We implanted D4M3A melanoma tumors in C57BL/6J mice and were treated as described in Methods. Tumors were harvested on day 29 and flow cytometry analysis revealed significant increases in the frequency of CD3⁺ and CD8⁺ T cells in both injected (Fig 29A) and contralateral (un-injected) tumors (Fig 29B) following T-VEC treatment. We also observed a significant increase in levels of melanoma antigen gp100- and TRP2-specific, and HSV-1 glycoprotein-B (gB)-specific CD8⁺ T cells in injected (Fig 29C) and contralateral tumors (Fig 29D). We next compared the levels of antigen specific CD8⁺ T cells in the injected vs. contralateral tumors of individual mice and observed that melanoma antigen specific CD8⁺ T cells were present in relatively higher numbers in injected lesions compared to contralateral tumors while the levels of HSV-1 gB-specific CD8⁺ T were similar (Fig 29E). The level of PD-L1 expression on tumor cells and percent CD45⁺ cells expressing PD-1 was significantly higher in injected compared to un-injected tumors (Fig 29F). These data suggest that T-VEC treatment induces both melanoma-specific and HSV-1-specific CD8⁺ T cells in injected and contralateral STING^{lo} melanoma tumors.

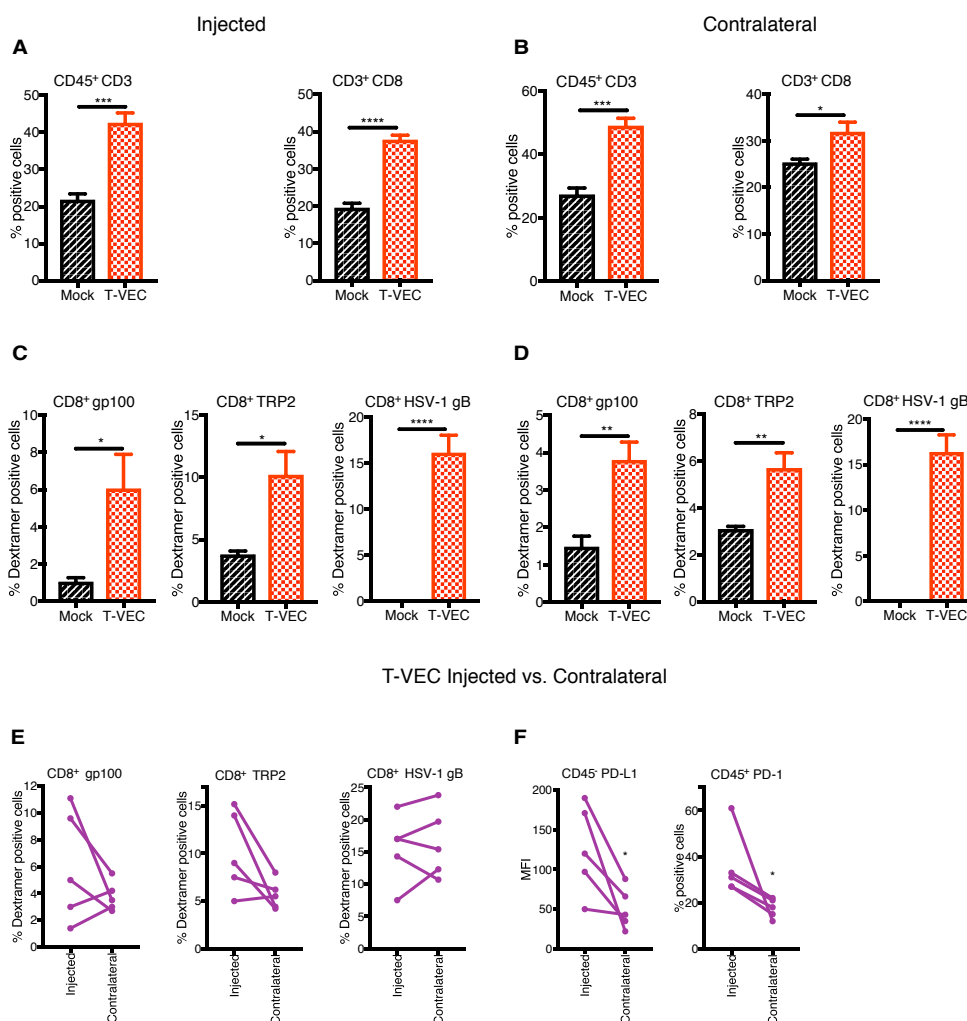


Figure 29. T-VEC treatment induces host immunity in STING-deficient melanoma model.

Mice ($n = 5/\text{group}$) were implanted subcutaneously in the right flank with 3×10^5 D4M3A cells on day 0 and treated with 6×10^6 pfu T-VEC or mock injection on days 17, 20, 23, 25 and 27. Tumors were harvested on day 29 and flow cytometry was performed using fluorochrome-conjugated antibodies as described in Methods. **(A)** Bar graph indicating percentage $\text{CD45}^+\text{CD3}^+$ T cells and $\text{CD3}^+\text{CD8}^+$ T cells from T-VEC and mock injected tumors and **(B)** contralateral tumors. **(C)** Bar graph indicating the percentage of CD8^+ T cells specific for murine gp100 or TRP2 and HSV-1 glycoprotein B (HSV-1 gB), respectively, from T-VEC and mock injected tumors and **(D)** contralateral tumors. **(E)** Line graphs indicating percent CD8^+ T cells specific for indicated antigens from either T-VEC injected or contralateral tumors. **(F)** PD-L1 expression of CD45^+ cells (left panel) and percent of $\text{CD45}^+\text{PD-1}^+$ cells (right panel) from T-VEC injected and contralateral tumors. Each experiment was performed two or more times with similar results. Data are presented as mean \pm SEM and statistical differences between groups was measured by student's t test. *** $p < 0.001$, **** $p < 0.0001$.

To further evaluate T-VEC induced systemic pro-inflammatory responses in STING^{lo} melanoma, gene expression analysis was performed on RNA derived from tumors treated with T-VEC. The Nanostring Pan Cancer immune gene expression panel was applied to tumors derived from both injected and contralateral tumor sites (Fig. 30). Gene expression analysis revealed upregulation of genes involved in: antigen presentation (*H2-DMb-2*, *H2-Ab1*), costimulation (*CD80*, *ICOS*), chemokines (*Cxcl10*, *Cxc19*), and genes involved with CD8⁺ T cell activation (*CD8 α* , *GZMa*, *GZMb*, and *Pdcd1*) in both injected (Fig 31A) and un-injected contralateral tumors (Fig 31B). We also analyzed gene expression changes in commonly involved immune response pathways and found that T-VEC treatment caused pronounced upregulation of these genes in injected lesions (Fig 31C), with a smaller increase in the contralateral tumors (Fig 31D). Together, these data support the ability of T-VEC to induce systemic inflammation and induce the recruitment of viral-specific and melanoma-associated antigen specific T cells to melanoma cells even when intracellular STING is low.

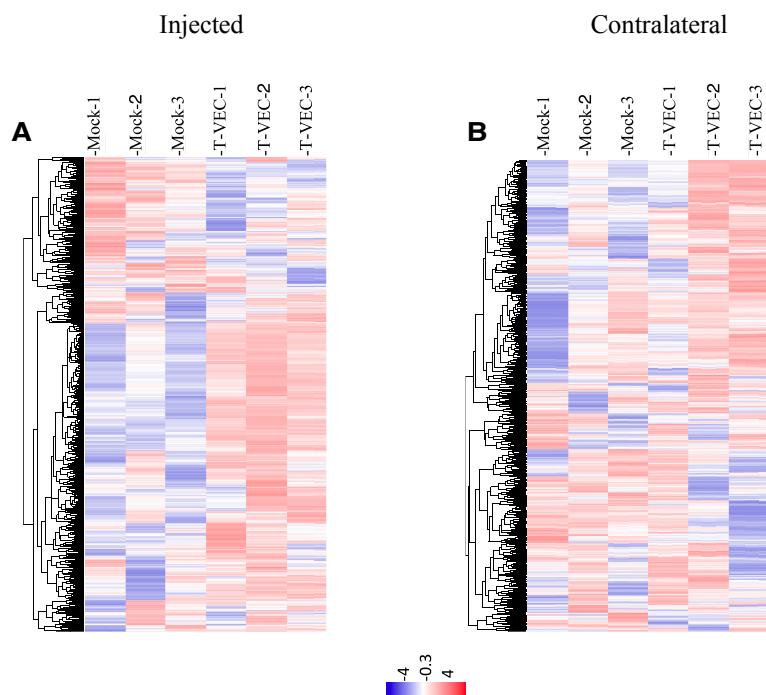


Figure 30. Global gene expression of injected and contralateral tumors during T-VEC treatment.

(A-B) C57BL/6J mice ($n = 3/\text{group}$) were implanted subcutaneously in the right flank with 3×10^5 D4M3A murine melanoma cells on day 0 and treated either with 6×10^6 plaque forming units of T-VEC or mock at days 17, 20, 23, 25 and 27. Tumors were harvested on day 29 and total RNA was isolated using a Qiagen RNAeasy kit. Gene expression analysis was performed using the NanoString PanCancer Immune panel. (A) Heat map indicating the global gene expression profile changes in T-VEC injected tumors and (B) contralateral tumors.

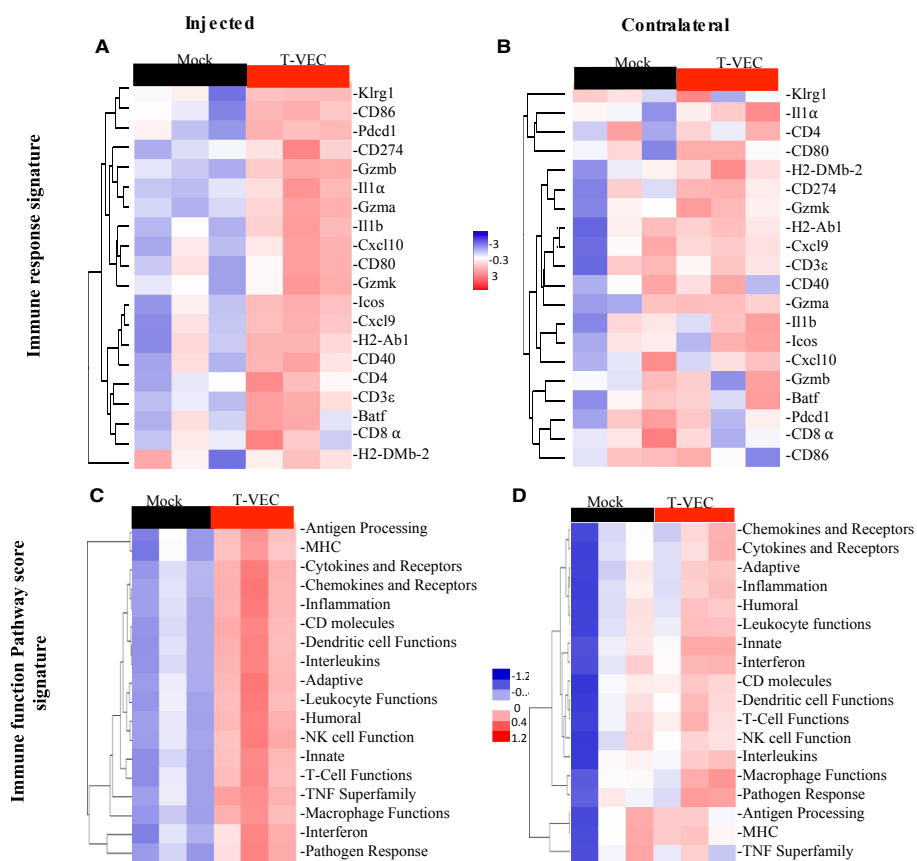


Figure 31. T-VEC treatment induces a systemic pro-inflammatory gene signature in STING-deficient tumors *in vivo*.

Mice (n = 3/group) were treated as outlined in Fig 28. Tumors were harvested on day 29 and total RNA was isolated and Nano string analysis performed using the pan cancer immune gene profiling kit as described in Methods. **(A)** Heatmap showing gene expression levels of genes involved in Immune response signature in the injected tumors and **(B)** contralateral tumors. **(C)** Heatmap showing Immune function Pathway score signature in the injected tumors and **(D)** contralateral tumors.

DISCUSSION

Oncolytic viruses are emerging as a new class of immunotherapeutic agents for cancer treatment. Clinical proof-of-concept has been provided in patients with advanced melanoma who demonstrated improved objective and durable response rates when treated with talimogene laherparepvec (T-VEC), an oncolytic HSV-1 encoding GM-CSF (17). In addition, there is emerging evidence that combination of T-VEC and immune checkpoint blockade may be beneficial with improved therapeutic responses without increased toxicity (28) (16). While these clinical data have been encouraging, the basic mechanisms by which T-VEC, and other oncolytic viruses, mediate anti-tumor activity is incompletely understood. We have previously reported that T-VEC also induces tumor cell apoptosis, following infection (21). In this report, we sought to further investigate which intracellular factors might influence T-VEC permissiveness in melanoma cells, and whether T-VEC can induce antitumor immune responses in tumors with low expression of STING, which usually correlates to lack of response to immunotherapies(10).

Pre-clinical studies have suggested a multi-modal mechanism of action in which oncolytic viruses promote tumor regression through direct cell lysis and secondary induction of host anti-tumor immunity (13). Our data confirms that T-VEC does induce Immunogenic cell death (ICD) with corresponding release of danger associated molecular pattern (DAMP) factors, including HMGB1, ATP and ecto-calreticulin. While traditional ICD has focused on DAMP release, we also demonstrated that T-VEC could induce an immune response *in vitro* and *in vivo*. This included evidence of TNF- α production (29), as well as infiltration

of CD8⁺ T cells and increased pro-inflammatory gene expression in both injected and un-injected tumors in mice. We also demonstrated an increase in PD-1 expression following *in vivo* treatment with T-VEC, highlighting the natural counter-regulatory mechanism wherein viral-induced type 1 interferons inhibit T cells through engagement of the PD-1/PD-L1 pathway. While this may limit therapeutic activity of oncolytic viruses, it also provides strong biologic rationale for combining T-VEC with PD-1/PD-L1 blockade. While these data are important for understanding how T-VEC contributes to the anti-tumor response, other oncolytic viruses may mediate host anti-tumor immunity through other mechanisms. For example, in a recent report of an oncolytic Newcastle disease virus (NDV) in lung cancer cell lines, NDV induced DAMP release as seen with T-VEC but autophagy also played an important role in mediating cell death (30). As the field develops, it will be critical to confirm how tumor cells die with each oncolytic virus to better identify relevant clinical indications and optimize combination approaches. We also explored the levels of various HSV-1 cell surface entry receptors. The expression of viral entry receptors across cancer cells and the relative contribution of receptor levels to therapeutic effectiveness of T-VEC is not well known. In screening a panel of melanoma cell lines with differential sensitivity to T-VEC-mediated killing, we found variable expression of the major HSV-1 entry receptors, HVEM and nectin-1, but expression of at least one receptor on all cell lines, except possibly LOXIMVI. Although further confirmation of cell entry receptors on fresh melanoma specimens would be helpful, it does not appear that lack of cell entry receptor expression appreciably inhibits T-VEC infection.

The initial response to HSV-1 infection occurs when viral DNA is “sensed” by elements of the anti-viral machinery(31). Indeed, one of the reasons for selective tumor cell replication for many DNA-based oncolytic viruses is due to deficiencies in anti-viral machinery elements (32, 33). Using a panel of human melanoma cell lines with variable sensitivity to T-VEC infection, we observed an inverse correlation between STING expression and T-VEC permissiveness. We did not find any impact of PKR or cGAS on T-VEC-mediated killing suggesting that STING may be particularly important. Recent studies have also identified STING expression as an integral intracellular factor in promoting lymphocyte recruitment to tumors and supporting sensitivity to immunotherapy(10). In tumor cells, STING may be triggered by aberrant tumor cell DNA, which then activates cytokines that coordinate with extrinsic STING to induce antigen presentation and trigger host anti-tumor immunity. This pathway has been targeted by STING agonists as a strategy for restoring local T cell recruitment and immunotherapy sensitivity, although clinical trials are still in early development (14). The improved replication of T-VEC in cells with STING deficiency, however, suggests that an alternative approach may be to use oncolytic DNA viruses, which exhibit preferential replication in tumor cells and may be able to overcome STING deficiency to restore innate and adaptive host anti-tumor immunity.

To further confirm the central role of STING in mediating T-VEC-related ICD we developed a STING knockout LOX-IMVI cell line became more permissive to T-VEC infection in the absence of STING. Interestingly, while T-VEC was able to induce TNF α , loss of STING was associated with less TNF α production but significantly increased IL-

1 β release. Although the basis for this is not clear, TNF α has been shown to increase PD-L1 expression in murine tumor-associated macrophages (34), and increased IL-1 β production might be due to increased inflammatory effects due to enhanced cell killing. In addition to STING, it is also possible that additional intracellular factors may be involved in mediating initial cytokine release induced by T-VEC. Further studies are needed to better understand the implications of altered cytokine release in promoting anti-tumor immunity and immunotherapy.

In order to examine immune responses in an immune-competent melanoma model, we used the D43M cell line which has very low STING expression and is resistant to treatment with anti-PD-1 immune checkpoint inhibitor. In this model employing a bilateral tumor design, T-VEC was able to induce a strong anenestic response with regression of injected and un-injected tumors with improved survival. In addition, we demonstrated the accumulation of viral- and tumor antigen-specific T cells within injected and un-injected lesions. In addition, increased pro-inflammatory gene expression was detected in all tumors suggesting a systemic anti-tumor immune response had been generated. This included numerous genes associated with multiple aspects of immune cell function, including antigen presentation, innate immunity, and T cell activation and recruitment. This supports the concept that T-VEC could overcome innate STING deficiency within the melanoma cells to promote ICD and anti-tumor immunity. It is important to note that while T-VEC exhibited immune infiltration to both injected and non-injected lesions, these responses can even be augmented by using mT-VEC and other combinations as previously described (21). These data are also supported by results of a recent phase I trial of T-VEC and pembrolizumab,

which demonstrated 62% objective response rate in melanoma patients treated with the combination (16). In this small trial, patients harboring tumors without PD-L1 expression responded. While PD-L1 expression has not completely correlated with therapeutic activity to checkpoint blockade in melanoma, this may be significant when considering other cancers where PD-L1 expression may be important for clinical activity with checkpoint blockade.

In summary, we have shown that T-VEC induces immunogenic cell death, DAMP release, cytokine production and induction of inflammatory gene expression. STING also emerged as a critical factor in mediating melanoma cell sensitivity to T-VEC infection, killing, and immune activation. This observation might also support STING expression as a predictive biomarker of T-VEC response, although this requires clinical validation. Previous studies have shown that oncolytic HSV-1 can mediate regression of STING-low tumor cells (32). It is possible that T-VEC may mediate anti-tumor responses through different pathways in STING expressing and STING deficient tumors. A better understanding of how T-VEC kills melanoma cells and promotes systemic anti-tumor immunity should promote more rational combination studies and could help identify patients with tumors most likely to respond to treatment with oncolytic viruses.

CHAPTER FOUR

SUMMARY AND CONCLUSION

In my studies, we sought to address two major hypotheses. First, we investigated the hypothesis that MAPK inhibition can enhance T-VEC mediated cell killing in-vitro and how the combination can improve anti-tumor immunity in-vivo. Indeed, we confirmed an additive cell killing effect when human melanoma cell lines are treated using a combination of T-VEC and MEK inhibitor regardless of BRAF mutation status. We also demonstrated increased viral replication and tumor cell apoptosis in cells treated with combination therapy. The combination was associated with therapeutic activity in human xenograft and immune competent murine melanoma models, as well as in the CT26 colon carcinoma model. Therapeutic responses are associated with the induction of viral- and tumor-specific CD8⁺ T cells and immunologic memory. Combination treatment also induced interferon- γ related inflammatory gene signature, which resulted in increased expression of PD-1 and PD-L1. This led us to test triple combination therapy using T-VEC, MEKi and PD-1 blocker. The triple combination further improved therapeutic responses both in melanoma and colon cancer mouse models. In our studies, we did not observe overt signs of toxicity in mice supporting a more favorable therapeutic window even with triple combination therapy, although clinical confirmation is needed. Collectively, these data provide a pre-clinical rationale for triple combination treatment of T-VEC, MEK inhibition and PD-1 blockade in patients with melanoma.

Next, we hypothesized that host intracellular factors contribute to the resistance of T-VEC mediated killing, and also sought to confirm if T-VEC treatment induces immunogenic cell death (ICD) as previously shown with other oncolytic viruses. Initially, we treated a panel of melanoma cell lines with T-VEC and observed that melanoma cells exhibit differential sensitivity to T-VEC treatment. Using a moderately sensitive cell line, we confirmed that T-VEC treatment caused ICD and led to the release of HMGB1, ATP and also upregulated ecto-calreticulin expression, confirming that T-VEC induces ICD. Next, we examined the protein levels of defined host anti-viral DNA and RNA sensors in these cell lines and identified high levels of STING protein expression as being associated with melanoma cell resistance to T-VEC replication. To confirm that STING contributes to T-VEC resistance, using CRISPR-CAS9 we generated cell lines that lack different components of the STING pathway. In our studies, only STING but not PKR or cGAS loss resulted in enhanced T-VEC-mediated lysis. Previously, STING has been shown to play a crucial role in mediating anti-tumor immunity and responses to immune checkpoint inhibition. Several preclinical studies have shown a direct correlation between STING expression and response to immune checkpoint inhibitors. Thus, we further aim to test if T-VEC can activate anti-tumor immune responses in STING^{lo} melanoma model that is resistant to immune checkpoint inhibition. Using a STING^{lo}-PD-1 resistant melanoma model we showed that T-VEC can rescue STING deficiency and can lead to anti-tumor immunity. Using Nanostring gene expression analysis, we also confirmed that T-VEC treatment leads to an increased immune inflammatory gene signature in both injected and contralateral tumors. These data collectively support the hypothesis that

STING expression contributes to T-VEC mediated cell killing in-vitro and further that T-VEC overcomes STING deficiency in-vivo resulting in systemic anti-tumor immunity.

FUTURE DIRECTIONS

Our study supports the proof of concept for therapeutic activity of T-VEC in combination with trametinib (MEKi), and PD-1 blockade. Therapeutic responses were shown in BRAF V600E mutant D4M3A H-2K^b mouse melanoma model and also in H-2K^d murine CT26 colon carcinoma models. Next, it is essential to evaluate the systemic anti-tumor benefits of the triple combination therapy. These studies can be performed by treating mice harboring tumors on both the right and left flanks. Using gene expression profiling and flow cytometry we can identify molecular signatures and key components which can either augment or subside the effects of the triple combination. Recognizing the critical molecular elements that mediate the therapeutic benefit can help us better understand the mechanisms of action by which all these three drugs work together. Finally, as all the three agents are currently approved for the treatment of melanoma, a clinical trial comprising two arms, one arm with T-VEC alone and other arm using a combination of T-VEC, MEKi, PD-1 inhibitor should be tested in the clinic to evaluate the translation of the study to melanoma patients. Next, this combination should be tested in other solid tumors which can be accessible for intratumoral injection of T-VEC. Currently, treatment of melanoma using a combination of PD-1 and CTLA4 immune checkpoint inhibitors have achieved favorable responses, but most often associated with increased side effects. In my experiments, we showed that triple combination has not only achieved favorable therapeutic responses in

mice but exhibited no visible side effects. Mice treated with the triple combination did not lose weight or showed no symptoms of distress in comparison with mock-treated mice.

Next, we investigated the components of host innate anti-viral machinery that can mediate resistance to T-VEC mediated melanoma killing. We observed that host DNA sensing factor STING could contribute to resistance to T-VEC. While our study showcases the role of STING in T-VEC mediated killing in melanoma cell lines, further studies are needed to expand the hypothesis to other tumor cell lines. It is necessary to validate our finding using a more extensive cell array, which includes at least a handful of cell lines from each tumor type. Another essential take-home point is that, while the loss of STING enhanced the ability of T-VEC to kill particular tumor cell lines, this effect was predominant with the higher multiplicity of infections of T-VEC treatment. This can infer the importance of other host anti-viral factors which might act in conjunction with STING pathway. A CRISPR array targeting a broader set of relevant genes can be performed to identify the contribution of other host factors that might mediate resistance to T-VEC treatment. Further, it is also essential to evaluate the effects of other host anti-viral factors in mediating anti-tumor responses in-vivo. We generate preliminary data suggesting that IRF-3 and IRF-7 may also be critical factors in mediating T-VEC replication. It will be particularly interesting to pursue additional experiments on the role of these factors in mediating T-VEC-induced ICD and inducing host anti-viral and anti-tumor immunity. We expect T-VEC might be able to achieve anti-tumor responses in tumors with both high as well as low levels of host anti-viral factor expression but might exhibit different mechanisms of actions based on expression levels of host anti-viral machinery, and these could be potential predictive

biomarkers although clinical validation is needed. Understanding the mechanisms of action of T-VEC in tumor models with differential expression of host anti-viral factors might help us to develop rational combinatorial treatment strategies.

CONCLUDING REMARKS

Finally, I want to conclude by stating that we are in a new, exciting and rapidly evolving phase of cancer treatment. Utilizing our body's immune system to fight cancer has been proven to be successful. During the last decade, we have experienced an exponential increase in the number of clinical trials being conducted using immunotherapy. Currently, there are almost 10,000 clinical trials registered on ClinicalTrials.gov that aim to evaluate the efficacy of either single agent or combination approaches utilizing immunotherapy for cancer treatment. While this is exciting, many trials have already failed to show therapeutic benefit. It is now essential for the National Cancer Institute to increase funding for basic research, which can help scientists to further dissect the mechanisms of action of these individual agents as a monotherapy and in combinational approaches. Novel strategies for identification of biomarkers have to be implemented to not only access the studies which have succeeded but also to evaluate the therapies which have failed during clinical development. Our research findings make significant contributions to the field by identifying fundamental pre-clinical mechanisms of action of each agent and by evaluating a rational combinatorial approach using these agents which are currently approved for the treatment of melanoma and provide a biologic rationale for clinical translation.

REFERENCES

1. Bommarreddy PK, Shettigar M, Kaufman HL. 2018. Integrating oncolytic viruses in combination cancer immunotherapy. *Nat Rev Immunol* 18: 498-513
2. Kaufman HL, Kohlhapp FJ, Zloza A. 2015. Oncolytic viruses: a new class of immunotherapy drugs. *Nat Rev Drug Discov* 14: 642-62
3. Bommarreddy PK, Aspromonte S, Zloza A, Rabkin SD, Kaufman HL. 2018. MEK inhibition enhances oncolytic virus immunotherapy through increased tumor cell killing and T cell activation. *Sci Transl Med* 10
4. Koshenkov VP, Broucek J, Kaufman HL. 2016. Surgical Management of Melanoma. *Cancer Treat Res* 167: 149-79
5. Gershenwald JE, Scolyer RA, Hess KR, Sondak VK, Long GV, Ross MI, Lazar AJ, Faries MB, Kirkwood JM, McArthur GA, Haydu LE, Eggermont AMM, Flaherty KT, Balch CM, Thompson JF, for members of the American Joint Committee on Cancer Melanoma Expert P, the International Melanoma D, Discovery P. 2017. Melanoma staging: Evidence-based changes in the American Joint Committee on Cancer eighth edition cancer staging manual. *CA Cancer J Clin* 67: 472-92
6. Luke JJ, Flaherty KT, Ribas A, Long GV. 2017. Targeted agents and immunotherapies: optimizing outcomes in melanoma. *Nat Rev Clin Oncol* 14: 463-82
7. Larkin J, Chiarion-Sileni V, Gonzalez R, Grob JJ, Cowey CL, Lao CD, Schadendorf D, Dummer R, Smylie M, Rutkowski P, Ferrucci PF, Hill A, Wagstaff J, Carlino MS, Haanen JB, Maio M, Marquez-Rodas I, McArthur GA, Ascierto PA, Long GV, Callahan MK, Postow MA, Grossmann K, Sznol M, Dreno B, Bastholt L, Yang A, Rollin LM, Horak C, Hodi FS, Wolchok JD. 2015. Combined Nivolumab and Ipilimumab or Monotherapy in Untreated Melanoma. *N Engl J Med* 373: 23-34
8. Wolchok JD, Chiarion-Sileni V, Gonzalez R, Rutkowski P, Grob JJ, Cowey CL, Lao CD, Wagstaff J, Schadendorf D, Ferrucci PF, Smylie M, Dummer R, Hill A, Hogg D, Haanen J, Carlino MS, Bechter O, Maio M, Marquez-Rodas I, Guidoboni M, McArthur G, Lebbe C, Ascierto PA, Long GV, Cebon J, Sosman J, Postow MA, Callahan MK, Walker D, Rollin L, Bhore R, Hodi FS, Larkin J. 2017. Overall Survival with Combined Nivolumab and Ipilimumab in Advanced Melanoma. *N Engl J Med* 377: 1345-56
9. Long GV, Stroyakovskiy D, Gogas H, Levchenko E, de Braud F, Larkin J, Garbe C, Jouary T, Hauschild A, Grob JJ, Chiarion Sileni V, Lebbe C, Mandala M, Millward M, Arance A, Bondarenko I, Haanen JB, Hansson J, Utikal J, Ferraresi V, Kovalenko N, Mohr P, Probachai V, Schadendorf D, Nathan P, Robert C, Ribas A, DeMarini DJ, Irani JG, Casey M, Ouellet D, Martin AM, Le N, Patel K, Flaherty K. 2014. Combined BRAF and MEK inhibition versus BRAF inhibition alone in melanoma. *N Engl J Med* 371: 1877-88
10. Griffin M, Scotto D, Josephs DH, Mele S, Crescioli S, Bax HJ, Pellizzari G, Wynne MD, Nakamura M, Hoffmann RM, Ilieva KM, Cheung A, Spicer JF, Papa S, Lacy KE, Karagiannis SN. 2017. BRAF inhibitors: resistance and the promise of combination treatments for melanoma. *Oncotarget* 8: 78174-92

11. Villanueva J, Infante JR, Krepler C, Reyes-Uribe P, Samanta M, Chen HY, Li B, Swoboda RK, Wilson M, Vultur A, Fukunaba-Kalabis M, Wubbenhorst B, Chen TY, Liu Q, Sproesser K, DeMarini DJ, Gilmer TM, Martin AM, Marmorstein R, Schultz DC, Speicher DW, Karakousis GC, Xu W, Amaravadi RK, Xu X, Schuchter LM, Herlyn M, Nathanson KL. 2013. Concurrent MEK2 mutation and BRAF amplification confer resistance to BRAF and MEK inhibitors in melanoma. *Cell Rep* 4: 1090-9
12. Grimaldi AM, Simeone E, Festino L, Vanella V, Palla M, Ascierto PA. 2015. Novel mechanisms and therapeutic approaches in melanoma: targeting the MAPK pathway. *Discov Med* 19: 455-61
13. Flaherty KT, Robert C, Hersey P, Nathan P, Garbe C, Milhem M, Demidov LV, Hassel JC, Rutkowski P, Mohr P, Dummer R, Trefzer U, Larkin JM, Utikal J, Dreno B, Nyakas M, Middleton MR, Becker JC, Casey M, Sherman LJ, Wu FS, Ouellet D, Martin AM, Patel K, Schadendorf D, Group MS. 2012. Improved survival with MEK inhibition in BRAF-mutated melanoma. *N Engl J Med* 367: 107-14
14. Robert C, Karaszewska B, Schachter J, Rutkowski P, Mackiewicz A, Stroiakovski D, Lichinitser M, Dummer R, Grange F, Mortier L, Chiarion-Sileni V, Drucis K, Krajsova I, Hauschild A, Lorigan P, Wolter P, Long GV, Flaherty K, Nathan P, Ribas A, Martin AM, Sun P, Crist W, Legos J, Rubin SD, Little SM, Schadendorf D. 2015. Improved overall survival in melanoma with combined dabrafenib and trametinib. *N Engl J Med* 372: 30-9
15. Larkin J, Ascierto PA, Dreno B, Atkinson V, Liskay G, Maio M, Mandala M, Demidov L, Stroyakovskiy D, Thomas L, de la Cruz-Merino L, Dutriaux C, Garbe C, Sovak MA, Chang I, Choong N, Hack SP, McArthur GA, Ribas A. 2014. Combined vemurafenib and cobimetinib in BRAF-mutated melanoma. *N Engl J Med* 371: 1867-76
16. Ebert PJR, Cheung J, Yang Y, McNamara E, Hong R, Moskalenko M, Gould SE, Maecker H, Irving BA, Kim JM, Belvin M, Mellman I. 2016. MAP Kinase Inhibition Promotes T Cell and Anti-tumor Activity in Combination with PD-L1 Checkpoint Blockade. *Immunity* 44: 609-21
17. Hu-Lieskovan S, Robert L, Homet Moreno B, Ribas A. 2014. Combining targeted therapy with immunotherapy in BRAF-mutant melanoma: promise and challenges. *J Clin Oncol* 32: 2248-54
18. Bommareddy PK, Patel A, Hossain S, Kaufman HL. 2017. Talimogene Laherparepvec (T-VEC) and Other Oncolytic Viruses for the Treatment of Melanoma. *Am J Clin Dermatol* 18: 1-15
19. Zamarin D, Holmgaard RB, Subudhi SK, Park JS, Mansour M, Palese P, Merghoub T, Wolchok JD, Allison JP. 2014. Localized oncolytic virotherapy overcomes systemic tumor resistance to immune checkpoint blockade immunotherapy. *Sci Transl Med* 6: 226ra32
20. Kohlhapp FJ, Kaufman HL. 2016. Molecular Pathways: Mechanism of Action for Talimogene Laherparepvec, a New Oncolytic Virus Immunotherapy. *Clin Cancer Res* 22: 1048-54

21. Workenhe ST, Mossman KL. 2014. Oncolytic virotherapy and immunogenic cancer cell death: sharpening the sword for improved cancer treatment strategies. *Mol Ther* 22: 251-6
22. Schumacher TN, Schreiber RD. 2015. Neoantigens in cancer immunotherapy. *Science* 348: 69-74
23. Fehres CM, Unger WW, Garcia-Vallejo JJ, van Kooyk Y. 2014. Understanding the biology of antigen cross-presentation for the design of vaccines against cancer. *Front Immunol* 5: 149
24. Garcia-Diaz A, Shin DS, Moreno BH, Saco J, Escuin-Ordinas H, Rodriguez GA, Zaretsky JM, Sun L, Hugo W, Wang X, Parisi G, Saus CP, Torrejon DY, Graeber TG, Comin-Anduix B, Hu-Lieskovan S, Damoiseaux R, Lo RS, Ribas A. 2017. Interferon Receptor Signaling Pathways Regulating PD-L1 and PD-L2 Expression. *Cell Rep* 19: 1189-201
25. Gleason MK, Lenvik TR, McCullar V, Felices M, O'Brien MS, Cooley SA, Verneris MR, Cichocki F, Holman CJ, Panoskaltsis-Mortari A, Niki T, Hirashima M, Blazar BR, Miller JS. 2012. Tim-3 is an inducible human natural killer cell receptor that enhances interferon gamma production in response to galectin-9. *Blood* 119: 3064-72
26. Wojton J, Kaur B. 2010. Impact of tumor microenvironment on oncolytic viral therapy. *Cytokine Growth Factor Rev* 21: 127-34
27. Tysome JR, Lemoine NR, Wang Y. 2013. Update on oncolytic viral therapy - targeting angiogenesis. *Oncotargets Ther* 6: 1031-40
28. Naik S, Russell SJ. 2009. Engineering oncolytic viruses to exploit tumor specific defects in innate immune signaling pathways. *Expert Opin Biol Ther* 9: 1163-76
29. Jhawar SR, Thandoni A, Bommareddy PK, Hassan S, Kohlhapp FJ, Goyal S, Schenkel JM, Silk AW, Zloza A. 2017. Oncolytic Viruses-Natural and Genetically Engineered Cancer Immunotherapies. *Front Oncol* 7: 202
30. Andtbacka RH, Kaufman HL, Collichio F. 2015. Talimogene Laherparepvec Improves Durable Response Rate in Patients with Advanced Melanoma. In *J Clin Oncol*
31. Chesney J, Puzanov I, Collichio F, Singh P, Milhem MM, Glaspy J, Hamid O, Ross M, Friedlander P, Garbe C, Logan TF, Hauschild A, Lebbe C, Chen L, Kim JJ, Gansert J, Andtbacka RHI, Kaufman HL. 2017. Randomized, Open-Label Phase II Study Evaluating the Efficacy and Safety of Talimogene Laherparepvec in Combination With Ipilimumab Versus Ipilimumab Alone in Patients With Advanced, Unresectable Melanoma. *J Clin Oncol*: JCO2017737379
32. Ribas A, Dummer R, Puzanov I, VanderWalde A, Andtbacka RHI, Michielin O, Olszanski AJ, Malvey J, Cebon J, Fernandez E, Kirkwood JM, Gajewski TF, Chen L, Gorski KS, Anderson AA, Diede SJ, Lassman ME, Gansert J, Hodi FS, Long GV. 2017. Oncolytic Virotherapy Promotes Intratumoral T Cell Infiltration and Improves Anti-PD-1 Immunotherapy. *Cell* 170: 1109-19 e10
33. Rojas JJ, Sampath P, Hou W, Thorne SH. 2015. Defining Effective Combinations of Immune Checkpoint Blockade and Oncolytic Virotherapy. *Clin Cancer Res* 21: 5543-51
34. Hu JC, Coffin RS, Davis CJ, Graham NJ, Groves N, Guest PJ, Harrington KJ, James ND, Love CA, McNeish I, Medley LC, Michael A, Nutting CM, Pandha

- HS, Shorrock CA, Simpson J, Steiner J, Steven NM, Wright D, Coombes RC. 2006. A phase I study of OncoVEXGM-CSF, a second-generation oncolytic herpes simplex virus expressing granulocyte macrophage colony-stimulating factor. *Clin Cancer Res* 12: 6737-47
35. Senzer NN, Kaufman HL, Amatruda T, Nemunaitis M, Reid T, Daniels G, Gonzalez R, Glaspy J, Whitman E, Harrington K, Goldsweig H, Marshall T, Love C, Coffin R, Nemunaitis JJ. 2009. Phase II clinical trial of a granulocyte-macrophage colony-stimulating factor-encoding, second-generation oncolytic herpesvirus in patients with unresectable metastatic melanoma. *J Clin Oncol* 27: 5763-71
 36. Kaufman HL, Kim DW, DeRaffele G, Mitcham J, Coffin RS, Kim-Schulze S. 2010. Local and distant immunity induced by intralesional vaccination with an oncolytic herpes virus encoding GM-CSF in patients with stage IIIc and IV melanoma. *Ann Surg Oncol* 17: 718-30
 37. Andtbacka RH, Ross M, Puzanov I, Milhem M, Collichio F, Delman KA, Amatruda T, Zager JS, Cranmer L, Hsueh E, Chen L, Shilkrut M, Kaufman HL. 2016. Patterns of Clinical Response with Talimogene Laherparepvec (T-VEC) in Patients with Melanoma Treated in the OPTiM Phase III Clinical Trial. *Ann Surg Oncol*
 38. Bommarreddy PK, Silk AW, Kaufman HL. 2017. Intratumoral Approaches for the Treatment of Melanoma. *Cancer J* 23: 40-7
 39. Jenkins MH, Steinberg SM, Alexander MP, Fisher JL, Ernstoff MS, Turk MJ, Mullins DW, Brinckerhoff CE. 2014. Multiple murine BRAf(V600E) melanoma cell lines with sensitivity to PLX4032. *Pigment Cell Melanoma Res* 27: 495-501
 40. Hebert CG, DiNardo N, Evans ZL, Hart SJ, Hachmann AB. 2018. Rapid quantification of vesicular stomatitis virus in Vero cells using Laser Force Cytology. *Vaccine*
 41. Liu L, Mayes PA, Eastman S, Shi H, Yadavilli S, Zhang T, Yang J, Seestaller-Wehr L, Zhang SY, Hopson C, Tsvetkov L, Jing J, Zhang S, Smothers J, Hoos A. 2015. The BRAF and MEK Inhibitors Dabrafenib and Trametinib: Effects on Immune Function and in Combination with Immunomodulatory Antibodies Targeting PD-1, PD-L1, and CTLA-4. *Clin Cancer Res* 21: 1639-51
 42. Hildner K, Edelson BT, Purtha WE, Diamond M, Matsushita H, Kohyama M, Calderon B, Schraml BU, Unanue ER, Diamond MS, Schreiber RD, Murphy TL, Murphy KM. 2008. Batf3 deficiency reveals a critical role for CD8alpha+ dendritic cells in cytotoxic T cell immunity. *Science* 322: 1097-100
 43. Spranger S, Dai D, Horton B, Gajewski TF. 2017. Tumor-Residing Batf3 Dendritic Cells Are Required for Effector T Cell Trafficking and Adoptive T Cell Therapy. *Cancer Cell* 31: 711-23 e4
 44. Ayers M, Luceford J, Nebozhyn M, Murphy E, Loboda A, Kaufman DR, Albright A, Cheng JD, Kang SP, Shankaran V, Piha-Paul SA, Yearley J, Seiwert TY, Ribas A, McClanahan TK. 2017. IFN-gamma-related mRNA profile predicts clinical response to PD-1 blockade. *J Clin Invest* 127: 2930-40
 45. Roulstone V, Pedersen M, Kyula J, Mansfield D, Khan AA, McEntee G, Wilkinson M, Karapanagiotou E, Coffey M, Marais R, Jebar A, Errington-Mais F, Melcher A, Vile R, Pandha H, McLaughlin M, Harrington KJ. 2015. BRAF- and

- MEK-Targeted Small Molecule Inhibitors Exert Enhanced Antimelanoma Effects in Combination With Oncolytic Reovirus Through ER Stress. *Mol Ther* 23: 931-42
46. Gholami S, Chen CH, Gao S, Lou E, Fujisawa S, Carson J, Nnoli JE, Chou TC, Bromberg J, Fong Y. 2014. Role of MAPK in oncolytic herpes viral therapy in triple-negative breast cancer. *Cancer Gene Ther* 21: 283-9
 47. Bagheri N, Shiina M, Lauffenburger DA, Korn WM. 2011. A dynamical systems model for combinatorial cancer therapy enhances oncolytic adenovirus efficacy by MEK-inhibition. *PLoS Comput Biol* 7: e1001085
 48. Botta G, Passaro C, Libertini S, Abagnale A, Barbato S, Maione AS, Hallden G, Beguinot F, Formisano P, Portella G. 2012. Inhibition of autophagy enhances the effects of E1A-defective oncolytic adenovirus dl922-947 against glioma cells in vitro and in vivo. *Hum Gene Ther* 23: 623-34
 49. Smith KD, Mezhir JJ, Bickenbach K, Veerapong J, Charron J, Posner MC, Roizman B, Weichselbaum RR. 2006. Activated MEK suppresses activation of PKR and enables efficient replication and in vivo oncolysis by Deltagamma(1)34.5 mutants of herpes simplex virus 1. *J Virol* 80: 1110-20
 50. Veerapong J, Bickenbach KA, Shao MY, Smith KD, Posner MC, Roizman B, Weichselbaum RR. 2007. Systemic delivery of (gamma)134.5-deleted herpes simplex virus-1 selectively targets and treats distant human xenograft tumors that express high MEK activity. *Cancer Res* 67: 8301-6
 51. Gilmartin AG, Bleam MR, Groy A, Moss KG, Minthorn EA, Kulkarni SG, Rominger CM, Erskine S, Fisher KE, Yang J, Zappacosta F, Annan R, Sutton D, Laquerre SG. 2011. GSK1120212 (JTP-74057) is an inhibitor of MEK activity and activation with favorable pharmacokinetic properties for sustained in vivo pathway inhibition. *Clin Cancer Res* 17: 989-1000
 52. Xia T, Konno H, Barber GN. 2016. Recurrent Loss of STING Signaling in Melanoma Correlates with Susceptibility to Viral Oncolysis. *Cancer Res* 76: 6747-59
 53. Vella LJ, Pasam A, Dimopoulos N, Andrews M, Knights A, Puaux AL, Louahed J, Chen W, Woods K, Cebon JS. 2014. MEK inhibition, alone or in combination with BRAF inhibition, affects multiple functions of isolated normal human lymphocytes and dendritic cells. *Cancer Immunol Res* 2: 351-60
 54. Itamura H, Shindo T, Tawara I, Kubota Y, Kariya R, Okada S, Komanduri KV, Kimura S. 2016. The MEK inhibitor trametinib separates murine graft-versus-host disease from graft-versus-tumor effects. *JCI Insight* 1: e86331
 55. Woo SR, Fuertes MB, Corrales L, Spranger S, Furdyna MJ, Leung MY, Duggan R, Wang Y, Barber GN, Fitzgerald KA, Alegre ML, Gajewski TF. 2014. STING-dependent cytosolic DNA sensing mediates innate immune recognition of immunogenic tumors. *Immunity* 41: 830-42
 56. Chevolet I, Speeckaert R, Schreuer M, Neyns B, Krysko O, Bachert C, Hennart B, Allorge D, van Geel N, Van Gele M, Brochez L. 2015. Characterization of the in vivo immune network of IDO, tryptophan metabolism, PD-L1, and CTLA-4 in circulating immune cells in melanoma. *Oncoimmunology* 4: e982382
 57. Deken MA, Gadiot J, Jordanova ES, Lacroix R, van Gool M, Kroon P, Pineda C, Geukes Foppen MH, Scolyer R, Song JY, Verbrugge I, Hoeller C, Dummer R,

- Haanen JB, Long GV, Blank CU. 2016. Targeting the MAPK and PI3K pathways in combination with PD1 blockade in melanoma. *Oncoimmunology* 5: e1238557
58. Torti N, Walton SM, Murphy KM, Oxenius A. 2011. Batf3 transcription factor-dependent DC subsets in murine CMV infection: differential impact on T-cell priming and memory inflation. *Eur J Immunol* 41: 2612-8
59. Corrales L, Matson V, Flood B, Spranger S, Gajewski TF. 2017. Innate immune signaling and regulation in cancer immunotherapy. *Cell Res* 27: 96-108
60. Toda M, Rabkin SD, Kojima H, Martuza RL. 1999. Herpes simplex virus as an in situ cancer vaccine for the induction of specific anti-tumor immunity. *Hum Gene Ther* 10: 385-93
61. Disis ML, Wallace DR, Gooley TA, Dang Y, Slota M, Lu H, Coveler AL, Childs JS, Higgins DM, Fintak PA, dela Rosa C, Tietje K, Link J, Waisman J, Salazar LG. 2009. Concurrent trastuzumab and HER2/neu-specific vaccination in patients with metastatic breast cancer. *J Clin Oncol* 27: 4685-92
62. Memarnejadian A, Meilleur CE, Shaler CR, Khazaie K, Bennink JR, Schell TD, Haeryfar SMM. 2017. PD-1 Blockade Promotes Epitope Spreading in Anticancer CD8(+) T Cell Responses by Preventing Fratricidal Death of Subdominant Clones To Relieve Immunodomination. *J Immunol* 199: 3348-59
63. Kawaguchi K, Igarashi K, Murakami T, Zhao M, Zhang Y, Chmielowski B, Kiyuna T, Nelson SD, Russell TA, Dry SM, Li Y, Unno M, Eilber FC, Hoffman RM. 2017. Tumor-Targeting Salmonella typhimurium A1-R Sensitizes Melanoma With a BRAF-V600E Mutation to Vemurafenib in a Patient-Derived Orthotopic Xenograft (PDOX) Nude Mouse Model. *J Cell Biochem* 118: 2314-9
64. Yamamoto M, Zhao M, Hiroshima Y, Zhang Y, Shurell E, Eilber FC, Bouvet M, Noda M, Hoffman RM. 2016. Efficacy of Tumor-Targeting Salmonella A1-R on a Melanoma Patient-Derived Orthotopic Xenograft (PDOX) Nude-Mouse Model. *PLoS One* 11: e0160882
65. Kawaguchi K, Igarashi K, Murakami T, Kiyuna T, Zhao M, Zhang Y, Nelson SD, Russell TA, Dry SM, Singh AS, Chmielowski B, Li Y, Unno M, Eilber FC, Hoffman RM. 2017. Salmonella typhimurium A1-R targeting of a chemotherapy-resistant BRAF-V600E melanoma in a patient-derived orthotopic xenograft (PDOX) model is enhanced in combination with either vemurafenib or temozolomide. *Cell Cycle* 16: 1288-94
66. Kohlhapp FJ, Huelsmann EJ, Lacey AT, Schenkel JM, Lusciks J, Broucek JR, Goldufsky JW, Hughes T, Zayas JP, Dolubizno H, Sowell RT, Kuhner R, Burd S, Kubasiak JC, Nabatiyan A, Marshall S, Bommareddy PK, Li S, Newman JH, Monken CE, Shafikhani SH, Marzo AL, Guevara-Patino JA, Lasfar A, Thomas PG, Lattime EC, Kaufman HL, Zloza A. 2016. Non-oncogenic Acute Viral Infections Disrupt Anti-cancer Responses and Lead to Accelerated Cancer-Specific Host Death. *Cell Rep* 17: 957-65

APPENDIX

APPENDIX A. ABBREVIATIONS USED

ANOVA: analysis of variance

ATCC: American Type Culture Collection ATG: start codon for methionine

ATP: adenosine triphosphate

BRAF: b-raf serine/threonine kinase

CD8: (cluster of differentiation 8) is a transmembrane glycoprotein that serves as a co-receptor for the T cell receptor (TCR)

cGAS: Cyclic GMP-AMP synthase

COMBO: combination

CRISPR: clustered regularly interspaced short palindromic repeats

DAMP: Damage associated molecular patterns

DMEM: Dulbecco's Modified Eagle Medium

DMSO: dimethyl sulfoxide

DNA: deoxyribonucleic acid

EDTA: ethylenediaminetetraacetic acid

ERK: extracellular signal-regulated kinase

FFPE: formalin-fixed, paraffin-embedded

GMCSF: Granulocyte-macrophage colony-stimulating factor

HSV-1: Herpes simplex virus type 1

H&E: hematoxylin & eosin

HMGB1: High mobility group box 1

ICP: Infected cellular protein

IFN- γ : Interferon-gamma

IgG: immunoglobulin G

IHC: immunohistochemistry

IC-50: half maximal inhibitory concentration

ICD: Immunogenic cell death

IL: interleukin

Ki-67: proliferation marker protein Ki-67

MAPK: mitogen-activated protein kinase

MEK: mitogen activated protein kinase

MTS: [3-(4,5-dimethylthiazol-2-yl)-5-(3- carboxymethoxyphenyl)-2-(4-sulfophenyl)-2H-tetrazolium]

NSG: NOD, non-obese diabetic /SCID, severe combined immunodeficiency/ GAMMA, interleukin 2 receptor γ null

PARP: poly (ADP-ribose) polymerase

PDX: patient-derived xenograft

PD-1: Programmed cell death protein 1

PD-L1: Programmed death-ligand 1

RAS: RAS proto-oncogene, GTPase

shRNA: short hairpin ribonucleic acid

STING: Stimulator of interferon genes

TNF α : Tumor necrosis factor alpha

T-VEC: Talimogene laherparepvec. T-VEC first oncolytic herpes simplex virus type -1 therapy approved by the U.S. FDA for patients with advanced melanoma

APPENDIX B. SUPPLEMENTARY TABLES

Table S1. Antibodies

| REAGENT or RESOURCE | SOURCE | IDENTIFIER |
|---|----------------|---------------------------------|
| Antibodies | | |
| FITC anti-mouse CD4 | BioLegend | Cat#100406, RRID:AB_312713 |
| PE anti-mouse CD3 | BioLegend | Cat#100206, RRID:AB_312663 |
| Pacific Blue™ anti-human/mouse Granzyme B | BioLegend | Cat#515408, RRID:AB_2562195 |
| Brilliant Violet™ 605 anti-mouse PD-L1 | BioLegend | Cat#124321, RRID:AB_2563635 |
| Brilliant Violet 650™ anti-mouse CD45 | BioLegend | Cat#103151, RRID:AB_2565884 |
| Brilliant Violet 711™ anti-mouse IFN- γ | BioLegend | Cat#505836, RRID:AB_11219588 |
| Brilliant Violet 785™ anti-mouse CD8a | BioLegend | Cat#100750, RRID:AB_2562610 |
| APC anti-mouse FOXP3 | Thermo Fischer | Cat#17-5773-82, RRID:AB_469457 |
| Alexa Fluor® 700 anti-mouse Ki-67 | BioLegend | Cat#652420, RRID:AB_2564285 |
| APC/Cy7 anti-mouse I-A/I-E (MHCII) | BioLegend | Cat#107628, RRID:AB_2069377 |
| APC anti-mouse F4/80 | BioLegend | Cat#123115; RRID:AB_893493 |
| PerCP/Cy5.5 anti-mouse CD3 | BioLegend | Cat#100218, RRID:AB_893318 |
| PE/Cy7 anti-mouse CD11c | BioLegend | Cat#117318, RRID:AB_493568 |
| Brilliant Violet 421™ anti-mouse Ly-6G/Ly-6C (Gr-1) | BioLegend | Cat#108434, RRID:AB_2562219 |
| Brilliant Violet™ 605 anti-mouse PD-1 | BioLegend | Cat#135220, RRID:AB_2562616 |
| Brilliant Violet 650™ anti-mouse CD44 | BioLegend | Cat#103049, RRID:AB_2562600 |
| Brilliant Violet 711™ anti-mouse CD11b | BioLegend | Cat#101242, RRID:AB_2563310 |
| Brilliant Violet 785™ anti-mouse CD8a | BioLegend | Cat#100750, RRID:AB_2562610 |
| Alexa Fluor® 700 anti-mouse CD45 | BioLegend | Cat#103128, RRID:AB_493715 |
| APC/Cy7 anti-mouse CD4 | BioLegend | Cat#100414, RRID:AB_312699 |
| FITC anti-mouse CD103 | BioLegend | Cat#121420, RRID:AB_10714791 |
| APC/Cy7 anti-mouse PD-L1 | Thermo Fischer | Cat#46-598282, RRID:AB_2573819 |
| PerCP/Cy5.5 anti-mouse CD4 | BioLegend | Cat#100434, RRID:AB_893324 |
| Brilliant Violet 605™ anti-mouse F4/80 | BioLegend | Cat#123133, RRID:AB_2562305 |
| Anti-mouse PD-1 | BioXCell | Cat#BE0146; RRID:AB_10949053 |
| Anti-mouse CD4 | BioXCell | Cat#BE0003-1; RRID:AB_1107636 |
| Anti-mouse CD8 | BioXCell | Cat#BE0061; RRID:AB_1125541 |
| InVivoMAb Rat IgG2b | BioXCell | Cat#BE0090; RRID:AB_1107780 |
| InVivoMAb Syrian Hamster IgG | BioXCell | Cat#BE0087; RRID:AB_1107782 |
| Anti-mouse CD8a | Thermo Fischer | Cat#14-0808-80; RRID:AB_2572860 |
| Cleaved caspase-3 (Asp175) antibody | Cell Signaling | Cat#9661; RRID:AB_2341188 |
| Phospho-p44/42 MAPK (Erk1/2) | Cell Signaling | Cat#4376; RRID:AB_331772 |
| Anti-Ki67 | Abcam | Cat#ab16667; RRID:AB_302459 |
| HRP anti-rat IG | Vector Lab | Cat#MP-7444-15; RRID:AB_2336530 |
| Calreticulin (D3E6) XP® Rabbit mAb | Cell Signaling | Cat#12238S |
| STING (D2P2F) Rabbit mAb | Cell Signaling | Cat#13647S |
| PKR (D7F7) Rabbit mAb | Cell Signaling | Cat#12297S |
| cGAS (D1D3G) Rabbit mAb | Cell Signaling | Cat#15102S |

Table S2. Chemicals

| REAGENT or RESOURCE | SOURCE | IDENTIFIER |
|--|---------------------------|-------------------|
| Chemicals | | |
| RPMI 1640 Medium | Thermo Fischer Scientific | Cat#11875093 |
| DMEM (Dulbecco's Modified Eagle Medium) | Thermo Fischer Scientific | Cat#11965118 |
| DMEM/F-12 | Thermo Fischer Scientific | Cat#10565018 |
| Trypsin-EDTA (0.25%) | Thermo Fischer Scientific | Cat#25200056 |
| Penicillin-Streptomycin-Glutamine | Thermo Fischer Scientific | Cat#10378016 |
| TRIzol | Thermo Fischer Scientific | Cat#15596018 |
| Fetal Bovine Serum | Sigma Aldrich | Cat#12306C |
| TWEEN 80 | Sigma Aldrich | Cat#SKU-P4780 |
| (Hydroxypropyl)methyl cellulose | Sigma Aldrich | Cat#SKU-H7509 |
| Phenazine methosulfate (PMS) | Sigma Aldrich | Cat#SKU-P9625 |
| CellTiter 96® AQueous MTS Reagent Powder | Promega | Cat#G1111 |
| Standard macrophage depletion kit | Encapsula nanoscience | Cat#SKU-8901 |
| DAB+ substrate chromogen system | Dako | Cat#K3468 |
| Hematoxylin 2 | Thermo Fischer Scientific | Cat#7231 |
| Eosin Y 1% alcoholic solution | Fisher Scientific | Cat#245-658 |
| 10% Formalin W/V | Fisher Chemical | Cat#SF98-4 |
| Cytoseal XYL | Thermo Fischer Scientific | Cat#8312-16E |
| Trametinib (GSK1120212) | Selleck Chemicals | Cat#S2673 |
| Vemurafenib (PLX4032, RG7204) | Selleck Chemicals | Cat#S1267 |
| Z-VAD-FMK | Selleck Chemicals | Cat#S7023 |
| FITC TRP2 Dextramer | Immudex | Cat# JD2199 |
| PE GP-100 Dextramer | Immudex | Cat# JA3570 |
| APC HSV-1 gB Dextramer | Immudex | Cat#JD2670 |
| PKR shRNA (h) Lentiviral Particles | SantaCruz Biotechnology | Cat#SC-36263-V |
| TMEM173 shRNA (h) Lentiviral Particles | SantaCruz Biotechnology | Cat#SC-92042-V |
| TMEM173 CRISPR/Cas9 KO Plasmid (h) | SantaCruz Biotechnology | Cat#SC-403148 |
| TMEM173 HDR Plasmid (h) | SantaCruz Biotechnology | Cat#SC-403148-HDR |
| UltraCruz® Transfection Reagent | SantaCruz Biotechnology | Cat#SC-395739 |
| Puromycin dihydrochloride, 25 mg | SantaCruz Biotechnology | Cat#SC-108071 |

Table S3. Commercial Assays

| REAGENT or RESOURCE | SOURCE | IDENTIFIER |
|------------------------------------|-------------------------|-----------------------|
| Commercial Assays | | |
| LookOut Mycoplasma PCR kit | Sigma | Cat#MP0035 |
| Mouse Pan-cancer immune gene panel | NanoString Technologies | XT_PGX_MmV1_CancerImm |
| Apoptosis Detection Kit | BioLegend | Cat#640914 |
| RNeasy plus mini kit | Qiagen | Cat#74134 |

Table S4. Experimental cell lines.

| REAGENT or RESOURCE | SOURCE | IDENTIFIER |
|--------------------------------|---------------------------------|------------|
| Experimental cell lines | | |
| Human: SK-MEL-28 | ATCC | HTB-72 |
| Human: SK-MEL-2 | ATCC | HTB-68 |
| Human: SK-MEL-5 | ATCC | HTB-70 |
| Mouse: B16-F10 | ATCC | CRL-6475 |
| Mouse: B16-F10-Nectin | Amgen | N/A |
| Mouse: D4M3A | (Jenkins et al., 2014) (Ref 39) | N/A |
| Mouse: CT26 | ATCC | CRL-2639 |

ATCC - American Type Culture Collection

Table S5. Experimental Models

| REAGENT or RESOURCE | SOURCE | IDENTIFIER |
|--|--------------|--------------|
| Experimental Models: Organisms/strains | | |
| Mouse: C57BL/6J | Jackson Labs | Stock#000664 |
| Mouse: NOD.Cg-Prkdc ^{scid} Il2rg ^{tm1Wjl} /SzJ | Jackson Labs | Stock#005557 |
| Mouse: B6.129S(C)-Batf3 ^{tm1Kmm} /J | Jackson Labs | Stock#013755 |
| Mouse: BALB/c | Jackson Labs | Stock#000651 |